Relating the properties of cellulose fibers to structure

Thesis Submitted to AcSIR for the Award of
the Degree of
DOCTOR OF PHILOSOPHY
In Engineering Science

By
Aakash Sharma
Registration Number: 20EE14A26051

Under the guidance of
Dr. Guruswamy Kumaraswamy and Dr. Shirish Thakre

Polymer Science and Engineering Division
CSIR-National Chemical Laboratory, Pune 411008

सीएसआयआर–राष्ट्रीय रासायनिक प्रयोगशाला

(वैज्ञानिक तथा औद्योगिक अनुसंधान परिषद्)

डॉ. होमी भाभा मार्ग, पुणे – 411 008. भारत

CSIR-NATIONAL CHEMICAL LABORATORY

(Council of Scientific & Industrial Research)

Dr. Homi Bhabha Road, Pune - 411008. India

CERTIFICATE

This is to certify that the work incorporated in this Ph.D. thesis entitled "**Relating the properties of cellulose fibers to structure**" submitted by Mr. Aakash Sharma to Academy of Scientific and Innovative Research (AcSIR) in fulfilment of the requirement for the award of the Degree of Doctor of Philosophy, embodies original research work under our guidance. We further certify that this work has not been submitted to any other University or Institution in part or full for the award of any degree or diploma. Research material obtained from other sources has been duly acknowledged in the thesis. Any text, illustration, table etc., used in the thesis from other sources have been duly cited and acknowledged.

It is also certified that this work done by the student, under our supervision, is plagiarism free.

Aakash Sharma

(Student)

Dr. Guruswamy Kumaraswamy

(Supervisor)

Dr. Shirish Thakre

(Co-supervisor)

CERTIFICATE

This is to certify that the work incorporated in this Ph.D. thesis entitled **"Relating the properties of cellulose fibers to structure"** submitted by Mr. Aakash Sharma to Academy of Scientific and Innovative Research (AcSIR) in fulfilment of the requirement for the award of the Degree of Doctor of Philosophy, embodies original research work under our guidance. We further certify that this work has not been submitted to any other University or Institution in part or full for the award of any degree or diploma. Research material obtained from other sources has been duly acknowledged in the thesis. Any text, illustration, table etc., used in the thesis from other sources have been duly cited and acknowledged.

It is also certified that this work done by the student, under our supervision, is plagiarism free.

Aakash Sharma

(Student)

Dr. Guruswamy Kumaraswamy

(Supervisor)

Dr. Shirish Thakre

(Co-supervisor)

Declaration by the Candidate

I hereby declare that the thesis entitled **"Relating the properties of cellulose fibers to structure"** submitted by me for the Degree of Doctor of Philosophy to Academy of Scientific & Innovative Research (AcSIR) is the record of work carried out by me at Polymer Sciences & Engineering Division (PSE), CSIR- National Chemical Laboratory, Pune - 411008, India, under the supervision of Dr. Guruswamy Kumaraswamy and Dr. Shirish Thakre. The work is original and has not formed the basis for the award of any degree, diploma, associateship and fellowship titles in this or any other university or other institute of higher learning. I further declare that the material obtained from other resources has been duly acknowledged in the thesis.

Aakash Sharma   June 2019
AcSIR ID: 20EE14A26051
Polymer Science and Engineering Division
CSIR-National Chemical Laboratory
Dr. Homi Bhabha Road, Pashan
Pune – 411008
Maharashtra, India

Dedicated to Papa

Abstract

Polymer fibers are ubiquitous. Applications of polymer fibers are wide ranging, spanning diverse fields such as textiles, biomedical materials, etc. These fibers are manufactured using very different processing techniques. For example, silk is spun by silkworms, PET fibers are spun from the melt state, polyethylene fibers are spun from gels. This thesis is focused on the structural investigation of semicrystalline regenerated cellulose fibers and on structure-property relations in these materials.

To convert cellulose into continuous filaments, it is dissolved and regenerated using two dominant industrially practiced processes – Viscose and Lyocell. Differences in processing techniques induce structural differences in regenerated cellulose fibers. Fibers manufactured using Viscose technique are characterized by skin core morphology whereas, Lyocell fibers show radial uniformity throughout the fiber diameter. Also, the shape of the fiber cross-section is different for Viscose and Lyocell fibers. Such structural differences manifest at length scales varying from O(Å) to O(μm). Implications of the structural differences are observed as differences in the fiber properties. For example, Lyocell fibers have higher modulus than Viscose fibers, Viscose fiber show better fibrillation resistance when soaked in water as compared to Lyocell fibers. Due to the hierarchy of structural differences, ascertaining the microstructural origin of the variations in these properties is a challenging task. Therefore, we present a systematic investigation of the structural features of regenerated cellulose fibers using tools that allow us to probe different length scales e.g. wide angle X-ray diffraction for Å-scale structure, small angle X-ray scattering for structure at tens of nm, ultra-small angle neutron scattering for structure at hundreds of nm, etc. We study the mechanical response of these fibers using a rheometer and relate the mechanical properties to the structure of the fibers.

We demonstrate that polymer fibers, including natural silk and synthetic fibers, exhibit universal viscoelastic response. On stretching below yield, they show logarithmic stress decay. On unloading fibers with a glassy amorphous phase, the stress recovers. A simple phenomenological model accurately describes data from independent mechanical experiments and provides insights into the microstructural origins of the fiber response. Counter to intuition, the model indicates that it is the crystalline regions, rather than the amorphous glass, that deform predominantly on stretching fibers at high strain rates. On

holding a stretched fiber, stress decays as a consequence of relaxations in amorphous regions. Finally, unloading the fiber transfers stress from the amorphous to crystalline regions resulting in stress recovery. Model parameters correlate well with the fiber microstructure. Crystal and amorphous moduli from the model match those from X-ray diffraction. Activation energies for the temperature dependence of the peak relaxation time are similar to those reported in the literature. Thus, a simple model that invokes only crystal-amorphous coexistence can successfully model the mechanical response of a wide variety of polymer fibers.

We employ this model to compare commercially available regenerated cellulose fibers manufactured using Viscose and Lyocell processes. Single fibers are subjected to a variety of mechanical deformations to obtain stress-strain, stress relaxation and stress recovery data. Lyocell fibers are characterized by higher values of crystalline modulus relative to Viscose. Lyocell fibers also have a higher amorphous phase modulus and a wider relaxation spectrum than Viscose, suggesting that amorphous and crystalline phases are dispersed in close connectivity in Lyocell. Viscose and Lyocell fibers exhibit qualitative similarities in their mechanical response. On stretching, there is a transition in the stress-strain curve from a low strain elastic response at a critical value of strain. This critical strain has been incorrectly attributed to yielding of the fiber. We establish that this critical value corresponds to an apparent yield. When subjected to strains higher than this apparent yield point, the fibers develop a memory of the mechanical deformation. This memory decays slowly, logarithmically with time and is lost over about a day as the fiber structure transitions back to the original as spun fiber. We also demonstrate that on wetting the fibers with water, there is an increase in the apparent yield strain for Viscose fibers, but not for Lyocell. We interpret these results in terms of the semicrystalline microstructure of the fibers.

We study the effect of stretching and stress relaxation on the orientation of crystal and amorphous phases of Lyocell and Viscose fibers. Our results show that on stretching, orientation in both crystal and amorphous phases increases linearly with strain, correlating with the increase in stress and with the stretching of the crystalline unit cell along the c-axis. On holding after stretching to a particular strain, the stress relaxes logarithmically in time, correlating with a decrease in the strain along the c-axis of the crystal unit cell. The stress relaxation is also correlated with a logarithmic increase in amorphous orientation, while crystalline orientation stays constant. We attribute the stress development during stretching to deformation of the crystal unit cell, while crystal reorientation in the fiber direction results in

increase in the crystalline orientation parameter. On holding the fiber at a fixed total strain, the stress relaxes as strain is transferred from crystal to amorphous regions. Thus, the strain on the unit cell c-axis decreases and amorphous orientation increases. There are quantitative differences between the rate of increase in amorphous phase orientation during stress relaxation for Lyocell and Viscose fibers. For dry fibers, Lyocell shows a slower increase in orientation during stress relaxation. On wetting the fibers, their structural response changes qualitatively. We combine wide angle X-ray diffraction and birefringence experiments with our model to infer that that on stretching the wet fiber, the crystalline phase is neither strained nor oriented. However, orientation develops in the amorphous phase. During stress relaxation in wet condition, Lyocell fibers shows a faster increase in amorphous orientation than Viscose fibers, in line with the comparison of relaxation time spectra for wet Viscose and Lyocell fibers.

We use small angle scattering to characterize the microvoids in regenerated cellulose fibers that might govern the onset of mechanical failure in these. In regenerated cellulose fibers, scattering of X-rays or neutrons at small angles is largely dominated by scattering from microvoids. We demonstrate that small angle X-ray scattering (SAXS) over the q-range that is typical for most commercial instruments arises from Porod scattering from the microvoid surfaces, viz. the scattered intensity scales as q^{-4}. Therefore, it is not possible to extrapolate this data to lower q to obtain microvoid dimensions and volume fraction. We combine SAXS with medium resolution small angle neutron scattering (MSANS) to characterize the microvoids in regenerated cellulose fibers. Specifically, we compare fibers produced using the Viscose process with those from the Lyocell process. For both Viscose and Lyocell fibers, microvoids have a high aspect ratio and are elongated in the fiber direction. Also, the volume fraction occupied by the microvoids is comparable for Viscose and Lyocell fibers (0.04% - 0.05%). However, there are differences in the microvoid size: Microvoids are more highly oriented for Lyocell fibers and have a larger average length and diameter, compared with Viscose fibers. This result might have important implications for understanding failure of these fibers.

In summary, this thesis reports a detailed study of the structural differences between Lyocell and Viscose fibers at multiple length scales. We have developed a set of sophisticated methodologies for structural characterization of regenerated cellulose fibers. We report the non-intuitive structural response of Lyocell and Viscose fibers subjected to mechanical deformations and develop structure-property relations for these fibers. Our work uncovers the

microstructural origins of the differences between Viscose and Lyocell fibers, and presents results that have implications for relations between semicrystalline microstructure and properties in general.

Acknowledgements

There is a long list of people in and out of NCL whom I wish to acknowledge. The first person who I am deeply thankful to, is my advisor **Dr. Guruswamy Kumaraswamy** (who is a *Guru* in true sense). It was one of the best decisions of my life to join his group. I have always admired his depth in so many different subjects, his passionate but very careful approach towards scientific problems and his practical thought process. I cannot thank him enough for what he has done for me and my fellow researchers.

Next, I would like to thank my Doctoral Advisory Committee members. I have been benefitted by inputs of Dr. Ashish Lele who has an extraordinarily accurate intuition and vast knowledge of diverse scientific tools, methodologies and subjects. I have had long discussions on the subject of fibers and physics of polymeric materials with Dr. Kadhiravan Shanmuganathan that helped me understand the gist of this subject. Dr. Ashish Orpe has always been very kind to entertain me whenever I approached him for discussing mathematical modelling. Dr. B.L.V. Prasad has helped me in polishing this work by asking insightful questions during my presentations and by giving useful feedbacks on the practical issues.

I also thank my co-adviser Dr. Shirish Thakre and our collaborator Aditya Birla Science and technology company for funding my PhD. I thank the members of fibers and textile team at ABSTC – Shailesh, Lalaso, Vivek, Sachin, Kadam for their insights from the processing point of view and for showing interest in my work.

I am thankful to all the course instructors – Dr. Guruswamy Kumaraswamy, Dr. Chetan Gadgil, Dr. Amol Kulkarni, Dr. Pankaj Doshi, Dr. Rajnish Kumar, Dr. Sudip Roy, Dr. Ashish Orpe, Dr. Sarika Bhattacharyya and Dr. Mugdha Gadgil. I have been fortunate to learn variety of subjects from these experts and will be using the learnings throughout my life.

I have been lucky to have made many close friends in NCL, from whom I have learnt about diverse fields of research. I am grateful to Aniket Thosar who was the first person I met after coming to NCL. I admire his truthfulness towards research, his open and strong criticism during our discussions and his passionate attitude towards science. He has been a great roommate, an annoying friend ☺ and a colleague whom I respect a lot. Next person in the list in Anees bhai who cofounded Research Discussions Forum with other members. Anees is a

person with impressive optimism and patience. We have had hours long discussions on science, RDF, politics, philosophy etc. and I have learnt a great deal from him. I am thankful to Sudhakar for handling my aggressive and naive queries with maturity and for being a *friend in need*. I am also thankful to Saurabh Usgaonkar who has always been there for deep discussions and has shown very helping attitude towards me. I am grateful to Arun Torris for extending experimental help. I admire his commitment towards his duties at NCL and his highly professional nature.

I would like to thank the whole team of Research Discussions Forum – Dr. Anuya Nisal. Dr. Anees Khan, Aniket Thosar, Ramendra, Harshal, Karan, Amruta, Karthika, Aniket Gudadhe, Prashant Yadav, Emanuel, Arun, Bipul, Prophesar. I thank Aniket Gudadhe and Prashant Yadav for running this activity for significantly long time and for their efforts to keep it interesting. I have learnt a lot from the sessions of RDF and am glade that we had this kind of forum where we could widen our knowledge in different topics, learn to teach and try to foresee the future needs of scientific and technological research.

Other than above mentioned, I am very thankful to many friends for making this PhD time joyful – Prashant Patil, Dhanalaxami, Nirmalya, Subrajeet, Parul, Neelanshi, Parnashri, Suranjana, Somyajyoti, Muzzammil, Mrityunjay, Rajesh, Jayesh, Varun, Yash, Pratap, Nikhil and all others who I might forget to mention here. My special thanks to Dr. Anuya Nisal for her encouragement, for believing in my capabilities and for tolerating my jokes.

I would like to thank Dr. Khuntia who has inspired me to pursue the field of research. I also thank Mr. Pardeshi for handling the financial issues very smoothly.

In the end, I would like to thank my family. I thank my wife Amruta for being a great friend, colleague and for always extending her support when I needed it most. I admire her inputs and her skill of asking right questions that have helped me refine my work. Being with her, I have learnt so many different subjects that I might have never worked on by myself. I am highly grateful to my father, Vinod Sharma for making me think big, for his modern viewpoints, for his consistence encouragement, guidance and support towards my career. He is a person with superior intellect, incredible positivity, and unimaginable capabilities to simplify a problem –scientific or social. I am grateful to my mother, Sunita Sharma for teaching me management and multitasking skills, for her love and affection towards me and for always keeping my interests above her. It is impossible to express my gratitude towards these people using words.

Contents

List of Figures

List of Tables

Chapter 1.
Introduction

Semicrystalline polymer fibers are an important class of materials. About 300 MT of synthetic polymers are manufactured every year,[1] out of which, about one fourth is spun into fiber form. Synthetic fibers like polyethylene, polyethylene terephthalate etc. are used in making ropes, nets, raincoats, etc. Natural fibers like silk and cellulose find major application in textile industries. The suitability of fibers for specific applications is determined by the fiber properties. For example, the high strength of ultra-high molecular weight polyethylene fibers makes them suitable for demanding heavy weight applications. The fiber properties are governed by structure development during the fiber manufacturing process. A wide variety of processing techniques are used to make fibers. For example, PET fibers are spun in the melt state, silk is produced naturally by silk worms, regenerated cellulose fibers are produced using solvent extrusion technique, etc. These differences in processing methods give rise to different structural features in the fiber morphology. **Figure 1.1** shows the SEM images taken for conventionally produced regenerated cellulose fibers and *B. mori* silk. One can notice that regenerated cellulose fibers exhibit non-uniform surface morphological features whereas silk fibers show uniform surface morphology.
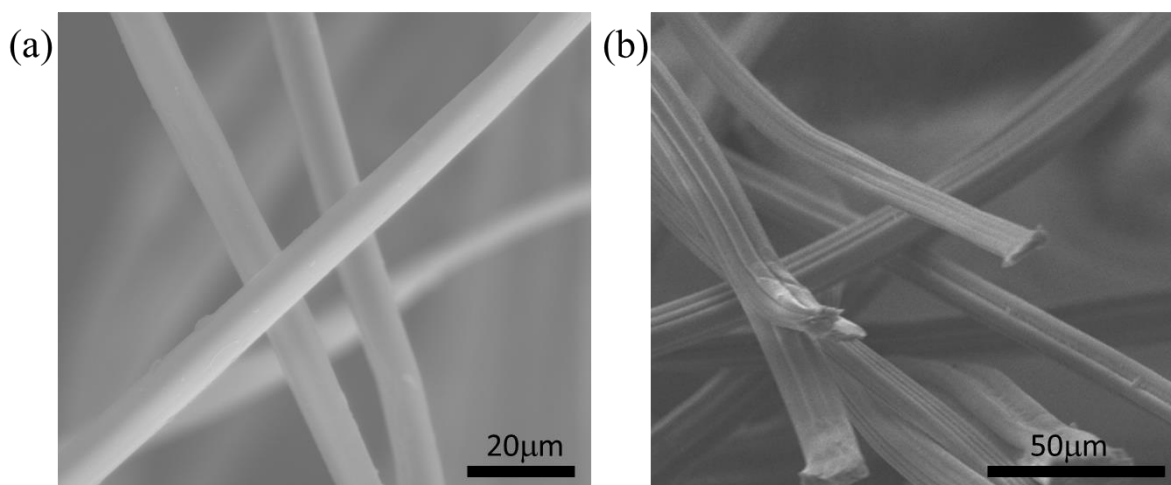
Figure 1.1 SEM images of (a) *B. mori* silk fibers and (b) regenerated cellulose fibers manufactured using Viscose process.

Introduction

1.1 Regenerated cellulose fibers:

The main focus of this thesis is to study structure-property relations in commercial regenerated cellulose fibers. These are bio-derived materials spun into semicrystalline fiber form. Regenerated cellulose fibers are manufactured by dissolving native cellulose obtained from the wood pulp in a solvent and by extruding the so formed "dope" into a non-solvent. There are many processing methods reported for the manufacture of regenerated cellulose fibers,[2–5] that produce fibers with variations in morphology and in properties. Out of these, two processing techniques are chiefly practiced at industrial scale to manufacture regenerated cellulose fibers – these are the Lyocell and Viscose processes. While the Viscose process is the conventional process for manufacture of regenerated cellulose fibers, there are several environmental concerns related to the chemicals used in this process.[2,6] Therefore, there is a strong drive to adopt the Lyocell process, since this process does not use carbon disuphide. However, the fibers produced using the Lyocell process exhibit very different properties as compared to the Viscose fibers. To rationally suggest process changes to obtain desirable properties in regenerated cellulose fibers, it is essential to understand the relation between their structure and the resultant properties. Unfortunately, a detailed quantitative account of structure-property relationship for these fibers is currently lacking. Further, even the appropriate tools and methodologies required for characterization of the important structural features of these fibers is missing. In this thesis, we present a systematic study of the structural characterization of regenerated cellulose fibers and their relation with fiber properties. We also present insights into the relations between these structural differences and the fiber manufacturing process. This could represent a useful starting point for varying process parameters to obtain the fiber structure required for the desired properties. While this thesis is predominantly focused on the study of regenerated cellulose fibers and the development of tools to characterize them, we note that the methodologies developed here could find application to study a wide range of similar systems. In this Chapter, we present a detailed literature survey of the literature on regenerated cellulose fibers: the processes used to manufacture these, fiber structure and properties. We start by presenting details of the manufacturing process for Viscose and Lyocell fibers.

1.1.1 Viscose process:

Viscose fibers, also known as rayon were first made in 1891 and were patented in 1893. The process of preparing rayon starts by dissolving cotton or wood cellulose into

agitated aqueous sodium hydroxide (17-19%) to form sodium cellulosate. This is represented as follows:

$$(C_6H_{10}O_5)_n \quad + \quad nNaOH \quad \rightarrow \quad (C_6H_9O_4ONa)_n \quad + \quad H_2O$$

Cellulose   **Sodium hydroxide**   **Sodium cellulosate**   **Water**
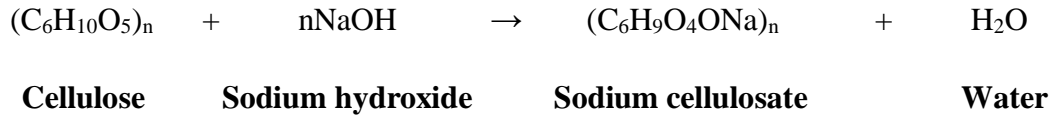
The yellow viscous solution so formed is called alkcell. It is pressed to remove excess alkali and is shredded into smaller pieces. For effective reaction of amorphous as well as the crystalline cellulose domains and to dissolve the short chains, the process is carried out at 45-55°C. At this point, the alkcell viscosity is very high, rendering it difficult to process. Therefore, alkcell is mercerized or pre-aged to decrease the degree of polymerization (DP) from 750-850 to 270-350. This range of DP is low enough so that it is processable and yet sufficiently high to obtain good tensile strength in the fiber. During mercerization, shredded sodium cellulosate is homogenized well at 40-60°C for up to 5 hours.

In the next step, mercerized cellulosate is reacted with CS_2 vapours under vacuum at 25-37°C. This process is carried out for up to 1.5 hours to maximize the reaction extent. The cellulose xanthate so formed is called viscose dope. The reaction is as follows:

$$(C_6H_9O_4ONa)_n \quad + \quad nCS_2 \quad \rightarrow \quad (C_6H_9O_4OCS_2^-Na^+)_n$$

Sodium cellulosate   **Carbon disulphide**   **Sodium cellulose xanthate**

The viscose dope is then aged for even distribution of CS_2 and is filtered for removing particulates. Then, the dope is de-aerated using vacuum and air bubbles are removed to the extent possible. Finally, the dope is extruded through a spinneret into a coagulation bath. In commercial plants, each spinneret has around 30000 – 50000 holes, where each hole has a diameter in a range of 40–60 μm. The coagulation bath contains predominantly sulphuric acid and small concentrations of zinc sulphate and sodium sulphate. Cellulose filaments are regenerated by the neutralization reaction that takes place in the acid bath as follows:

$$2(C_6H_9O_4OCS_2^-Na^+)_n + nH_2SO_4 \quad \rightarrow \quad (C_6H_{10}O_5)_n \quad + \quad nNa_2SO_4 \quad + \quad 2nCS_2$$
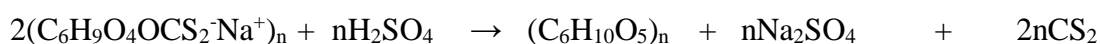
Sodium cellulose   **Sulphuric acid**   **Cellulose**   **Sodium sulphate**   **Carbon disulphide**
xanthate

Cellulose filaments are stretched at high draw ratios using rollers to achieve the desired properties. Finally, the fibers are washed to remove solvents and are dried.

1.1.2 Lyocell process:

The first pilot plant for the Lyocell process was established in 1983 and the process was commercialized in 1984. In this process, cellulose pulp is dissolved in aqueous N-methyl morpholine-N-oxide (NMMO). NMMO can easily hydrogen bond with cellulose due to its N-O dipoles therefore, replacing intermolecular and intramolecular hydrogen bonds. However, there is a small region in the ternary phase of water, NMMO and cellulose shown by the shaded region in **Figure 1.2**, where cellulose is efficiently dissolved. The temperature of this dissolution is in the range 90-120°C.
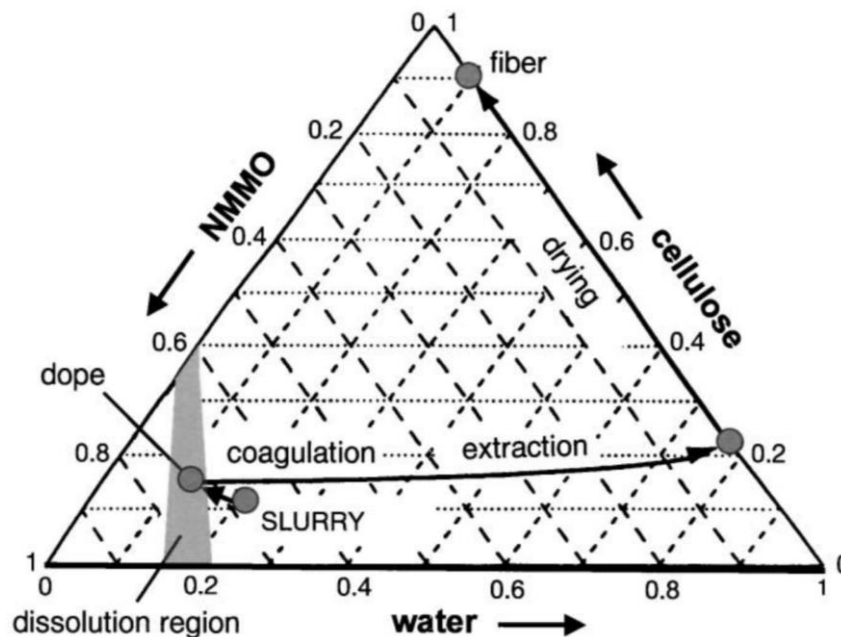
Figure 1.2 Ternary phase diagram of Cellulose-NMMO-Water. *Reused with permission from reference[7] Copyright (2001) Elsevier.*

The DP of cellulose in the brownish cellulose dope formed by dissolution in NMMO is 500-600. This dope is then filtered for removing any impurities before extruding using spinnerets.

The spinning process of Lyocell fibers is called dry jet-wet spinning process. During the spinning step, dope is extruded through tiny holes of spinnerets. An air gap is present just after the spinnerets such that air is blown on the fibers as they are extruded out of the spinneret and before the non solvent bath. This air gap is critical to the fiber properties. It has been found that the air gap length governs the strength and the orientation properties of the final fiber.[6] After the air gap, filaments are introduced to the spinning bath containing water as a non-solvent. As represented in the **Figure 1.2**, water extracts the NMMO out of the cellulose filaments and the cellulose fibers thus formed are stretched, washed and dried.

Draw ratios in the range of 4-20 are usually used.[2] It is reported that the amount of solvent recovered in Lyocell process is > 99% which makes it considerably more efficient than the Viscose process in which about 70-75% of CS_2 is recovered.

1.2 Comparison of Lyocell and Viscose processes:

Lyocell and Viscose processes are different in many aspects. Here we list down the major differences in the processes that are known to critically affect the fiber properties.

- The first difference is in the type of solvents used. Due to different solvents, Viscose process involves reaction of cellulose to form a base and the regeneration takes placed by acid base neutralization reaction. On the other hand, regeneration of Lyocell occurs by solvent extraction process, which involves few, if any, side reactions.

- Degree of polymerization of cellulose is higher in Lyocell dope than the Viscose dope. This is reported to provide higher strength to the final fiber form in Lyocell process.[6]

- Another major difference between Lyocell and Viscose is the processing temperature. Lyocell spinning is carried out at elevated temperatures as compared to Viscose.

- A crucial factor that makes two fibers very different from each other is the type of spinning. Viscose is a wet spinning process where the extruded filaments are regenerated by spinning into the coagulation bath. Therefore, the filaments do not get enough time to crystallize and orient[6] whereas, Lyocell is a dry jet-wet spinning process in which before regeneration, the extruded filaments are passed through an air gap in which fibers get well oriented and achieve higher strengths.

Differences in the manufacturing processes of Lyocell and Viscose fibers, as summarized briefly here, cause the fibers to attain different structural features and different properties. The specifics of how various process parameters affect fiber structure is not completely understood at this point. However, there are some reports in the literature that elucidate differences in structural features for these fibers and the consequent variation in properties. We discuss structural and property differences in Lyocell and Viscose fibers in the next sections.

1.3 Structural differences in Lyocell and Viscose fibers:

Fiber microstructure develops at multiple length scales during the manufacturing process. It is well known that the cellulose fibers exhibit hierarchical structure present at various length scales as shown schematically in **Figure 1.3**.

$\sim O\,(\text{Å}) \qquad \sim O\,(10\ \text{nm}) \qquad \sim O\,(\mu m) \qquad \sim O\,(\text{cm})$
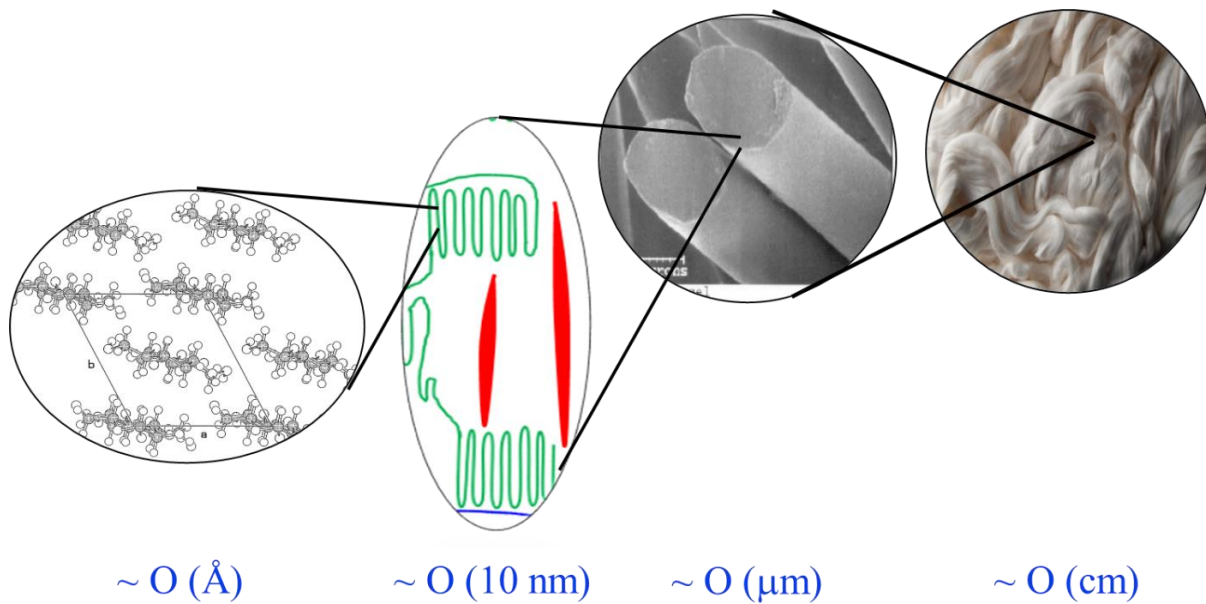
Figure 1.3 Hierarchical structure of regenerated cellulose fibers with representation of different features at each length scale. At ∼ O (μm) – SEM of single fibers, at ∼ O (10 nm) – schematic of microvoids (red streaks) and crystalline lamellae (green chain folded regions) and at ∼ O (Å) unit cell structure of regenerated cellulose. *Parts of figure are reused with permission from references*[2,8] *Copyright (2001) Elsevier*

In the next section, we discuss the structural features at each of these length scales and the differences in Lyocell and Viscose fibers, as reported in the literature.

1.3.1   *Micron (μm) length scale:*

Viscose and Lyocell fibers exhibit differences in surface morphologies and in the shape of the fiber cross section and, variations across the fiber length and in the radial direction etc. **Figure 1.4** shows SEM images of Viscose and Lyocell fibers. It is clearly observed that Viscose fibers exhibit a non-uniform surface morphology with an irregular cross section. On the other hand, Lyocell fibers show a uniform surface with a regular and more circular cross section than the Viscose fibers.
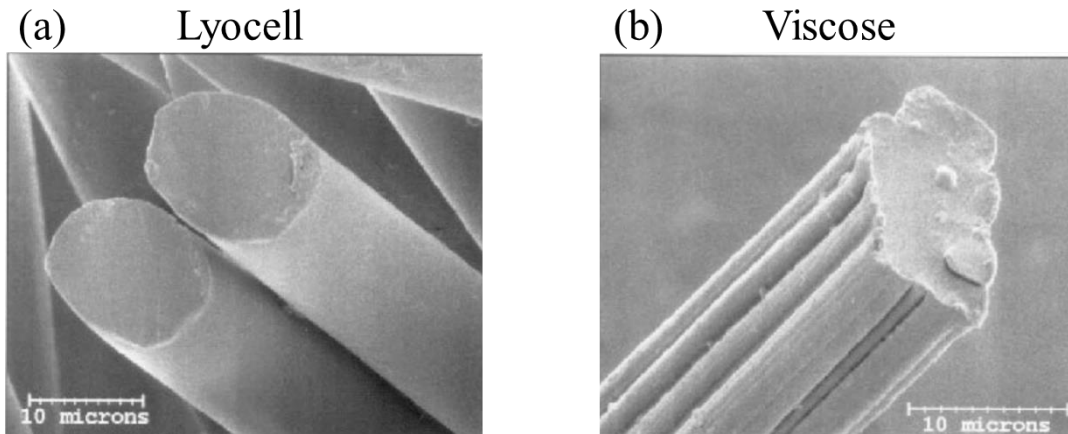
(a)   Lyocell   (b)   Viscose

Figure 1.4 SEM images of Lyocell and Viscose fibers. *Reused with permission from reference[2] Copyright (2001) Elsevier*

Other than the differences in the surface morphology, Lyocell and Viscose fibers also show radial differences across fiber cross section that are not apparent in the SEM images. Several research groups have reported dye uptake studies that show that Viscose fibers possess a skin-core structure. Abu-Rous et. al[9] have studied diffusion of Uvitex BHT dye across the thin fiber cross section with time as shown in **Figure 1.5**. They have shown that the dye penetration is restricted to the skin of Viscose fiber cross sections whereas, for Lyocell, dye keeps diffusing into the core at a constant rate until finally the whole cross section is stained. Therefore, radial variation across the cross section is not observed in Lyocell fibers. Using X-ray diffraction studies it has been shown that the skin of Viscose fibers contains smaller crystallites that have higher orientation than the core.[10,11] Morehead et. al. has systematically studied and listed the process parameters that affect the skin formation in Viscose fibers.[10] For example, they have shown that skin thickness increases with increase in cellulose concentration in the dope, by decreasing the ageing time, by increasing the ion concentration in the bath etc.
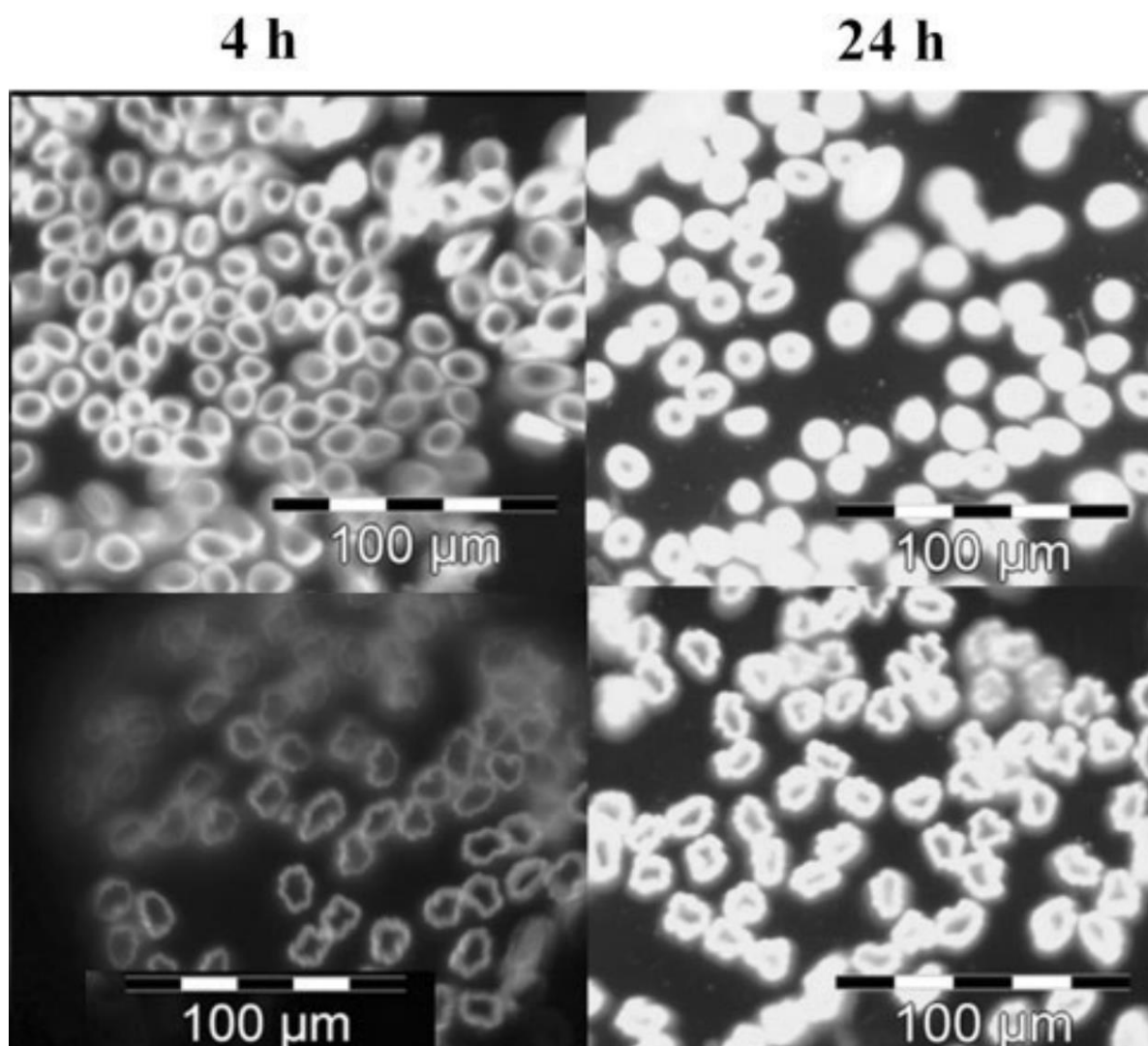
Figure 1.5 Diffusion of dye in Lyocell (top) and Viscose (bottom) cross sections observed at two time scales – after 4hrs and 24 hrs. *Reused with permission from reference*[9] *Copyright (2007) John Wiley and Sons*

1.3.2 Nanometer (nm) length scale:

Figure 1.3 shows the schematic of the structural features like microvoids and crystal/amorphous phases at nm length scales. The conventional tools to study these features are transmission electron microscopy (TEM), small angle X-ray and neutron scattering (SAXS/SANS). There are several reports that use these techniques to reveal the presence of fibrils, microvoids etc. We now discuss these reports in detail.

A typical SAXS pattern from regenerated cellulose fibers reported by Jiang et. al.[12] is shown in **Figure 1.6**. Ruland described this kind of scattering as fan like pattern.[13] He claimed that this kind of scattering originates from microvoids elongated in the fiber

direction. Using the spread of intensities in the azimuthal plan, he proposed a method to calculate the average misorientation and average length of the microvoids. Later this method was extensively used by many other research groups. Jiang et. al. used this method to compare the average length and the misorientation of microvoids in Viscose, modified Viscose, Lyocell and fibers manufactured using ionic liquids as solvents.[12] They showed that the Viscose fibers possess longest microvoids with highest misorientation.
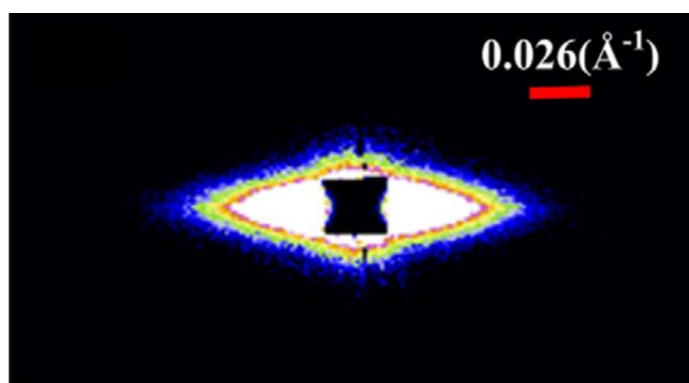
Figure 1.6 2D SAXS pattern for regenerated cellulose fibers *Reused with permission from reference[12] Copyright (2012) Elsevier*

To obtain the radii of microvoids, Jiang et. al.[12] plotted the intensities in the horizontal plane as a Guinier plot and resolved the scattering curve into successive tangents as shown in **Figure 1.7**. Accordingly, for circular cross section of microvoids. the intensity, I, depends on the average radius (R) of the scatterer as:

$$I = I(0) \, \exp(\frac{-q^2R^2}{4})$$

1.1

where, q is the scattering vector that depends on scattering angle (2θ) and wavelength of incident X-rays (λ) as q = 4πsin(θ)/λ) and I(0) is intensity at q = 0 nm^{-1}.

Using this method, they showed that there is no significant difference in microvoid radii between Lyocell and Viscose fibers. Therefore, according to their analysis, differences in the manufacturing process do not affect the microvoid radii. The same research group studied the effect of spinning speed on the microvoid size, measured using the aforementioned method.[14] They showed that on increasing spinning speed, the average microvoid length increases and average misorientation decreases. They also showed that the average radius of the microvoid cross section decreases on increasing the spinning speed during the process.
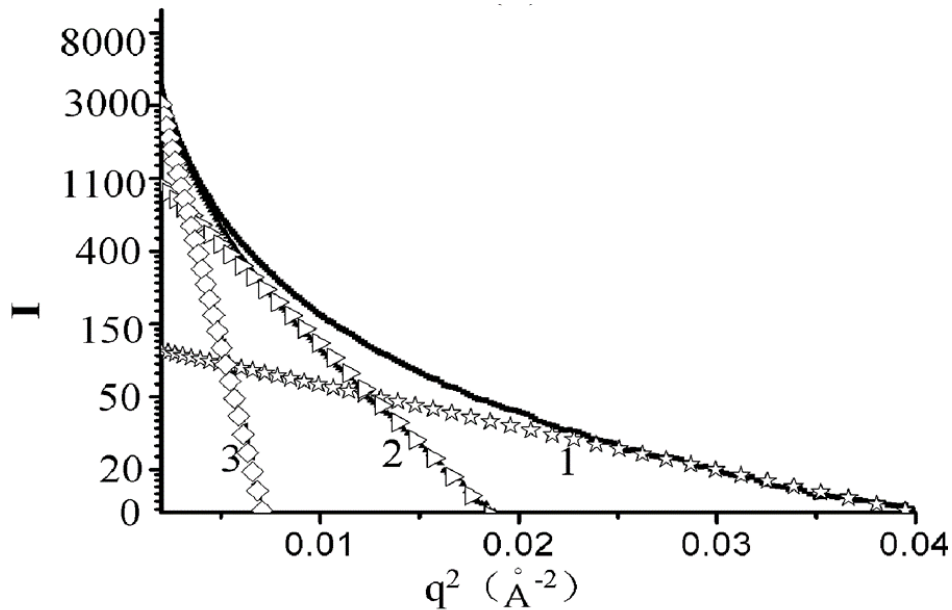
Figure 1.7 Guinier plot of intensities in the horizontal direction with successive tangents. *Reused with permission from reference*[12] *Copyright (2012) Elsevier*

Crawshaw et. al. have investigated the effect of drying on the chord length, radius of gyration, mean cross-section and volume fraction of microvoids in regenerated cellulose fibers.[15] They demonstrated that the average microvoid size consistently increases with drying the water swollen fiber and the void volume fraction decreases. They stated that, on drying, smaller microvoids close up, leading to a decrease in void volume fraction. Schurz et. al. investigated microvoid structure using the scattering invariant and obtained the average chord length and the microvoid volume fraction.[16] They claimed that elongated and well oriented microvoids might be responsible for superior mechanical properties of Lyocell fibers. Fischer et. al. performed small angle neutron scattering on selectively deuterated regenerated cellulose fibers to obtain the fibril dimensions using equation 1.[17]

The use of Guinier analysis to interpret the small angle scattering data, as reported in the literature, is valid only at sufficiently low q such that qR < 1. For uniaxially elongated microvoids, this should result in the scattered intensity, I scaling as q^{-1}. We note that the experimental data does not show this, calling the analysis in the literature into question. We elaborate on this point in Chapter 5 and demonstrate that the microvoid radii reported in the literature are incorrect.

Other than scattering experiments, transmission electron microscopy has been used to study the structure at nm length scales. Abu-Rous and co-workers[18] used the solvent exchange

technique to insert isoprene in the regenerated cellulose fibers swollen with water at first and then with acetone. Isoprene was polymerized inside the fibers and was stained with osmium tetraoxide. The microtomed cross sections of such samples were observed under TEM. They showed that Lyocell fibers exhibit a porous layer on the outer side of the cross section (**Figure 1.8**). In contrast, Viscose fibers showed pores throughout the cross section, characterized by a wide size distribution. Therefore, there are significant differences in the pore structure of swollen Lyocell and Viscose fibers that have been reported in the literature.
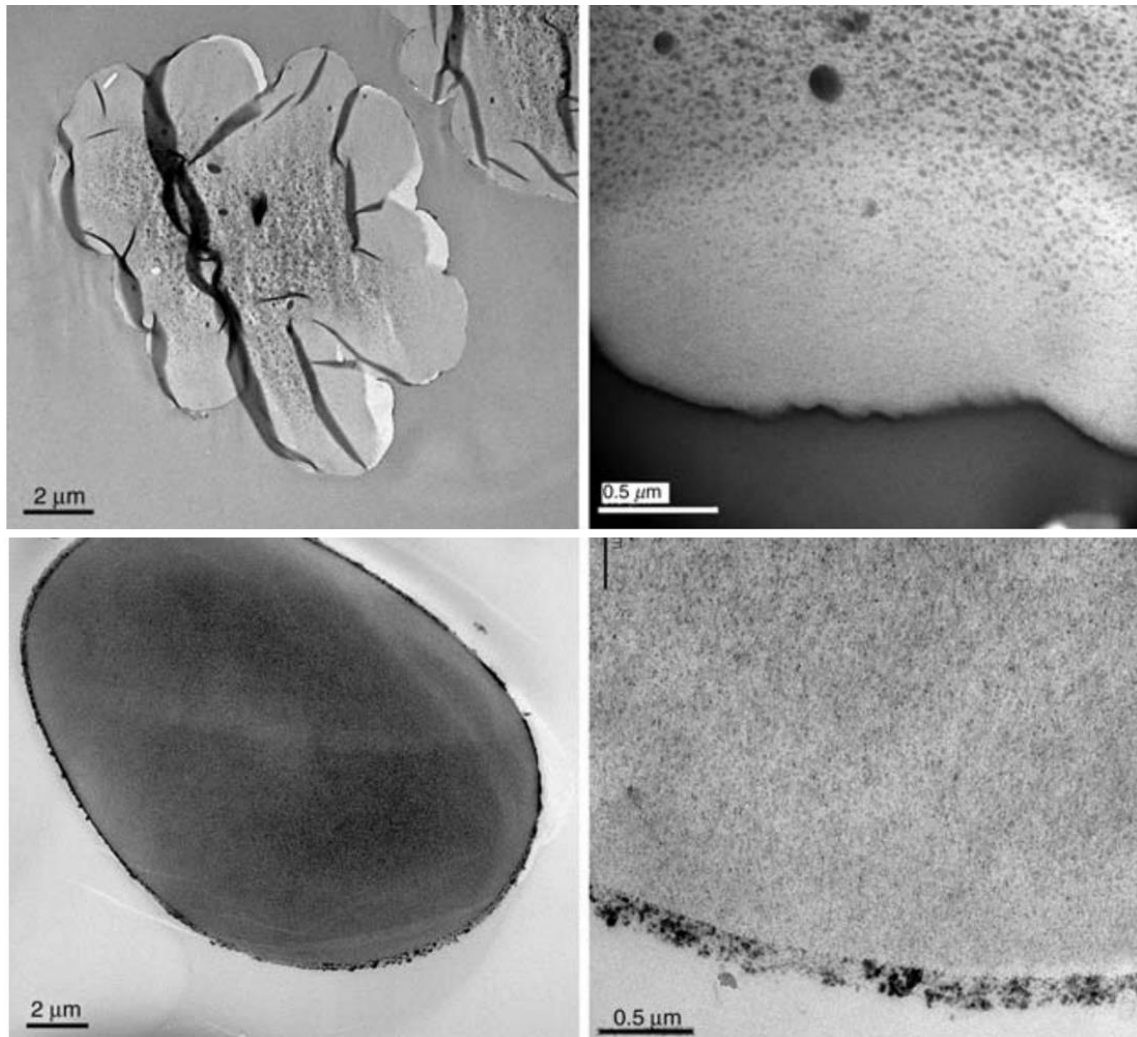
Figure 1.8 TEM images of stained cross section of Viscose (top) and Lyocell (bottom) fibers showing distribution of pores as black regions. *Reused with permission from reference*[18] *Copyright (2006) Springer Nature*

We note here that the pore structure shown in **Figure 1.8** has been obtained for swollen fibers and it is not clear how this relates to the microvoid structure in dry fibers.

1.3.3   Angstroms (Å) length scale:

As shown in **Figure 1.3**, at angstrom length scales, the unit cell structure of the cellulose crystal characterizes fiber structure. Wide angle X-ray diffraction is a widely used tool to study the unit cell structure of regenerated cellulose fibers. 2D WAXD pattern from regenerated cellulose fibers is shown in **Figure 1.9**.[19] Zugenmaier has summarized in his review that there are four major categories of cellulose allomorphs and regenerated cellulose fibers fall in the cellulose II category.[8] Two cellulose chains run antiparallel to form a monoclinic unit cell in regenerated cellulose fibers. The lattice parameter values for regenerated cellulose fibers, as reported by Kolpak et. al.[20] are a = 8.01 Å, b = 9.04 Å, c = 10.36 and γ = 117.1°. However, we note here that the values of lattice parameters reported in the literature vary over quite a significant range.[8,21,22]
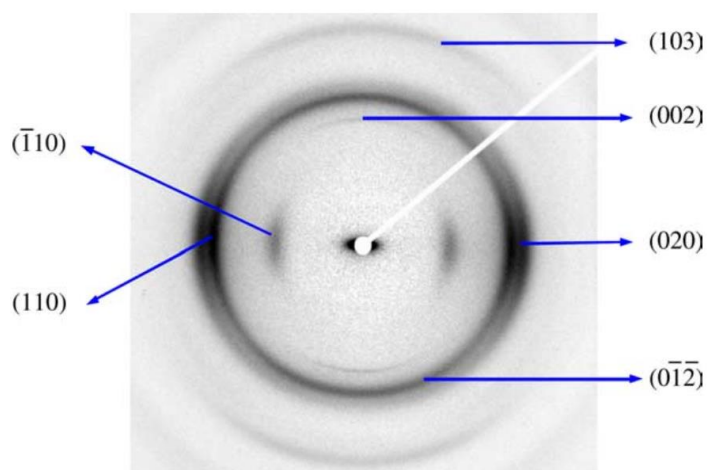
Figure 1.9 2D WAXD pattern of regenerated cellulose fibers. *Reused with permission from reference[19] Copyright (2006) Elsevier*

Figure 1.10 shows a 1D WAXD pattern of regenerated cellulose fibers,[19] showing scattering peaks from the crystalline regions on an amorphous halo. Various research groups have studied the WAXD pattern of Viscose and Lyocell fibers and obtained percentage crystallinity.[12,14,23–27] Again, a wide range of crystallinity values have been reported for these fibers varying from 15.5% to 74%. However, it is consistently observed that Lyocell fibers exhibit higher crystallinity than Viscose fibers.[12,14,24–27] Jiang et. al. have correlated the higher modulus and strength of Lyocell fibers with their higher crystallinity and smaller crystal size.[12]
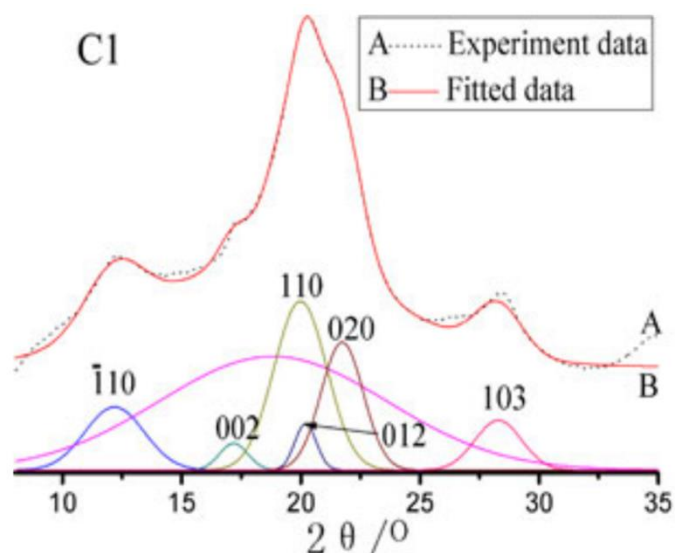
Figure 1.10 1D WAXD pattern of regenerated cellulose fibers with peaks fitted. *Reused with permission from reference[14] Copyright (2012) Springer Nature*

The 2D WAXD pattern in **Figure 1.9** indicates the oriented nature of crystalline units in regenerated cellulose fiber. A widely used method to quantify orientation of uniaxially oriented crystalline phase in literature is to calculate the Hermans orientation parameter.[28,29] It has been shown that Lyocell fibers exhibit higher crystalline orientation than Viscose fibers. Zhang et. al. reported that the major reason behind higher crystalline fraction and higher crystalline orientation of Lyocell fibers is the presence of an air gap during dry jet-wet processing of Lyocell.[6] Due to this air gap, cellulose chains orient and crystallize before the coagulation bath. Other than crystalline orientation, amorphous phase orientation has also been investigated by many groups using birefringence measurements.[12,14,30] It has been shown that the amorphous phase of cellulose fibers also exhibits orientation along with the crystalline phase. The amorphous phase has a higher orientation in case of Lyocell fibers as compared to Viscose fibers.[12,30] Jiang et. al. showed that percentage crystallinity, crystalline and amorphous orientations increase with increase in the spinning speed.[14]

A complete structural elucidation of regenerated cellulose fibers involves many other features including the details of the fibrillar structure, the hydrogen bonding network, etc. Here, we restrict our discussion to the features that are relevant for the current work. In summary, the aforementioned discussion demonstrates that regenerated cellulose fibers are characterized by a complicated hierarchical structure that develops differently in Viscose and Lyocell fibers. These differences in the structural features lead to differences in the properties of fibers. Next, we discuss the properties of regenerated cellulose fibers in detail along with

the literature on the differences in Viscose and Lyocell fibers, and the structural origin of these differences.

1.4 Properties of regenerated cellulose fibers:

1.4.1 Mechanical response:

The mechanical properties of regenerated cellulose fibers depend on their structure, and therefore, on the process of manufacture. There are several reports on the mechanical measurements on cellulose fibers and comparisons between Viscose and Lyocell fibers have also been reported. **Figure 1.11** shows a typical stress vs. strain response from regenerated cellulose fibers manufactured using Lyocell and Viscose processes. For both fibers, the stress increases linearly up to a strain of about 1% and beyond that the slope of stress strain curve decreases. On stretching further, the slope remains constant till the fibers fail. The kink at 1% strain has been reported in the literature as the yield point. As shown in **Figure 1.11**, Lyocell fibers have higher modulus than the Viscose fibers. Lyocell fibers also exhibit higher strength as compared to the Viscose fibers. However, the strain at which Lyocell fibers break is lower than the Viscose fibers. Kong et. al. have studied the effect of draw ratio on the stress strain reponse.[31] They showed that with increase in draw ratio, the modulus of fibers increases and the strain at break decreases.
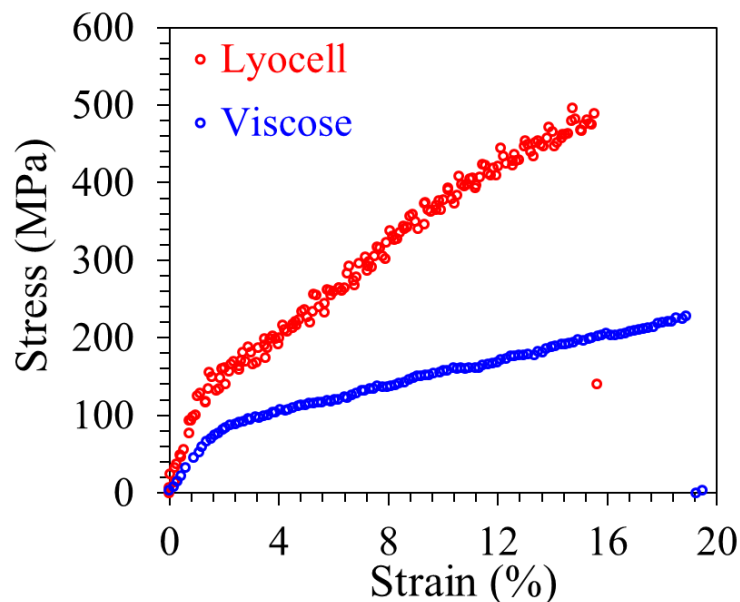
Figure 1.11 Stress vs strain data for regenerated cellulose fibers manufactured using Lyocell and Viscose processes.

It has been reported that the higher crystallinity of Lyocell fibers is responsible for its higher modulus.[6]

1.4.2 Cyclic loading/unloading:

Elasticity and plasticity of regenerated cellulose fibers have been tested by performing cyclic loading and unloading experiments. Gindl et. al. have reported that on stretching both Viscose and Lyocell fibers, an elastic linear region is observed for strains below kink strain.[32] **Figure 1.12** shows the cyclic loading/unloading response for Viscose and Lyocell fibers. Here, a single fiber is stretched to different increasing strain in each cycle, beyond kink. It could be seen that in each cycle, the strain at which the slope of stress strain curve decreases, changes to a new value. For both fibers, there is an increase in the elastic region in subsequent cycles when stretched beyond the kink. They have claimed that with each cycle, the elastic modulus of both fibers increases which is known as strain hardening. They have also reported that the strain hardening is more pronounces in case of Lyocell fibers than the Viscose fibers.
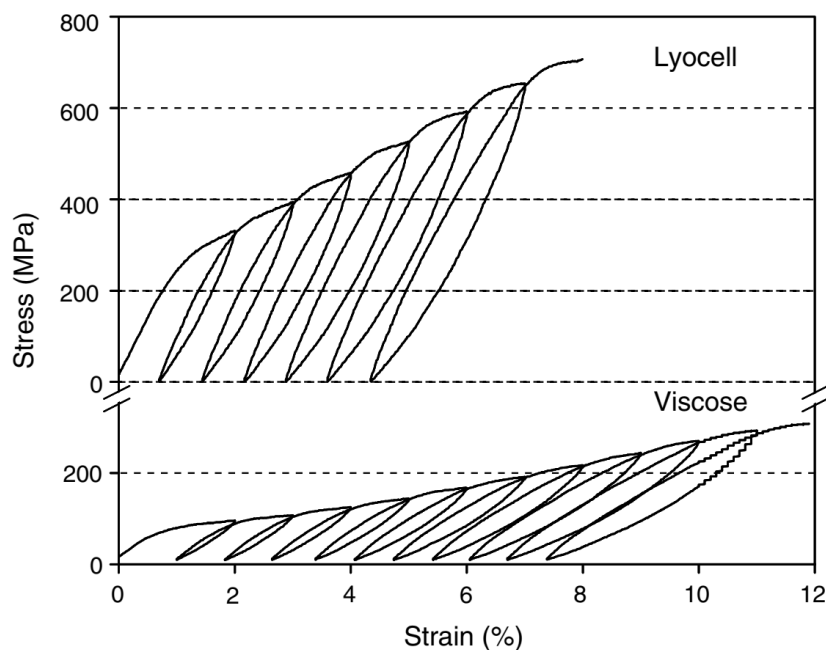
Figure 1.12 Cyclic loading/unloading data for Lyocell and Viscose fibers with increasing strain in each cycle. *Reused with permission from reference*[32] *Copyright (2006) Elsevier*

Meredith also performed cyclic loading/unloading experiments on Viscose Rayon fibers.[33] He showed that when the fiber is unloaded to zero strain after stretching beyond the kink strain, some fraction of strain is recovered. Therefore, along with the plastic deformation, some elastic recovery is also observed.

1.4.3 Stress relaxation:

Stress relaxation experiments on regenerated cellulose fibers have been reported in literature. In these experiments, a fiber is stretched to a particular strain value and is held at that strain for long time. Yamaguchi et. al.[34] and Meredith[35] performed stress relaxation experiments on Viscose Rayon fibers. Yamaguchi et. al. showed that the stress relaxes as a power law in time for regenerated cellulose fibers. **Figure 1.13** shows the stress relaxation moduli plotted against time for fibers stretched to different strains. It could be observed that the rate of stress relaxation is independent of the strain to which is the fiber is stretched. They fitted the stress relaxation data with a power law dependence of stress on time as shown in **Figure 1.13**. They showed that as compared to polyester and nylon fibers, stress relaxes faster for regenerated cellulose fibers. However, to the best of our knowledge, comparison of stress relaxation between Lyocell and Viscose fibers has not been thoroughly studied in literature.
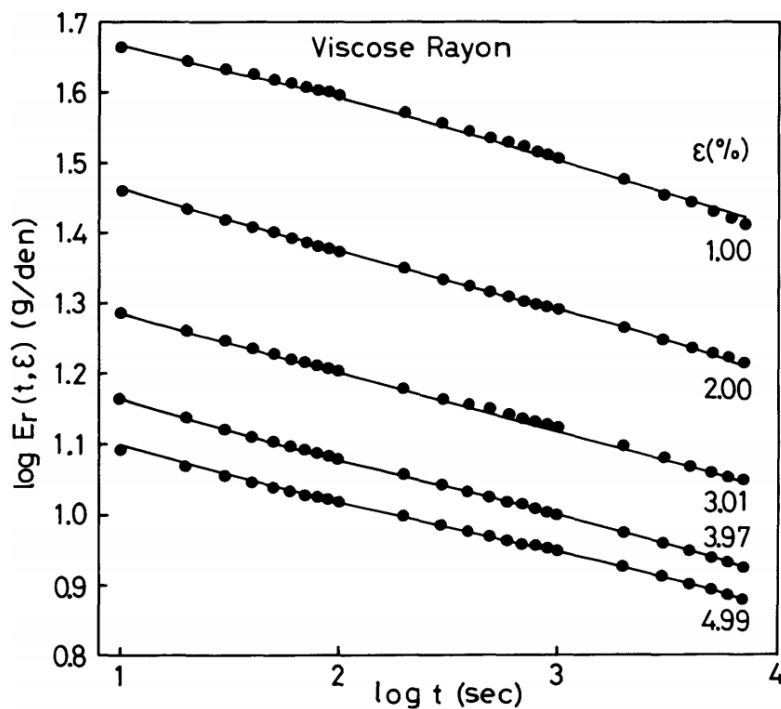
Figure 1.13 Stress relaxation data for Viscose Rayon fibers obtained at different strain. *Reused with permission from reference*[34] *Copyright (1981) The Textile Machinery Society of Japan*

1.4.4 Fibrillation:

Fibrillation is a phenomenon that is especially pronounced for Lyocell fibers. During this, the filaments of fiber start splitting apart as shown in **Figure 1.14** when the fiber is soaked in

water and subjected to mechanical shear. It is reported that Viscose fibers are not as prone to fibrillation as Lyocell fibers. Fibrillation is undesirable because the fibers lose their good wash and wear properties. There have been many attempts to solve the fibrillation problem in Lyocell fibers. Researchers have tried treatment with alkali, cross linking agents, etc. to reduce fibrillation.[36,37] Some models also have been proposed to explain the mechanism of fibrillation based on the parallel fibrillar structure of Lyocell fibers.[38] However, the exact reason behind fibrillation is not fully understood and more research needs to be done to understand and address this problem.
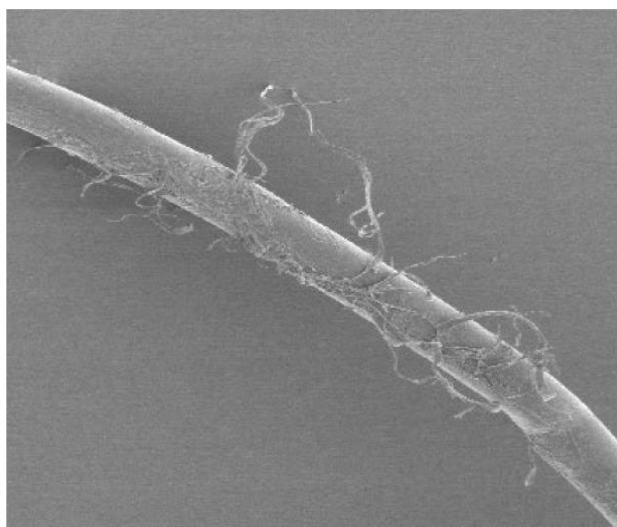
Figure 1.14 Fibrillation of Lyocell fibers in wet state. *Reused with permission from reference[2] Copyright (2001) Elsevier.*

1.4.5   Sorption and swelling properties:

The effect of water on regenerated cellulose fibers has been studied by various research groups. Water forms hydrogen bonds with cellulose and is capable of disrupting intra and inter chain hydrogen bonding in cellulose. Several reports compare the sorption behaviour of Lyocell and Viscose fiber[25,39,40] and it has been shown that Lyocell fibers absorb less moisture than the Viscose fibers. This has been attributed to the greater number of free –OH bonds present in Viscose fibers due to their low crystallinity. Also, Viscose fibers swell more than the Lyocell fibers when soaked in aqueous medium.

1.5   Structure property relationships:

We have discussed the structure and the properties of regenerated cellulose fibers manufactured using Viscose and Lyocell techniques. Now we discuss the literature relating the fiber properties to structure. It is clear from that the dependence of properties of cellulose

fibres on structure is not fully understood. Complications arise from the hierarchical organization of structure in regenerated cellulose fibers. Due to the presence of different structural features at each length scale, relating properties to structure unambiguously is extremely difficult. Although there are some literature reports that attempt to relate properties to structure, robust structure property relations remain elusive. Here we discuss the current literature regarding the dependence of properties on structure.

There are several reports on structure property relationships in regenerated cellulose fibers.[3,7,12,14,30,41–45] Kong et. al. studied the effect of domain orientation on the mechanical properties of regenerated cellulose fibers.[46] They showed using WAXD that the fibers with lower orientation show a rapid increase in orientation on stretching whereas fibers with higher domain orientation show a slower increase and undergo less reorientation. They reported that fibers with higher crystal orientation show high tensile modulus and proposed a model to relate the crystal shear stress to orientation. Many other reports also show that the tensile modulus increases with increase in crystalline orientation.[3,14,30] Jiang et. al. studied different regenerated cellulose fibers with variations in the crystallinity and crystalline orientation.[12,14] They showed that fibers with higher crystallinity exhibit higher modulus. Kong et al. showed that fibers with higher crystalline orientation fail at a lower strain.[47] Lenz et. al. investigated the origin of fibrillation and reported that the fibrillation of Lyocell fibers increases with increase in crystalline orientation.[30]

Zhang et. al. used mechanical models to fit the stress strain curve for regenerated cellulose fibers in dry and wet state.[48] Based on these models, they propose that the change in fiber properties on wetting arise from wetting-induced changes in the crystallinity and hydrogen bonded structure. Meredith and Haughton et. al. used reaction rate theory to obtain activation energies from the stress relaxation of regenerated cellulose fibers.[35,49] Haughton et. al showed that a bimodal distribution of activation energies is required to explain the relaxation and attribute the relaxation to the motion of glucose rings. Meredith also proposed a spring dashpot combination to explain the stress relaxation response.

As discussed above, there are several reports that study the dependence of properties on various structural features in regenerated cellulose fibers. Based on these results, some qualitative relations have been proposed. However, none of these studies is able to clearly establish quantitative structure-property links for regenerated cellulose fibers. Further, the models that have been employed in the literature are incapable of identifying the relevant

structural attribute that governs specific properties. Therefore, there is insufficient understanding on the subject of structure-property relations in regenerated cellulose fibers.

1.6 Objective of thesis:

Transitioning from Viscose to Lyocell process is important due to the lower environmental footprint of the Lyocell process. However, as the fibers obtained from Viscose and Lyocell processes exhibit differences in properties, it is important to understand the structural underpinning of the fiber properties to allow rational manipulation of structure by varying processing conditions. However, the current literature does not provide robust structure-property relations for regenerated cellulose fibers. Additionally, literature studies report inconsistent and, in some cases, incorrect structural data for cellulose fibers. Due to the structural complexity, in some cases, the appropriate tools to quantify structural features are not available. Therefore, one of the major objectives of this thesis is to present an elegant set of complementary experimental methodologies and analytical tools to accurately quantify various structural features in Viscose and Lyocell fibers at different length scales. Another objective is to identify the relevant structural features that govern different properties of these fibers. We establish structure-property relation for regenerated cellulose fibers and compare the properties and the structure of Viscose and Lyocell fibers. Specifically, we focus on mechanical properties of the fibers. Using wide angle, small angle and medium resolution small angle scattering, we develop methodologies to characterize microstructural features. Models are developed to relate these features to the properties and to identify the differences in Viscose and Lyocell fibers.

1.7 Outline of the thesis:

Chapter 1: This chapter presents the relevant literature on the subject of regenerated cellulose fibers and the gaps present in literature. We present our motivation for this work and summarize the approach adopted.

Chapter 2: We investigate the linear region mechanical response for a variety of semicrystalline fibers with glassy amorphous phase e.g. silk, regenerated cellulose, polyethylene terephthalate and polyacrylonitrile in different experiments. Response from these experiments is fitted using a simple phenomenological model. The model parameters are related to the structural features present at angstrom length scale using wide angle x ray diffraction. Briefly, we obtain crystalline and amorphous phase moduli from in-situ WAXD experiments during mechanical deformation and compare the values to the model parameters.

Introduction

The viscous dissipative response is related to the sub T_g relaxations in these systems. We show that the model predicts counterintuitive microstructural response for these fibers, that we validate using other experimental techniques. A major finding of this work is that the linear region mechanical response in semicrystalline polymer fibers with glassy amorphous phase is governed only by crystal-amorphous coexistence and other structural details at higher length scales are not relevant. This work presents quantitative structure-property relations for polymer fibers in the form of a simple model.

Chapter 3: We show that Viscose and Lyocell fibers exhibit qualitatively similar (but quantitatively different) response in mechanical experiments. We use the model developed in Chapter 2 to fit data from Viscose and Lyocell fibers. The fit parameters relate to structural features. Hence, by comparing the model parameters for Viscose and Lyocell fiber, we study the origin of quantitative difference in properties of these two fibers. On stretching the fibers beyond a particular strain, there is a transition in the slope of stress/strain response. This transition has been reported as yielding in the literature. We show that this transition is actually an apparent yield and the apparent plastic deformation observed on stretching the fibers beyond this point is, in fact, recoverable. We also show that this apparent yield point could be shifted to a new value by stretching the fiber. On wetting the Viscose and Lyocell fibers, there is an increase in the apparent yield point of Viscose fibers whereas for Lyocell fibers, there is no change. We describe the wet state behaviour of these fibers based on water absorption experiments.

Chapter 4: We perform in-situ WAXD and birefringence experiments on Viscose and Lyocell fibers during stretching and stress relaxation. We describe the effect of these deformation experiments on the crystalline and amorphous phase orientations. Crystal orientation does not change during stress relaxation whereas the amorphous phase orientation increases on holding the fibers at a constant strain. We also demonstrate the effect of water on the response of structure. Combined results from WAXD, birefringence and relaxation experiments show that, in water soaked condition, the crystalline phase does not get strained on stretching the fibers. Also, wetting reverses the trend of relaxation rates for Viscose and Lyocell fibers.

Chapter 5: We study the microvoid structure of Viscose and Lyocell fibers at O~(10-100 nm). We perform small angle X-ray scattering and medium resolution neutron scattering experiments on Lyocell and Viscose fibers in dry state. We show that the scattering arises

primarily from the elongated microvoids, oriented in the fiber direction. We demonstrate that the analyses of small angle scattering presented in the literature for cellulose fibers is erroneous. We show that medium small angle data is essential to obtain the microvoid size distribution and propose a methodology for analysing the scattering data. Our analysis gives information on the average microvoids length, radius, misorientation and the distribution of microvoid radii. We show that Lyocell fibers possess bigger microvoids than the Viscose fibers, which may relate to the mechanism of failure of Lyocell fibers.

Chapter 6: This chapter presents a summary of the work in this thesis and the scope for the future work on this subject.

1.8   References:

(1)   Geyer, R.; Jambeck, J. R.; Law, K. L. Production , Use , and Fate of All Plastics Ever Made. *Sci. Adv.* **2017**, *3* (7), e1700782.

(2)   Woodings, C. *Regenerated Cellulose Fibres*; Woodhead Publishing Limited, 2001.

(3)   Cai, J.; Zhang, L.; Zhou, J.; Qi, H.; Chen, H.; Kondo, T.; Chen, X.; Chu, B. Multifilament Fibers Based on Dissolution of Cellulose in NaOH/Urea Aqueous Solution: Structure and Properties. *Adv. Mater.* **2007**, *47* (22), 8676–8683.

(4)   Chen, J. H.; Guan, Y.; Wang, K.; Xu, F.; Sun, R. C. Regenerated Cellulose Fibers Prepared from Wheat Straw with Different Solvents. *Macromol. Mater. Eng.* **2015**, *300* (8), 793–801.

(5)   Li, X.; Li, N.; Xu, J.; Duan, X.; Sun, Y.; Zhao, Q. Cellulose Fibers from Cellulose/1-Ethyl-3-Methylimidazolium Acetate Solution by Wet Spinning with Increasing Spinning Speeds. *J. Appl. Polym. Sci.* **2014**, *131* (9), 1–9.

(6)   Zhang, S.; Chen, C.; Duan, C.; Hu, H.; Li, H. Regenerated Cellulose by the Lyocell Process , a Brief Review of the Process and Properties. *BioResources* **2018**, *13(2)*, 4577–4592.

(7)   Fink, H. P.; Weigel, P.; Purz, H. J.; Ganster, J. Structure Formation of Regenerated Cellulose Materials from NMMO-Solutions. *Prog. Polym. Sci.* **2001**, *26* (9), 1473–1524.

(8)   Zugenmaier, P. Conformation and Packing of Various Crystalline Cellulose Fibers.

Prog. Polym. Sci. **2001**, *26* (9), 1341–1417.

(9)   Abu-Rous, M.; Varga, K.; Bechtold, T.; Schuster, K. C. A New Method to Visualize and Characterize the Pore Structure of TENCEL (Lyocell) and Other Man-Made Cellulosic Fibres Using a Fluorescent Dye Molecular Probe. *J. Appl. Polym. Sci.* **2007**, *106* (3), 2083–2091.

(10)   Morehead, F. F.; Sisson, W. A. Skin Effect in Viscose Rayon. *Text. Res. J.* **1945**, *15*, 443–450.

(11)   Müller, M.; Riekel, C.; Vuong, R.; Chanzy, H. Skin/Core Micro-Structure in Viscose Rayon Fibres Analysed by X-Ray Microbeam and Electron Diffraction Mapping. *Polymer.* **2000**, *41* (7), 2627–2632.

(12)   Jiang, G.; Huang, W.; Li, L.; Wang, X.; Pang, F.; Zhang, Y.; Wang, H. Structure and Properties of Regenerated Cellulose Fibers from Different Technology Processes. *Carbohydr. Polym.* **2012**, *87* (3), 2012–2018.

(13)   Ruland, W. Small-Angle Scattering Studies on Carbonized Cellulose Fibers. *J. Polym. Sci. Part C Polym. Symp.* **1969**, *28* (1), 143–151.

(14)   Jiang, G.; Yuan, Y.; Wang, B.; Yin, X.; Mukuze, K. S.; Huang, W.; Zhang, Y.; Wang, H. Analysis of Regenerated Cellulose Fibers with Ionic Liquids as a Solvent as Spinning Speed Is Increased. *Cellulose* **2012**, *19* (4), 1075–1083.

(15)   Crawshaw, J.; Cameron, R. A Small Angle X-Ray Scattering Study of Pore Structure in Tencel Cellulose Fibres and the Effects of Physical Treatments. *Polymer (Guildf).* **2000**, *41*, 4691–4698.

(16)   Schurz, J.; Lenz, J.; Wrentschur, E. Inner Surface and Void System of Regenerated Cellulose Fibers. *Die Angew. Makromol. Chemie* **1995**, *229*, 175–184.

(17)   Fischer, E. W.; Herchenröder, P.; Stamm, M.; Manley, R. S. J. Small-Angle Neutron Scattering of Selectively Deuterated Cellulose. *Macromolecules* **1978**, *11* (1), 213–217.

(18)   Abu-Rous, M.; Ingolic, E.; Schuster, K. C. Visualisation of the Fibrillar and Pore Morphology of Cellulosic Fibres Applying Transmission Electron Microscopy. *Cellulose* **2006**, *13* (4), 411–419.

Introduction

(19) Chen, X.; Burger, C.; Fang, D.; Ruan, D.; Zhang, L.; Hsiao, B. S.; Chu, B. X-Ray Studies of Regenerated Cellulose Fibers Wet Spun from Cotton Linter Pulp in NaOH/Thiourea Aqueous Solutions. *Polymer.* **2006**, *47* (8), 2839–2848.

(20) Kolpak, F. J.; Blackwell, J. Determination of the Structure of Cellulose II. *Macromolecules* **1976**, *9* (2), 273–278.

(21) Langan, P.; Nishiyama, Y.; Chanzy, H. A Revised Structure and Hydrogen-Bonding System in Cellulose II from a Neutron Fiber Diffraction Analysis. *J. Am. Chem. Soc.* **1999**, *121* (43), 9940–9946.

(22) Kaduk, J. A.; Blanton, T. N. An Improved Structural Model for Cellulose II. *Powder Diffr.* **2013**, *28* (3), 194–199.

(23) Zhou, S.; Tashiro, K.; Hongo, T.; Shirataki, H.; Yamane, C.; Ii, T. Influence of Water on Structure and Mechanical Properties of Regenerated Cellulose Studied by an Organized Combination of Infrared Spectra, X-Ray Diffraction, and Dynamic Viscoelastic Data Measured as Functions of Temperature and Humidity. *Macromolecules* **2001**, *34* (5), 1274–1280.

(24) Kreze, T.; Jeler, S.; Strnad, S. Correlation between Structure Characteristics and Adsorption Properties of Regenerated Cellulose Fibers. *Mater. Res. Innov.* **2003**, *5* (6), 277–283.

(25) Kreze, T.; Stana-Kleinschek, K.; Ribitsch, V. The Sorption Behaviour of Cellulose Fibres. *Lenzinger Berichte* **2001**, *80*, 28–33.

(26) Stana-Kleinschek, K.; Ribitsch, V.; Kreže, T.; Sfiligoj-Smole, M.; Peršin, Z. Correlation of Regenerated Cellulose Fibres Morphology and Surface Free Energy Components. *Lenzinger Berichte* **2003**, *82*, 83–95.

(27) Röder, T.; Moosbauer, J.; Wöss, K.; Schlader, S.; Kraft, G. Man-Made Cellulose Fibres – a Comparison Based on Morphology and Mechanical Properties. *Lenzinger Berichte* **2013**, *91*, 7–12.

(28) Hermans, J. J.; Hermans, P. H.; Vermaas, D.; Weidinger, A. Quantitative Evaluation of Orientation in Cellulose Fibres From the X-Ray Pibre Diagram. *Recl. des Trav. Chim. des Pays-Bas* **1946**, *65* (6), 427–447.

(29) Alexander, L. E. *X-Ray Diffraction Methods in Polymer Science*; John Wiley & Sons,

Inc., 1969.

(30) Lenz, J.; Schurz, J.; Wrentschur, E. Properties and Structure of Solvent-Spun and Viscose-Type Fibres in the Swollen State. *Colloid Polym. Sci.* **1993**, *271* (5), 460–468.

(31) Kong, K.; Eichhorn, S. J. The Influence of Hydrogen Bonding on the Deformation Micromechanics of Cellulose Fibers The Influence of Hydrogen Bonding on the Deformation Micromechanics of Cellulose Fibers. *J. Macromol. Sci. Part B Phys.* **2005**, *44* (6), 1123–1136.

(32) Gindl, W.; Keckes, J. Strain Hardening in Regenerated Cellulose Fibres. *Compos. Sci. Technol.* **2006**, *66* (13), 2049–2053.

(33) Meredith, R. 12—a Comparison of the Tensile Elasticity of Some Textile Fibres. *J. Text. Inst. Trans.* **1945**, *36* (7), T147–T164.

(34) Yamaguchi, B. T.; Kitagawa, T.; Yanagawa, T.; Kimura, H. Relationship and Tensile between Recovery Stress Relaxation of Filament Yarns. *J. Text. Mach. Soc. Japan* **1981**, *27* (2), 43–49.

(35) Meredith, R. 27—Relaxation of Stress in Stretched Cellulose Fibres. *J. Text. Inst. Trans.* **1954**, *45* (6), T438–T461.

(36) Bates, I.; Maudru, E.; Phillips, D. a S.; Renfrew, a H. M.; Su, Y.; Xu, J. Cross-Linking Agents for the Protection of Lyocell against Fibrillation: Synthesis, Application and Technical Assessment of 2,4-Diacrylamidobenzenesulphonic Acid. *Color. Technol.* **2004**, *120* (6), 293–300.

(37) Zhang, W.; Okubayashi, S.; Bechtold, T. Fibrillation Tendency of Cellulosic Fibers. Part 1: Effects of Swelling. *Cellulose* **2005**, *12* (3), 267–273.

(38) Nemec, H.; Ag, L. Fibrillation of Cellulosic Materials - Can Previous Literature Offer a Solution? *Lenzinger Berichte* **1994**, *9*, 69–72.

(39) Persin, Z.; Stana-Kleinschek, K.; Kreze, T. Hydrophilic/Hydrophobic Characteristics of Different Cellulose Fibres Monitored by Tensiometry. *Croat. Chem. Acta* **2002**, *75* (1), 271–280.

(40) Kreze, T.; Strnad, S.; Stana-Kleinschek, K.; Ribitsch, V. Influence of Aqueous Medium on Mechanical Properties of Conventional and New Environmentally

Friendly Regenerated Cellulose Fibers. *Mater. Res. Innov.* **2001**, *4* (2–3), 107–114.

(41)   Fink, H. P.; Philipp, B.; Paul, D.; Serimaa, R.; Paakkari, T. The Structure of Amorphous Cellulose as Revealed by Wide-Angle X-Ray Scattering. *Polymer.* **1987**, *28* (8), 1265–1270.

(42)   Kim, D. B. Dry Jet-Wet Spinning of Cellulose/N-Methylmorpholine N-Oxide Hydrate Solutions and Physical Properties of Lyocell Fibers. *Text. Res. J.* **2005**, *75* (4), 331–341.

(43)   Adusumalli, R.-B.; Muller, U.; Weber, H.; Roeder, T.; Sixta, H.; Gindl, W. Tensile Testing of Single Regenerated Cellulose Fibres. *Macromol. Symp* **2006**, *244*, 83–88.

(44)   Gindl, W.; Martinschitz, K. J.; Boesecke, P.; Keckes, J. Changes in the Molecular Orientation and Tensile Properties of Uniaxially Drawn Cellulose Films. *Biomacromolecules* **2006**, *7* (11), 3146–3150.

(45)   Gindl, W.; Martinschitz, K. J.; Boesecke, P.; Keckes, J. Orientation of Cellulose Crystallites in Regenerated Cellulose Fibres under Tensile and Bending Loads. *Cellulose* **2006**, *13* (6), 621–627.

(46)   Kong, K.; Davies, R. J.; McDonald, M. A.; Young, R. J.; Wilding, M. A.; Ibbett, R. N.; Eichhorn, S. J. Influence of Domain Orientation on the Mechanical Properties of Regenerated Cellulose Fibers. *Biomacromolecules* **2007**, *8* (2), 624–630.

(47)   Kong, K.; Wilding, M. A.; Ibbett, R. N.; Eichhorn, S. J. Molecular and Crystal Deformation of Cellulose: Uniform Strain or Uniform Stress? *Faraday Discuss.* **2008**, *139*, 283–298.

(48)   Zhang, S.; Wang, W.; Li, F.; Yu, J. Non-Linear Viscoelastic Behavior of Novel Regenerated Cellulose Fiber in Dry and Wet Condition. *Cellul. Chem. Technol.* **2013**, *47*, 353–358.

(49)   Haughtont, P. M.; Sellen, D. B. Stress Relaxation in Regenerated Cellulose. *J. Phy. D Appl. Phys* **1973**, *6*, 1998–2011.

Chapter 2.
Modeling the universal viscoelastic response of semicrystalline polymer fibers

(Contents of this chapter are published in and reprinted with permission from Sharma, A.; Kumaraswamy, G.; Thakre, S. Modeling the Universal Viscoelastic Response of Polymer Fibers. *Phys. Rev. Mater.* **2018**, *2* (6), 062601). *Copyright (2018) American Physical Society*

2.1 Graphical Abstract:
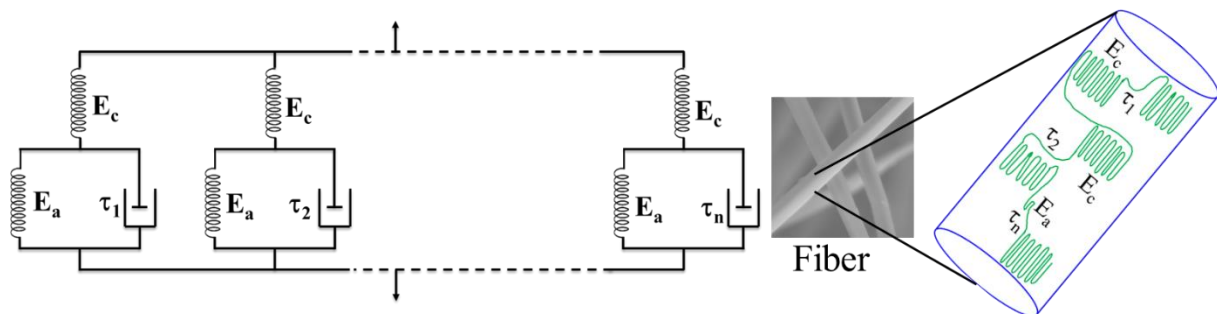
2.2 Introduction:

Polymer fibers are ubiquitous in nature (for example, silk or cellulosic plant fibers) as well as in industrial practice (for example, PET or nylon). The toughness of natural silks and the springiness of synthetic fibers woven into carpets are determined by the fiber microstructure.[1-6] A majority of polymer fibers, including silk and PET, are semicrystalline. Such polymers have a regular chemical structure that allows them to crystallize. However, the long chain nature of polymer molecules precludes complete crystallization and amorphous and crystal phases coexist in the semicrystalline state. Two phase coexistence over a wide range of temperature and pressure violates the Gibbs rule and is indicative of the non-equilibrium nature of semicrystalline polymers. Further, at temperatures below the glass transition temperature (T_g) of the polymer, the amorphous phase is glassy.

Modelling the mechanical response of semicrystalline polymer fibers is challenging due to their structural complexity. Polymers crystallize to form lamellae that are tens of nanometres thick. Since the thickness of the lamellar crystal is much smaller than the typical polymer contour length, a polymer chain spans multiple lamellae.[7] Parts of a chain that are between

crystalline lamellae are in the amorphous state. Further complexity, such as the presence of microvoids or a core-shell structure might arise from the spinning process that produces the fiber. Thus, semicrystalline microstructure is characterized by ordering over a wide range of length scales, making it difficult to develop tractable molecular models to capture their behaviour. Several attempts have been made over the last several decades to develop phenomenological models for the viscoelastic response of polymer fibers.[8–12] For example, the response of silk fibers to cyclic loading has recently been modelled.[10] However, this model is incapable of capturing stress recovery observed on unloading silk fibers. Phenomenological models have also been developed that capture the response of polyethylene fibers.[8,13] Here, we demonstrate that a wide variety of semicrystalline polymer fibers, including natural and synthetic fibers, exhibit universal viscoelastic response. We present a phenomenological model, that is independent of fiber chemistry, that captures data from independent mechanical experiments and offers insights into the microstructural origins of the mechanical response.

2.3   Materials and Methods:

We examine semicrystalline polymer fibers of polyacrylonitrile (PAN), polyethylene terephthalate (PET), regenerated cellulose, and silk fibroin. PAN and PET fibers are synthetic whereas regenerated cellulose is obtained from natural cellulose.[14–16] Silk is a natural fiber obtained from silkworms.[17,18] At room temperature, PET, PAN, regenerated cellulose, and silk fibroin have a glassy amorphous phase. Thus, our experiments investigate synthetic as well as natural semicrystalline polymer fibers, prepared using a wide range of spinning methods (including solution and melt spinning and reactive regeneration).

2.3.1   *Mechanical Measurements:*

We isolate individual fibers and stretch them at a constant rate ($= 4 \times 10^{-3}$ s^{-1}) to investigate their stress-strain response. All mechanical measurements are performed using ARES G2 rheometer (TA instruments). For each test, a single fiber is clamped in the torsion fixture of the rheometer using a paper frame, as described by Adusumalli and co-workers[19] with gauge length between 10 to 11 mm. Each measurement is repeated at least 10 times to ensure reproducibility. Variation in the data across fibers was less than 10%. Here, representative data from one fiber is presented. In stress relaxation, a fiber is stretched (at 4×10^{-3} s^{-1}) to a strain below the yield strain and the stress is monitored while holding the fiber at that strain.

The normal force transducer gives the force values during stretching, relaxation and recovery tests. We ensure that the forces, even for single fiber measurements are at least 10-fold greater than the resolution limit of the transducer. To calculate stress on a fiber, we obtain the fiber cross-sectional area as follows. We straighten fibers and embed them in epoxy. Then, we microtome the epoxy embedded fibers perpendicular to the fiber length and obtain the cross-sectional images using an optical microscope at 40X magnification. We use ImageJ software to measure the cross-sectional area of all embedded fibers. The average cross sectional area (averaged over at least 25 fibers) and standard deviation for all fibers is shown in **Table 2.1**. We obtain the stress as the force normalized by the average cross-sectional area.

Table 2.1 Average and standard deviation in cross-section area for fibers.

	AVERAGE (μm^2)	ST.DEV. (μm^2)
Regenerated Cellulose	151.8	15
Silk	86.9	13.11
PET	146.1	14.05
PAN	380.9	33.33

2.3.2   *In situ Wide Angle X-Ray Diffraction:*

WAXD measurements were performed by taking a bunch of fibers. All measurements were made using RIGAKU R AXIS IV[++] equipped with a microfocus source (Cu Kα radiation, λ = 0.154 nm, 1.2KW rotating anode generator). We mounted a stretching device (LINKAM Tensile Stress Testing System - TST350) on the WAXD instrument so that in situ measurements could be performed on fibers during stretching. WAXD was performed on unstretched fibers; then the samples were stretched at a strain rate of $4 \times 10^{-3} s^{-1}$ to a strain below (apparent) yield point and held for a period of 2 days. Then WAXD was performed on these relaxed fibers. 2D air background was subtracted from the measurements made on each sample after normalizing for scattering time. 2D data were converted to 1D data using RIGAKU 2DP software.

2.3.3   *Lattice parameters for regenerated cellulose fibers:*

Crystalline peaks in WAXD data of regenerated cellulose fibers are indexed based in the literature.[20,21] We calculate d spacing corresponding to the indexed peaks. Crystalline unit

cell of regenerated cellulose fibers is known to be monoclinic.[22] For monoclinic unit cell, the d spacing relates to the unit cell parameters as follows:

$$\frac{1}{d^2} = \frac{1}{(sin\,\theta)^2}\left[\frac{h^2}{a^2} + \frac{k^2}{b^2} - \frac{2hk\,cos\,\gamma}{ab}\right] + \frac{l^2}{c^2}$$

2.1

2.4 Results and Discussions:

2.4.1 Mechanical response:

At low strains, the stress is linear in strain for all fibers [**Figure 2.1**(a)]. We observe that the fibers apparently yield at a critical strain ε_y, above which the slope of the stress-strain data decreases. For strains $< \varepsilon_y$, stress-strain data is reversible, viz. the stress decreases to zero along the same path on unloading the fiber immediately after stretching. The elastic response of the fibers below ε_y is characteristic of the microstructure of the as spun fiber and is independent of the strain rate within a range of 2.5 x 10^{-4} s^{-1} to 4 x 10^{-3} s^{-1}. Here, we restrict our investigations to the elastic response region.
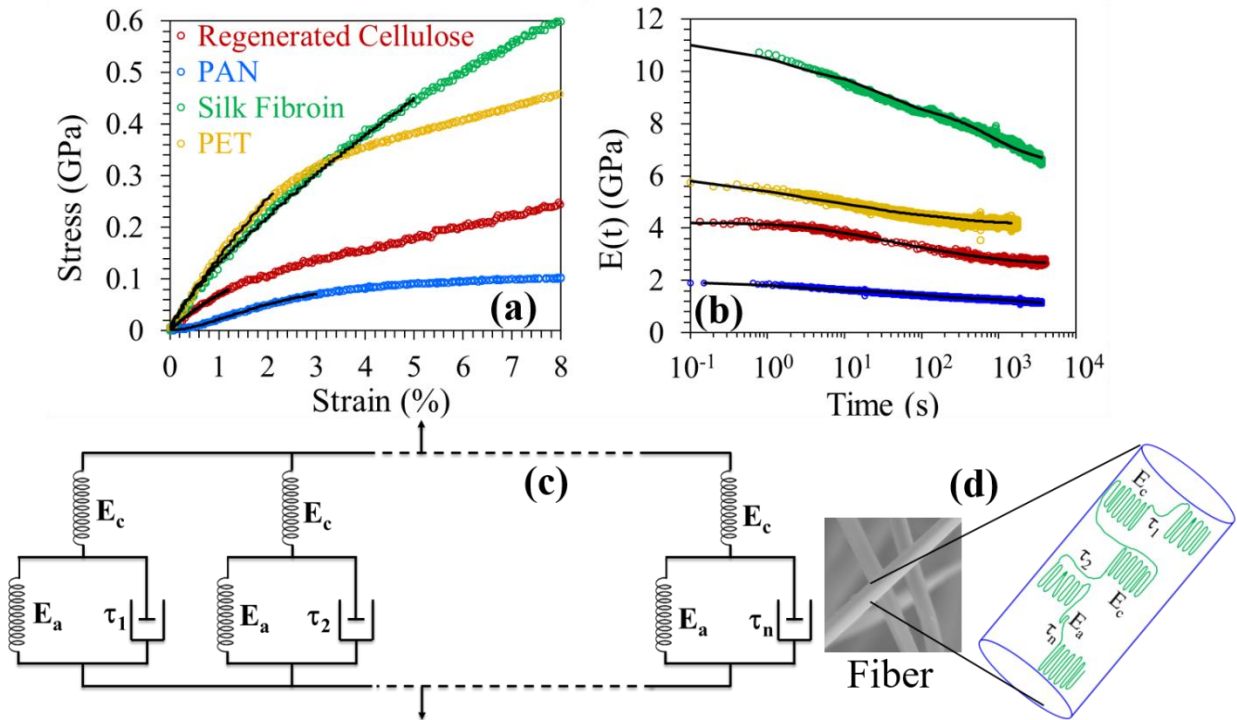
Figure 2.1 (a) Stress strain response from various semicrystalline fibers at a constant stretch rate of 4×10^{-3} s^{-1}. The (apparent) yield strain ε_y for Cellulose, PAN, PET, and silk fibers was determined to be 1.3%, 3.5%, 2.1%, and 7.6%, respectively. (b) Modulus, $E(t) = \sigma(t)/\varepsilon$ from stress relaxation experiments for fibers held after stretching to a strain, $\varepsilon_o < \varepsilon_y$. The black lines represent fits to the model shown in (c) comprising units with an elastic element in series with a Kelvin Voigt element. We assume a distribution of relaxation times in each unit that is represented schematically as a parallel combination. (d) Schematic representation of polymer chains spanning crystalline lamellae and amorphous domains in the semicrystalline fibers.

Polymer fibers are viscoelastic. We investigate the fiber viscoelastic response by performing stress relaxation experiments. For all semicrystalline fibers, the stress decays logarithmically with time [**Figure 2.1**(b)]. The stress does not decay to zero even after holding for several days. The logarithmic time decay of stress suggests that relaxation is governed by processes characterized by widely varying time scales.

2.4.2 Model:

We describe the mechanical response of the fibers using a phenomenological model as shown schematically in **Figure 2.1**(c). Each unit comprises a Kelvin-Voigt element (with elastic

modulus E_a and relaxation time τ) in series with an elastic spring with modulus E_c. This unit is described by the following equation:

$$\frac{d\sigma}{dt} + \frac{\sigma}{\tau} - \frac{E_c E_a}{\tau(E_c + E_a)}\varepsilon - E_c\frac{d\varepsilon}{dt} = 0$$

2.2

Since the polymer fibers exhibit logarithmic stress decay, we model the response using a spectrum of relaxation times, $P(\tau)$, corresponding to the spatial heterogeneity of the amorphous domains [**Figure 2.1** (d)]. From equation 2.2, we obtain the stress developed, σ_{s-s}, on stretching the fiber at a constant strain rate $\dot{\varepsilon}$ and the time-dependent stress relaxation (σ_r) as:

$$\sigma_{S-S} = \int_{-\infty}^{\infty} P(\tau)\ \frac{E_c}{E_c + E_a}\left[E_a\varepsilon + E_c\tau\dot{\varepsilon}(1 - e^{-\frac{t}{\tau}})\right]d\tau$$

2.3

$$\sigma_r = \int_{-\infty}^{\infty} P(\tau)\left\{\left[\sigma_0 - \frac{E_c E_a\varepsilon}{E_c + E_a}\right]e^{-\frac{t}{\tau}} + \frac{E_c E_a\varepsilon}{E_c + E_a}\right\}d\tau$$

2.4

For $E_a > 0$, the stress from this model never decays to zero during stress relaxation experiments.

Fiber stretching and stress relaxation are independent experiments. We obtain the fit parameters, E_c, E_a, and $P(\tau)$ by simultaneously fitting the model to data from these two independent experiments using CONTIN regularization.[23,24] Since we simultaneously fit stress-strain and stress relaxation data, the model converges robustly to the same fit parameters even with widely varying initial guesses. Fit parameters E_c and E_a are given in **Table 2.2** and the relaxation spectra $P(\tau)$ are shown in **Figure 2.2**. In all fibers, $E_c > E_a$. As anticipated from the stress decay data, $P(\tau)$ varies widely (**Figure 2.2**). We observe that $P(\tau)$ is monomodal for PET, PAN, and silk and is bimodal for the regenerated cellulose fibers.

Table 2.2 Moduli from fitting and WAXD.

		Moduli from fitting (GPa)	Moduli from WAXD (GPa)
Regenerated Cellulose	E_c	12.5	14.2
	E_a	1.1	1.78
Silk Fibroin	E_c	13	11.6
	E_a	4.57	4.96
PET	E_c	6.06	5.81
	E_a	2.27	2.32
PAN	E_c	2.17	--------------
	E_a	0.44	
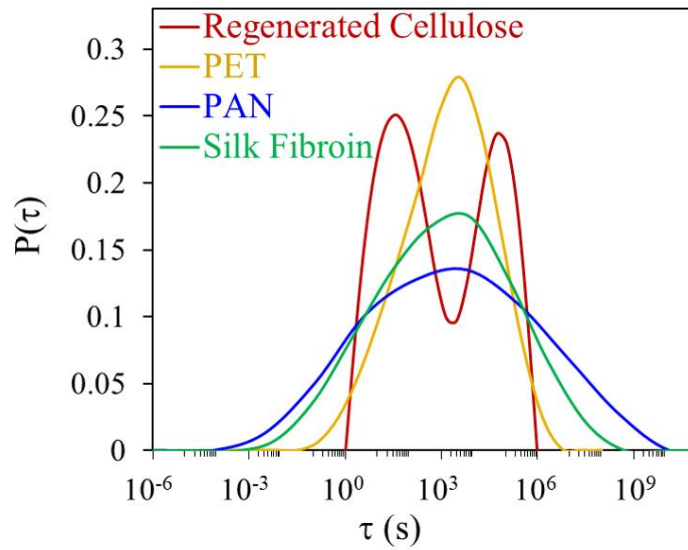
Figure 2.2 The best fit for the relaxation times, $P(\tau)$, obtained by fitting the experimental data to the model.

We now explore how these model parameters relate to the semicrystalline microstructure. Since $E_c > E_a$, it is possible that E_c represents the elastic modulus of the crystalline domains while E_a represents the low strain elastic response of the glassy amorphous domains. To verify this, we employ wide angle x-ray diffraction (WAXD) to independently estimate the elastic moduli associated with the crystalline and glassy amorphous domains.

2.4.3   *Wide angle x ray diffraction:*

We cannot perform WAXD on a single fiber. Therefore, we perform in-situ WAXD on a bunch of fibers stretched to strains below ε_y in a stretching device. The fiber spinning process induces strong uniaxial orientation in the crystalline phase, reflected in 2D-WAXD from aligned fibers. We perform WAXD on fibers that are held in the stretched state for two days, such that the stress approaches a steady state. The meridional WAXD peaks shift to lower 2θ when fibers are stretched. For example, we show the shift for the 002 peak on stretching regenerated cellulose fibers [**Figure 2.3**(a)]. From the WAXD peak positions, we can calculate crystalline unit cell parameters for unstretched and stretched fibers. For example, based on the equation 2.1, a, b, c parameters obtained for cellulose fibers in unstretched state are a=7.801 Å, b=9.212 Å, c=10.254 Å and for stretched fibers are a=7.788 Å, b=9.205 Å, c=10.297 Å. We observe that stretching induces an extension of the crystal unit cell along the c axis and a small compression along a and b axes. Since the polymer chain is aligned along the c axis of the crystalline unit cell,[22] stretching results in elongation of the polymer crystals along the chain axis. We calculate the crystalline strain, ε_c $(= \frac{\Delta c}{c})$, as the ratio of the change along the c axis, normalized by the unstretched unit cell distance along the c axis. It is well established in literature that the stress is homogeneously distributed on the crystal and amorphous parts of semicrystalline polymers.[25–27] Hence, crystalline and amorphous phases have been modelled as two springs connected in series by Dulmage and Sakurada.[28–31] We modify their method to estimate the strain on the amorphous regions as $\varepsilon_a = \varepsilon - \varepsilon_c$. At steady state, the stress corresponds to a series combination of the crystalline and glassy elastic elements. Thus, $\sigma = \frac{E_c E_a \varepsilon}{E_c + E_a}$. Therefore, we calculate the elastic moduli as:

$$E_c = \frac{\sigma}{\varepsilon_c} \qquad E_a = \frac{\sigma}{\varepsilon_a}$$

2.5

We use this method to estimate the elastic moduli for PET, silk, and regenerated cellulose fibers. PAN fibers show only equatorial peaks (200) and (310): Therefore, it is not possible to obtain the unit cell dimension along the c axis from WAXD and, we cannot use this method to estimate the elastic modulus for PAN fibers. The moduli, E_c and E_a, obtained from WAXD for PET, silk, and regenerated cellulose fibers agree reasonably well with those from the model fits (see   **Table 2.2**). This supports our assumption that E_c and E_a obtained from the

model can be interpreted as the elastic moduli corresponding to crystalline and amorphous domains of the semicrystalline fibers, respectively.
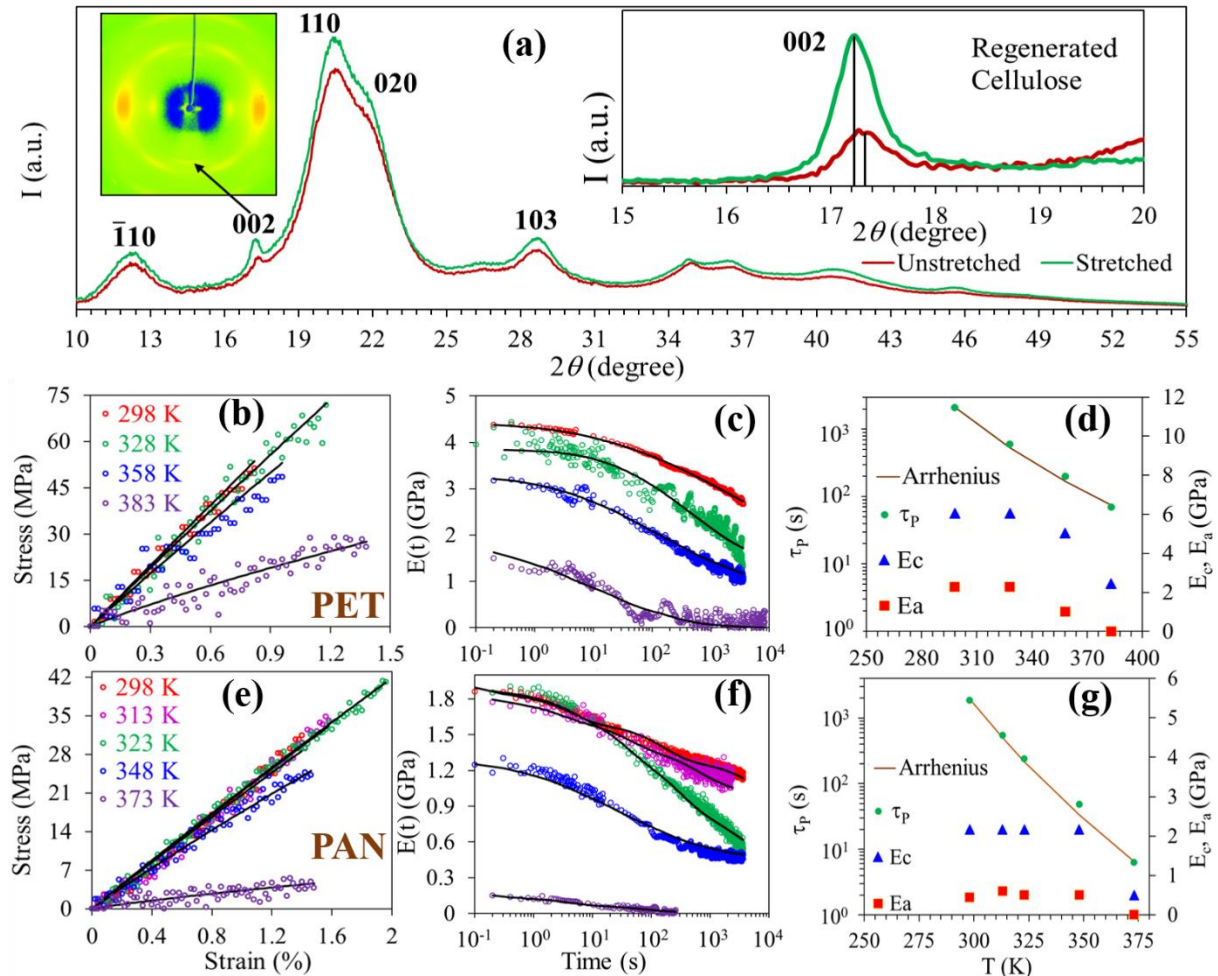
Figure 2.3 (a) Wide angle x-ray diffraction data for regenerated cellulose fiber in unstretched and stretched states. 2D data obtained from the WAXD is shown as an inset (left). The data are reduced to 1D (intensity versus 2θ) by circular averaging. WAXD peaks were indexed based on the literature.[20,21] The inset on the right clearly shows that the 002 peak shifts to lower 2θ upon stretching. Data for PET and PAN fibers are shown in the middle and bottom, respectively. (b), (e) Stress strain and (c), (f) stress relaxation experiments performed at temperatures of 298, 328, 358, and 383 K for PET and 298, 313, 323, 348, and 373 K for PAN fibers. Fits to the data are indicated as black lines. Temperature dependent model parameters are given in (d,g).

We now examine the temperature dependence of the model parameters, $P(\tau)$, E_c, and E_a, as PET and PAN fibers are heated to temperatures approaching their T_g. Fiber orientation results in an increase in the T_g for fibers. We measure T_g of 375 K and 389 K for PAN and PET fibers, respectively—higher than literature values for unoriented samples (PET—353 K, PAN—369 K). On heating PAN and PET fibers from 298 K to near T_g, there is a systematic decrease in the fiber modulus, suggesting softening of fibers with temperature [**Figure 2.3**(b) and (e)]. Correspondingly, model fits to the data show a two to five-fold decrease in E_c on approaching T_g. In contrast, near the polymer T_g there is a qualitative change in the stress relaxation for both fibers. Near T_g, the stress in both PET and PAN stretched fibers decreases to 0 upon holding for about 1000 s. Correspondingly, E_a decreases abruptly to 0 near T_g [**Figure 2.3**(c) and (f)]. Thus, the mechanical response of PET and PAN fibers on approaching the amorphous phase T_g is described by a simple Maxwell model comprising an elastic element in series with a viscous element.[32] The behaviour of E_a close to T_g is further evidence that E_a is related to the response of the amorphous domains.

On heating, there is also a shift in $P(\tau)$ to lower values as shown in **Figure 2.4**. We plot the temperature dependent decrease in the peak of the relaxation time distribution, τ_P [**Figure 2.3**(d) and (g)]. There is an exponential decrease in τ_P with temperature, characterized by an activation energy of 37.4 kJ/mol for PET and 70.2 kJ/mol for PAN. We note that these values for the activation energy compare favourably with those from dielectric measurements of β relaxation processes in these material.[33,34] Further, dielectric measurements yield broad relaxation spectra corresponding to β processes, comparable to the breadth of $P(\tau)$ from our model fits (PET,[35,36] PAN,[37] regenerated cellulose[38]). Thus, the amorphous relaxations that we obtain from our model correlate with sub - T_g motions reported for these polymers. Thus, the parameters of this simple model bear a remarkable correspondence with the microstructural features of semicrystalline fibers: The moduli correspond to the elastic response of crystalline and amorphous phases while the relaxation time spectra represent the contribution of sub-T_g processes in the amorphous regions.
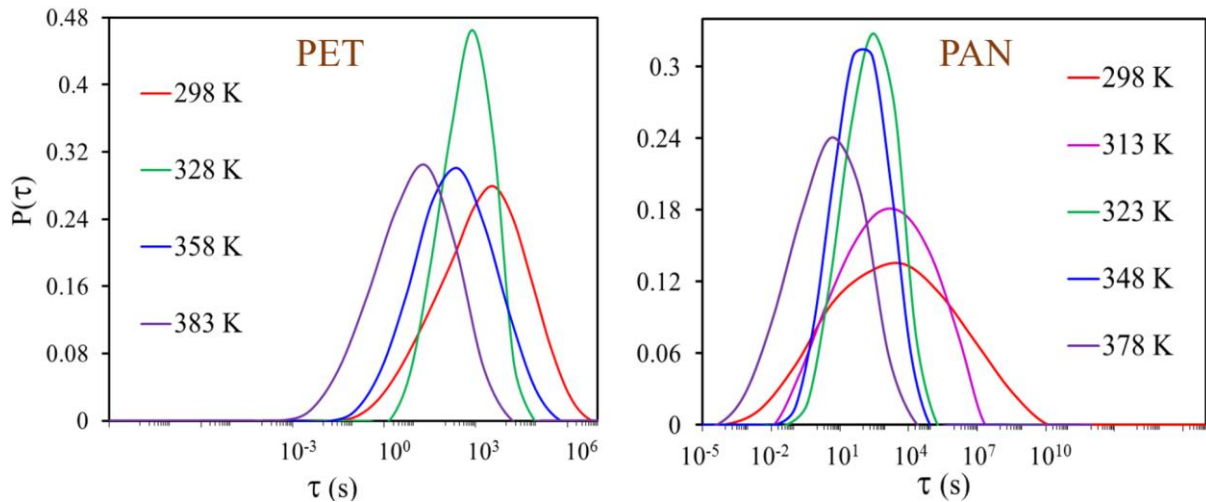
Figure 2.4 Relaxation time spectra of PET and PAN fibers shift to lower time scales with temperature.

Having established the connection between the model and semicrystalline microstructure, we now explore the predictions of the model. We calculate the strain in the crystalline and amorphous domains when regenerated cellulose fibers are stretched at 4×10^{-3} s^{-1}, using the model parameters calculated earlier. Counter to intuition, the model suggests that it is the crystalline regions that predominantly deform, and that there is minimum deformation of the glassy amorphous regions during stretching as shown in **Figure 2.5** (a). The time scales for the stretching experiment ($\dot{\varepsilon}^{-1}$ = 250 s) is significantly smaller than those that characterize glassy relaxation (**Figure 2.2**). Thus, the glassy amorphous phase is unable to respond during stretching and it is the crystalline regions that get strained. We now present three independent experiments that support this surprising prediction of the model.
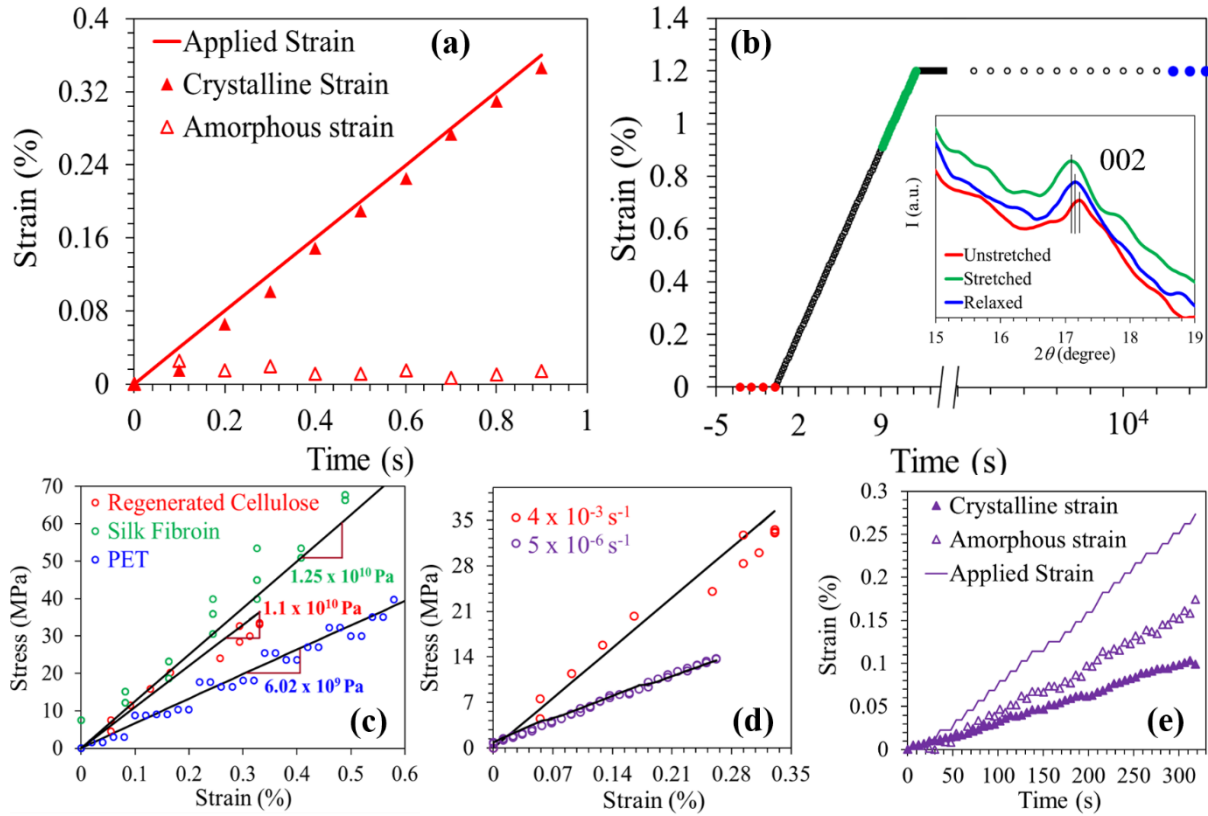
Figure 2.5 (a) Evolution of crystalline and amorphous strains from the model during stretching of cellulose fibers at 4×10^{-3} s^{-1}. (b) Variation of strain with time for cellulose fibers shows three regions where WAXD (shown in inset) is performed: Red (unstretched fibers), green (during stretching), and blue (relaxed fibers). (c) Initial slope of the stress vs strain curve for regenerated cellulose, PET, and silk fibers obtained at 4×10^{-3} s^{-1} [compare with the crystal modulus obtained from WAXD (**Table 2.2**)]. (d) Stress vs strain data for cellulose fibers stretched at (4×10^{-3} s^{-1}) and at extremely low strain rate (5×10^{-6} s^{-1}). (e) Evolution of crystalline and amorphous strains from model during stretching of cellulose fibers at (5×10^{-6} s^{-1}) [compare with (a)].

At first, we use WAXD to directly examine the crystalline strain when the cellulose fibers are stretched. We stretch cellulose fibers to a strain of 1.2% ($<\varepsilon_y$) and obtain WAXD data for 3 s, close to the peak strain [**Figure 2.5** (b)]. Since, the data acquisition time is small, we average data over five repeat measurements to improve signal to noise. Then, we allow the fibers to relax over two days and obtain WAXD at steady state. We observe that the crystal expands in the c-axis direction during stretching and subsequently shrinks as stress is transferred to the amorphous glassy phase during relaxation. This provides direct proof for deformation of the

crystalline phase during stretching. We note that crystal deformation happens during stretching only for semicrystalline samples with a glassy amorphous phase, for which our model is valid. When we stretch fibers of high molecular weight polyethylene, where the amorphous phase is rubbery, we observe no change in the position of the meridional peak in WAXD (**Figure 2.6**).[39] Next, we examine the slope of the stress-strain data during stretching and compare with the crystalline modulus obtained directly from WAXD measurements. We observe that for regenerated cellulose, PET, and silk fibroin stretched at 4×10^{-3} s^{-1}, the slope of the stress-strain curve as shown in **Figure 2.5** (c) is approximately equal to the crystalline modulus obtained from WAXD in   **Table 2.2**. Thus, the modulus obtained by stretching a composite structure comprised of interconnected crystalline and amorphous domains closely matches the crystalline modulus obtained independently from WAXD measurements. This strongly suggests that it is indeed the crystal regions that deform during stretching of semicrystalline fibers with a glassy amorphous phase. Finally, the model suggests that if we stretch the fibers at extremely low strain rates, then there will also be a contribution of the amorphous phase to the mechanical response. Here, the strain rates should be sufficiently low such that the time scale that characterizes deformation is comparable to the slowest relaxation times of the amorphous phase. We perform stretching experiments on regenerated cellulose fibers at a strain rate of 5×10^{-6} s^{-1}, three orders of magnitude lower than that in our previous experiments. We observe that the initial slope of the stress strain curve is lower than at higher strain rates (and therefore lower than the crystalline modulus [**Figure 2.5** (d)]). Using the model parameters obtained previously, we observe that in this experiment, the strain is taken up by both amorphous and crystalline regions [**Figure 2.5** (e)]. Thus, taken together, our data provide strong evidence for the non-intuitive predictions of the model.
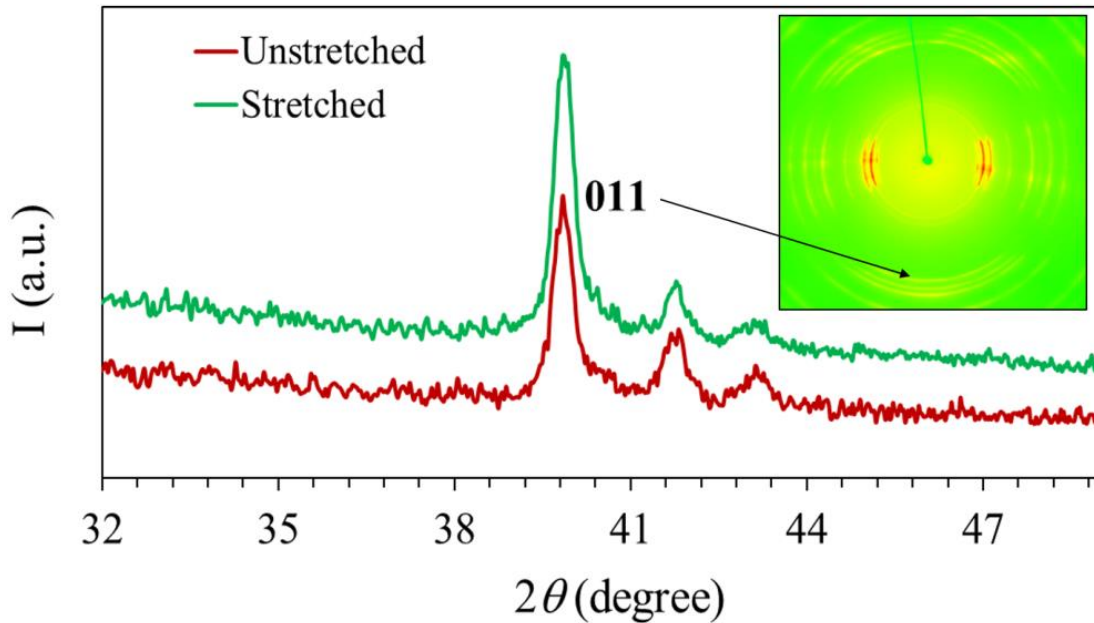
Figure 2.6 Meridional peak position (011) does not change on stretching for ultra-high molecular weight polyethylene as the amorphous phase is rubbery. The peak has been indexed based on the literature.[39,40]

In semicrystalline fibers where glassy amorphous domains are modelled as Voigt elements, stress relaxation does not correspond to irrecoverable viscous dissipation. Our model predicts that as strain is transferred to the glassy amorphous domains, the energy during stress relaxation is not lost. Rather, it is stored in the elastic component (E_a) of the Voigt element. This should result in an internal build-up of stress in the fiber. Thus, if the fiber is unloaded to zero stress after stress relaxation, then this internal built-up stress in the amorphous domain is transferred back to the crystalline domain, that should manifest as an increase in the fiber stress over the slow time scales that characterize the glassy amorphous phase.

To verify this prediction, we performed stress recovery experiments. Here, semicrystalline fibers with a glassy amorphous phase are stretched below yield and are allowed to relax for 3600 s. Then the fiber is unloaded by rapidly reducing strain (at 4×10^{-3} s^{-1}), until the stress decreases to zero. Stress decreases to zero at nonzero strain, as anticipated by the model. The fibers are then held at this strain and the stress is monitored [**Figure 2.7**(a)]. For all semicrystalline fibers investigated: PET, PAN, silk, and regenerated cellulose fibers, we observe an increase in stress with time as shown in **Figure 2.7** (b). Further, the increase in stress is quantitatively predicted by the model using the same parameters obtained from

fitting the stress-strain and stress relaxation data. The model fit is shown as a black line in **Figure 2.7** (b). Where $E_a = 0$, e.g., PET and PAN near T_g, those fibers do not show stress recovery.
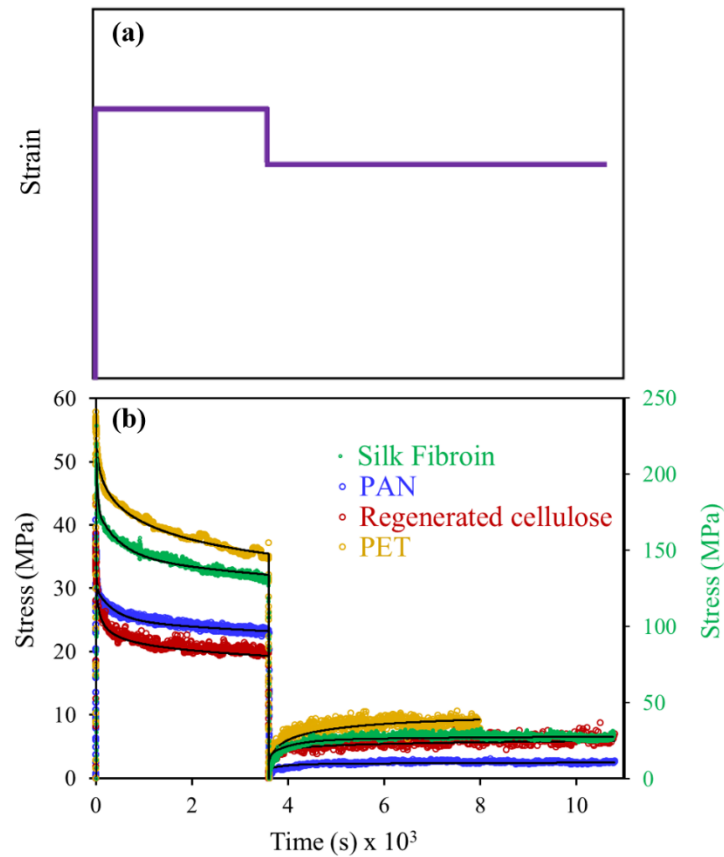
Figure 2.7 (a) Experimental protocol for strain imposed during stress recovery experiments. (b) The response from fibers with glassy amorphous phase shows recovery in stress after relaxation.

2.5 Conclusions:

We have demonstrated that a relatively simple model can quantitatively capture the mechanical response of a wide variety of semicrystalline fibers, for independent measurements (stress-strain, stress relaxation, and recovery) and over a wide temperature range. To the best of our knowledge, none of the models reported in the literature capture the response from such diverse experiments for different polymers.[41–47] Our model predicts the mechanical response of synthetic fibers (PET, PAN, regenerated cellulose) with different chemistries, manufactured using a wide variety of spinning processes, as well as of natural

fibers (silk). These fibers exhibit wide variations in crystallinity, orientation, and morphology. For example, reactively regenerated viscose cellulose fibers are characterized by an amorphous skin/crystalline core morphology, while other fibers do not show such dramatic radial variation. We do not account for such morphological differences—the fiber response is modelled as arising only from the amorphous/crystal connectivity in the semicrystalline microstructure. This appears to be sufficient to describe the mechanical response of the fibers. Further, model parameters are constrained by simultaneously fitting independent experiment results. These model parameters correlate to the semicrystalline microstructure in a physically meaningful way and fitted values match reasonably well with those from WAXD experiments and literature.

2.6 References:

(1)   Ward, I. M. *Structure and Properties of Oriented Polymers*; Springer Science & Business Media, 2012.

(2)   Northolt, M. G. Tensile deformation of poly (p-phenylene terephthalamide) fibres, an experimental and theoretical analysis. *Polymer.* **1980**, *21* (10), 1199–1204.

(3)   Cai, J.; Zhang, L.; Zhou, J.; Qi, H.; Chen, H.; Kondo, T.; Chen, X.; Chu, B. Multifilament Fibers Based on Dissolution of Cellulose in NaOH/Urea Aqueous Solution: Structure and Properties. *Adv. Mater.* **2007**, *47* (22), 8676–8683.

(4)   Kong, K.; Davies, R. J.; McDonald, M. A.; Young, R. J.; Wilding, M. A.; Ibbett, R. N.; Eichhorn, S. J. Influence of Domain Orientation on the Mechanical Properties of Regenerated Cellulose Fibers. *Biomacromolecules* **2007**, *8* (2), 624–630.

(5)   Jabbari-Farouji, S.; Lame, O.; Perez, M.; Rottler, J.; Barrat, J. L. Role of the Intercrystalline Tie Chains Network in the Mechanical Response of Semicrystalline Polymers. *Phys. Rev. Lett.* **2017**, *118* (21), 1–5.

(6)   Che, J.; Locker, C. R.; Lee, S.; Rutledge, G. C.; Hsiao, B. S.; Tsou, A. H. Plastic Deformation of Semicrystalline Polyethylene by X-Ray Scattering: Comparison with Atomistic Simulations. *Macromolecules* **2013**, *46* (13), 5279–5289.

(7)   Hsiao, B. S.; Yang, L.; Somani, R. H.; Avila-Orta, C. A.; Zhu, L. Unexpected Shish-Kebab Structure in a Sheared Polyethylene Melt. *Phys. Rev. Lett.* **2005**, *94* (11), 1–4.

(8)   Wilding, M. A.; Ward, I. M. Creep and Stress-Relaxation in Ultra-High Modulus

Linear Polyethylene. *J. Mater. Sci.* **1984**, *19* (2), 629–636.

(9)   Shi, F. Modeling Stretching-Relaxation Properties of Yarns. *Fibres Text. East. Eur.* **2013**, *98* (2), 51–55.

(10)   Krasnov, I.; Diddens, I.; Hauptmann, N.; Helms, G.; Ogurreck, M.; Seydel, T.; Funari, S. S.; Muller, M. Mechanical Properties of Silk: Interplay of Deformation on Macroscopic and Molecular Length Scales. *Phys. Rev. Lett.* **2008**, *100* (4), 2–5.

(11)   Krasnov, I.; Seydel, T.; Müller, M. Fractional Dynamics in Silk: From Molecular Picosecond Subdiffusion to Macroscopic Long-Time Relaxation. *Phys. Rev. E - Stat. Nonlinear, Soft Matter Phys.* **2015**, *91* (4), 4–7.

(12)   Manich, A. M.; Marino, P. N.; Castellar, M. D. D. E.; Saldivia, M.; Sauri, R. M. Viscoelastic Modeling of Natural and Synthetic Textile Yarns. *J. Appl. Polym. Sci.* **2000**, *76*, 2062–2067.

(13)   Djokovic, V.; Kostoski, D.; Galovic, S.; Dramicanin, M. D.; Kacarevic-Popovic, Z. Influence of Orientation and Irradiation on Stress Relaxation of Linear Low-Density Polyethylene (LLDPE): A Two-Process Model. *Polymer.* **1999**, *40* (10), 2631–2637.

(14)   Morris, E. A.; Weisenberger, M. C.; Bradley, S. B.; Abdallah, M. G.; Mecham, S. J.; Pisipati, P.; McGrath, J. E. Synthesis, Spinning, and Properties of Very High Molecular Weight Poly (Acrylonitrile-Co-Methyl Acrylate) for High Performance Precursors for Carbon Fiber. *Polymer.* **2014**, *55* (25), 6471–6482.

(15)   Chen, G. Y; Cuculo, J. A.; Tucker, P. A. Effects of Spinning Conditions on Morphology and Properties of Polyethylene Terephthalate Fibers Spun at High Speeds. *J. Appl. Polym. Sci.* **1992**, *44* (3), 447–458.

(16)   Woodings, C. *Regenerated Cellulose Fibres*; Woodhead Publishing Limited, 2001.

(17)   Jin, H.-J.; Kaplan, D. L. Mechanism of Silk Processing in Insects and Spiders. *Nature* **2003**, *424* (6952), 1057–1061.

(18)   Fu, C.; Shao, Z.; Fritz, V. Animal Silks: Their Structures, Properties and Artificial Production. *Chem. Commun.* **2009**, No. 43, 6515.

(19)   Adusumalli, R.-B.; Muller, U.; Weber, H.; Roeder, T.; Sixta, H.; Gindl, W. Tensile Testing of Single Regenerated Cellulose Fibres. *Macromol. Symp* **2006**, *244*, 83–88.

(20) Chen, X.; Burger, C.; Fang, D.; Ruan, D.; Zhang, L.; Hsiao, B. S.; Chu, B. X-Ray Studies of Regenerated Cellulose Fibers Wet Spun from Cotton Linter Pulp in NaOH/Thiourea Aqueous Solutions. *Polymer.* **2006**, *47* (8), 2839–2848.

(21) Jiang, G.; Yuan, Y.; Wang, B.; Yin, X.; Mukuze, K. S.; Huang, W.; Zhang, Y.; Wang, H. Analysis of Regenerated Cellulose Fibers with Ionic Liquids as a Solvent as Spinning Speed Is Increased. *Cellulose* **2012**, *19* (4), 1075–1083.

(22) Zugenmaier, P. Conformation and Packing of Various Crystalline Cellulose Fibers. *Prog. Polym. Sci.* **2001**, *26* (9), 1341–1417.

(23) Provencher, S. W. Contin : A General Purpose Constrained Regularization Program for Inverting Noisy Linear Algebraic and Integral Equations. *Comput. Phys. Commun.* **1982**, *27*, 4655.

(24) I.-G. Marino, Regularized Inverse Laplace Transform, MATLAB Central File Exchange, Retrieved September 03 2016 (**2007**) https://www.mathworks.com/matlabcentral/fileexchange/6523-rilt.

(25) Sirichaisit, J.; Brookes, V. L.; Young, R. J.; Vollrath, F. Analysis of Structure/Property Relationships in Silkworm (Bombyx Mori) and Spider Dragline (Nephila Edulis) Silks Using Raman Spectroscopy. *Biomacromolecules* **2003**, *4* (2), 387–394.

(26) Yeh, W. Y.; Young, R. J. Molecular Deformation Processes in Aromatic High Modulus Polymer Fibres. *Polymer.* **1999**, *40* (4), 857–870.

(27) Young, R. J. Monitoring Deformation Processes in High-Performance Fibres Using Raman Spectroscopy. *J. Text. Inst.* **1995**, *86* (2), 360–381.

(28) Dulmage, W. J.; Contois, L. E. A Study of the Elastic Modulus and Extensibility of the Crystalline Regions in Highly Oriented Polymers. *J. Polym. Sci.* **1958**, *28* (117), 275–284.

(29) Sakurada, I.; Nukushina, Y.; Ito, T. Experimental Determination of the Elastic Modulus of Crystalline Regions in Oriented Polymers. *J. Polym. Sci.* **1962**, *57* (165), 651–660.

(30) Sakurada, I.; Ito, T.; Nakamae, K. Elastic Moduli of Polymer Crystals for the Chain Axial Direction. *Die Makromol. Chemie* **1964**, *75*, 1–10.

(31) Sakurada, I.; Ito, T.; Nakamae, K. Elastic Moduli of the Crystal Lattices of Polymers. *J. Polym. Sci. Part C Polym. Symp.* **1966**, *15* (1), 75–91.

(32) Ward, I.M. Sweeney, J. *An Introduction to The Mechanical Properties of Solid Polymers*; **2004**.

(33) Maxwell, A. S.; Monnerie, L.; Ward, I. M. Secondary Relaxation Processes in Polyethylene Terephthalate-Additive Blends: 2. Dynamic Mechanical and Dielectric Investigations. *Polymer.* **1998**, *39* (26), 6851–6859.

(34) Okajima, S.; Ikeda, M.; Takeuchi, A. A New Transition Point of Polyacrylonitrile. *J. Polym. Sci. Part A-1 Polym. Chem.* **1968**, *6* (7), 1925–1933.

(35) Neagu, E.; Pissis, P.; Apekis, L.; Gomez Ribelles, J. L. Dielectric Relaxation Spectroscopy of Polyethylene Terephthalate (PET) Films. *J. Phys. D. Appl. Phys.* **1997**, *30* (11), 1551–1560.

(36) Boyd, R. H. Relaxation Processes in Crystalline Polymers: Molecular Interpretation - a Review. *Polymer.* **1985**, *26* (8), 1123–1133.

(37) Hayakawa, R.; Nishi, T.; Arisawa, K.; Wada, Y. Dielectric Relaxation in the Paracrystalline Phase in Polyacrylonitrile. *J. Polym. Sci. Part A-2 Polym. Phys.* **1967**, *5* (1), 165–177.

(38) Einfeldt, J.; Meißner, D.; Kwasniewski, A. Contributions to the Molecular Origin of the Dielectric Relaxation Processes in Polysaccharides - The High Temperature Range. *J. Non. Cryst. Solids* **2003**, *320* (1–3), 40–45.

(39) McDaniel, P. B.; Deitzel, J. M.; Gillespie, J. W. Structural Hierarchy and Surface Morphology of Highly Drawn Ultra High Molecular Weight Polyethylene Fibers Studied by Atomic Force Microscopy and Wide Angle X-Ray Diffraction. *Polymer.* **2015**, *69*, 148–158.

(40) Butler, M. F.; Donald, A. M.; Bras, W.; Mant, G. R.; Derbyshire, G. E.; Ryan, A. J. A Real-Time Simultaneous Small- and Wide-Angle X-Ray Scattering Study of In-Situ Deformation of Isotropic Polyethylene. *Macromolecules* **1995**, *28* (19), 6383–6393.

(41) Kitagawa, M.; Mori, T.; Matsutani, T. Rate-Dependent Nonlinear Constitutive Equation of Polypropylene. *J. Polym. Sci. Part B Polym. Phys.* **1989**, *27* (1), 85–95.

(42)   Kitagawa, M.; Takagi, H. Nonlinear Constitutive Equation for Polyethylene under Combined Tension and Torsion. *J. Polym. Sci. Part B Polym. Phys.* **1990**, *28* (11), 1943–1953.

(43)   Hong, K.; Strobl, G. Network Stretching during Tensile Drawing of Polyethylene: A Study Using X-Ray Scattering and Microscopy. *Macromolecules* **2006**, *39* (1), 268–273.

(44)   Men, Y.; Rieger, J.; Strobl, G. Role of the Entangled Amorphous Network in Tensile Deformation of Semicrystalline Polymers. *Phys. Rev. Lett.* **2003**, *91* (9), 095502.

(45)   Hong, K.; Rastogi, A.; Strobl, G. A Model Treating Tensile Deformation of Semicrystalline Polymers: Quasi-Static Stress-Strain Relationship and Viscous Stress Determined for a Sample of Polyethylene. *Macromolecules* **2004**, *37* (26), 10165–10173.

(46)   Hong, K.; Rastogi, A.; Strobl, G. Model Treatment of Tensile Deformation of Semicrystalline Polymers: Static Elastic Moduli and Creep Parameters Derived for a Sample of Polyethylene. *Macromolecules* **2004**, *37* (26), 10174–10179.

(47)   Haward, R. N.; Thackray, G. The Use of a Mathematical Model to Describe Isothermal Stress-Strain Curves in Glassy Thermoplastics. *Proc. R. Soc. A Math. Phys. Eng. Sci.* **1968**, *302* (1471), 453–472.

Chapter 3.

Structure-property relations in regenerated cellulose fibers: Comparison of fibers manufactured using Viscose and Lyocell processes

3.1 Graphical Abstract:

In-situ WAXD   Mechanical Model   Apparent Yield
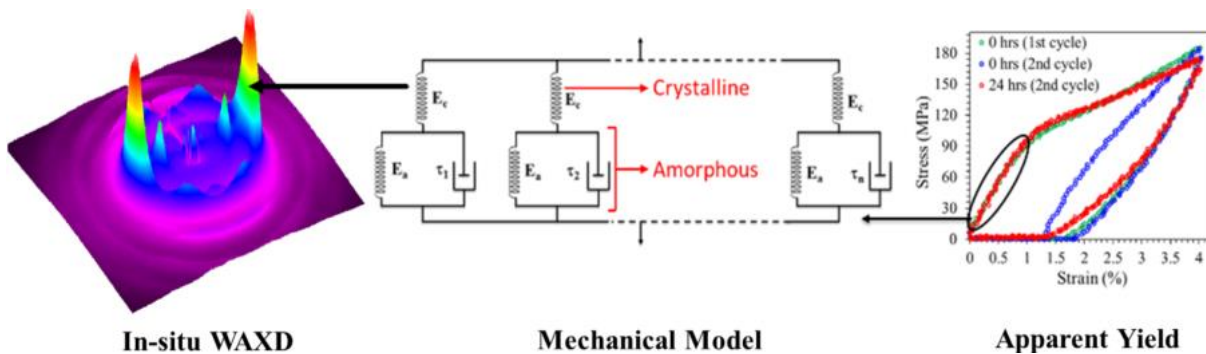
3.2 Introduction:

Cellulose is the most abundant natural polymer. It is a semicrystalline polymer where crystal and amorphous phases coexist, with the crystalline phase stabilized by strong hydrogen bonds. On heating, cellulose does not exhibit crystal melting – rather, the polymer undergoes degradation. Solvents that can disrupt intra-molecular hydrogen bonding can dissolve cellulose, offering a route to process it into useful products. To convert cellulose into continuous fiber form for use in textile applications, it has to be regenerated. In this process, the native cellulose is dissolved and regenerated fibers are produced by spinning the solution into a non-solvent coagulation bath. The details of the fiber regeneration process play a critical role in determining the microstructure of the regenerated fiber, and therefore in determining its properties.

Structure-Property Relations in Regenerated Cellulose Fibers: Comparison of Fibers Manufactured using Viscose and Lyocell Processes
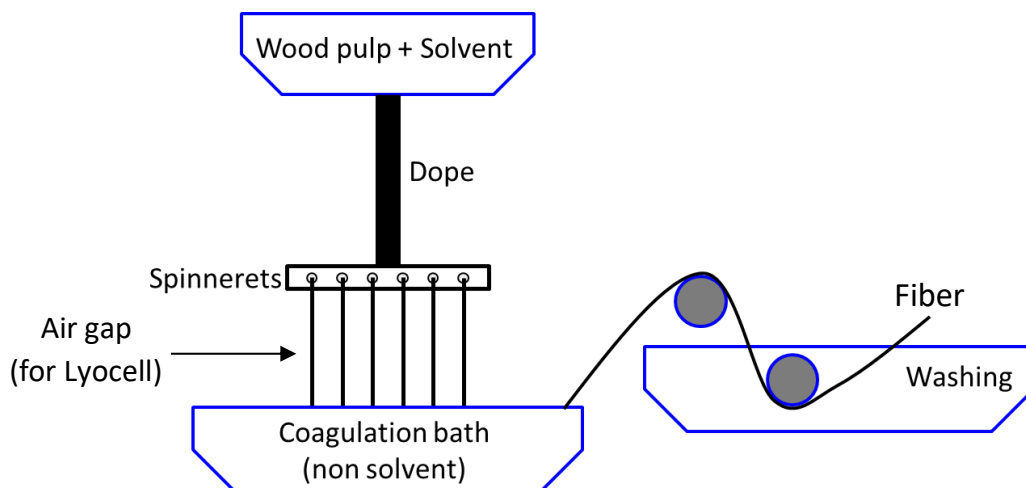
Figure 3.1 Regeneration process for the production of cellulose fibers.

The steps of cellulose fiber regeneration are schematically depicted in **Figure 3.1**. Wood pulp is dissolved in a solvent and the solution is extruded through spinneret holes into a coagulation bath that contains a non-solvent. The non-solvent extracts the solvent, regenerating the cellulose in fiber form. Several processes based on this general scheme have been developed for dissolution of native cellulose and its regeneration as fibers.[1,2] The two main industrially practiced processes are the Lyocell and Viscose processes, that we described in detail in Chapter 1. Here we reiterate the differences in these processes by giving a brief description of them.

The Viscose process was developed over a century ago, in 1891. Here, cellulose pulp is reactively dissolved in sodium hydroxide base to form sodium cellulosate.[2] This solution is aged at 40 – 60°C such that the degree of polymerization (DP) of cellulose is reduced from 750-850 to 270-350. This results in a decrease in solution viscosity to processable values. Sodium cellulosate is then treated with carbon disulphide to form sodium cellulose xanthate, which is dissolved in dilute sodium hydroxide to form Viscose dope. Subsequently, the solution is extruded through spinnerets into a coagulation bath containing sulphuric acid and salts, $ZnSO_4$ and Na_2SO_4. The xanthate reacts vigorously with the acid solution and is neutralized to cellulose. The fiber thus obtained is washed and dried. Cellulose undergoes recrystallization during the spinning and coagulation steps. The Lyocell process is more recent, and was first commercialized in 1984.[2] Here, cellulose pulp is dissolved in an aqueous solution of N-Methylmorpholine N-oxide (NMMO). The cellulose in solution has a DP of 500-600.[1] The solution (called dope) is then extruded using spinnerets, across an air gap, into

a coagulation bath containing water. In the coagulation bath, water acts as a non-solvent for the cellulose and extracts NMMO to regenerate the cellulose fiber.

In this work, we examine similarities and differences in the structure and properties of fibers from Viscose and Lyocell processes. We begin by summarizing aspects that have been previously reported in the literature[3–5] and, that are consistent with data on fibers investigated here. When examined using a scanning electron microscope (SEM), there are significant differences in the shapes of the fiber cross-section for Viscose and Lyocell fibers (**Figure 3.2** a and b). Viscose fibers exhibit a highly irregular cross section (**Figure 3.2** a). Lyocell fibers do not show a perfectly circular cross-section either – however, they are significantly more regular than the Viscose fibers (**Figure 3.2** b). The shape of the cross-section is a consequence of the regeneration process and the difference between Viscose and Lyocell fibers has been previously reported.[2]

Further, in experiments where the fibers are dyed and examined in cross-section under an optical microscope, we observe that the Viscose fibers possess a radial skin layer that exhibits higher dye uptake than the core (**Figure 3.2** c). In contrast, we observe uniform dye uptake throughout the cross-section of Lyocell fibers (**Figure 3.2** d). Thus, not only are the Lyocell fibers more uniformly shaped in cross-section, there are also no radial gradients that are reflected in the dye uptake. Reports in the literature suggest that the regeneration process of Viscose fibers results in the formation of a skin layer with a lower crystallinity than the core, resulting in the observed radial differences.[6,7]
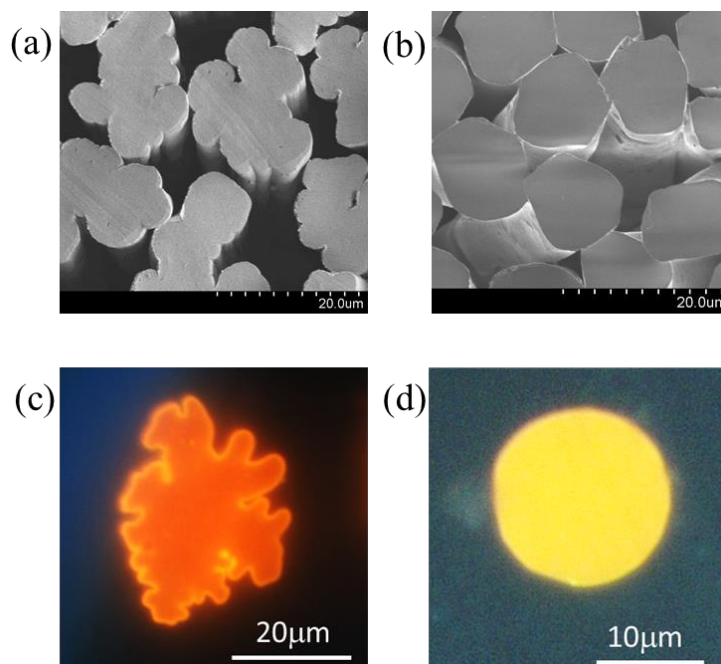
Figure 3.2 SEM images of the fiber cross sections for (a) Viscose and (b) Lyocell fibers. Representative optical microscopy images of dyed and microtomed cross section of (c) Viscose and (d) Lyocell fibers.

There are several reports that investigate the effect of regeneration processes on the structure and properties of cellulose fibers.[8–15] Jiang et al compared regenerated cellulose fibers made from Viscose, Lyocell and modifications of these processes.[9] They demonstrated that Lyocell fibers have higher specific modulus (viz. elastic modulus/specific gravity) and tenacity (viz. breaking load/linear density) in both dry and wet state, when compared with Viscose fibers. However, the strain at break is lower for Lyocell fibers relative to Viscose. They used wide-angle X ray diffraction (WAXD) to demonstrate that Lyocell fibers have a higher crystallinity relative to Viscose fibers and suggested that the higher modulus of the Lyocell fibers arises from their higher crystallinity. Reports have related the elongation at break to the crystallinity and crystalline orientation in cellulose fibers. Detailed analyses of the effects of processing parameters such as draw ratio, spinning speed etc. on properties and structure have been reported in the literature.[16–19] It has been shown that on increasing the spinning speed and draw ratio, the crystalline orientation increases. Fibers characterized by higher orientation fail at lower elongation relative to those with lower orientation, viz. spun at lower draw ratios.[20] On stretching, there is an increase in the orientation exhibited by fibers with a low initial orientation.[18,19] Previous studies have also reported the influence of wetting Lyocell and

Viscose cellulose fibers with water on their mechanical properties.[9,21,22] These reports indicate that the water uptake of Viscose fibers is higher relative to Lyocell. This results in a significant decrease in the tenacity of Viscose fibers on wetting. Since Lyocell fibers show a lower water uptake, the decrease in their wet state tenacity is lower.

The mechanical response of various cellulosic fibers have been described using phenomenological models as well as molecular mechanics.[18,23,24] These models typically capture the effect of molecular deformation and crystal domain orientation on the stress-strain behavior of these fibers. However, given the microstructural complexity of cellulose fibers, these models are inadequate to capture the behavior of cellulose fibers subjected to different mechanical histories. We reported (**Section 2.4.2**)[25] the development of a phenomenological model that accurately captures the mechanical response of semicrystalline fibers in the linear response regime. We demonstrated the use of this model to fit stress-strain, stress relaxation and recovery data for a wide variety of fibers, including natural fibers such as silk and regenerated cellulose as well as synthetic PET and PAN fibers. Notably, we demonstrated that for semicrystalline fibers with a glassy amorphous phase, the fit parameters could be directly related to microstructural features. Thus, this model provides important insights into the microstructural underpinnings of the mechanical response of glassy semicrystalline polymer fibers.

Here, we contrast the mechanical response of regenerated cellulose fibers prepared using Viscose and Lyocell processes. We subject Viscose and Lyocell fibers to mechanical deformation, and fit this data to our phenomenological model. The microstructural parameters obtained from this fit characterize the two fibers. At elongational strains of a few percent, regenerated cellulose fibers show a decrease in the slope of the stress-strain curve. This has been identified as the yield point in the literature.[26–28] We demonstrate that this does not represent a true yield point for either Viscose or Lyocell fibers. On wetting the fibers, there is a change in the apparent yield strain. The nature of this change is qualitatively different for Viscose and Lyocell fibers, indicative of structural differences between these fibers.

3.3   Material and Methods:

We perform experiments on commercial regenerated cellulose fibers manufactured using Lyocell and Viscose processes. These fibers were provided by Aditya Birla Science and Technology Company Pvt. Ltd. The linear mass density of Lyocell fibers is 1.15 ± 0.29 den and that of Viscose fibers is 1.2 ± 0.13 den. Viscose and Lyocell fibers are characterized by a crystallinity index of 0.3 and 0.4, respectively (from a ratio of intensity under crystalline peaks to total intensity in WAXD as described in **section 4.3.4**). Lyocell fibers show higher crystal orientation with a Hermans orientation parameter of 0.86, relative to 0.79 for Viscose. Experiments were performed on "dry" fibers, conditioned at 25ºC and 55% RH for over a day, as well as on fibers soaked in water for at least 30 minutes. During measurements on wet fibers, the fiber is kept in contact with a pool of water so that it does not dry out during the experiment.

3.3.1   Mechanical Measurements:

Fibers were subjected to different mechanical histories using the ARES G2 rheometer (TA Instruments). Specifically, we perform stress strain, cyclic loading/unloading, stress relaxation and stress recovery experiments. For each test, a single fiber is clamped in the torsion fixture of the rheometer using a paper frame set up as described by Gindl and co-workers[12] with gauge length between 10 and 11 mm. Each measurement is repeated at least 10 times and representative data are presented. We obtain the stress by dividing the force obtained from the rheometer by the average cross sectional area of the fiber.

Stress strain measurements are performed on single fibers stretched at a constant strain rate of 4×10^{-3} s^{-1} until failure. Cyclic loading/unloading experiments are performed by stretching a single fiber to a predetermined strain at a fixed rate (4×10^{-3} s^{-1}) after which the strain is decreased at the same rate to zero strain. These measurements are performed for different values of strains chosen below and above the apparent yield point. For stress relaxation measurements, fibers are stretched at a strain rate of 4×10^{-3} s^{-1} to a specified final strain. The strain is then held constant to monitor the evolution of stress. In stress recovery experiments, fibers are stretched to a final strain and are maintained at that strain for one hour. After one hour, strain on the fiber is decreased at 4×10^{-3} s^{-1} until the stress becomes zero. Subsequently, the fiber is held at that strain and the evolution of stress is monitored.

3.3.2   *Wide Angle X-Ray Diffraction (WAXD):*

WAXD measurements are made on fibers in dry state. The diameter of the X-ray spot is greater than the average fiber diameter – hence, WAXD measurements are made on a bundle of fibers. These fibers are combed to straighten them and are then clamped in the WAXD. All measurements are made using Rigaku R Axis IV++ equipped with a microfocus source (Cu K_α radiation, λ = 0.154 nm, 1.2 kW rotating anode generator).

We mount a stretching device (Linkam Tensile Stress Testing System - TST350) on the WAXD instrument to perform in situ diffraction measurements during stretching. WAXD measurement is performed first on combed, straightened fibers in the unstretched state at first; then the fibers are stretched at a strain rate of 4 x 10^{-3} s^{-1} to a specific value of final strain and are held at this strain for two days to allow the stress to relax to a plateau. Once the stress plateaus, WAXD is performed again on these stretched fibers (**Figure 3.3**).

2D air background is subtracted from the WAXD data obtained for each sample after normalizing for scattering time. 2D data is converted to 1D data using RIGAKU 2DP software.
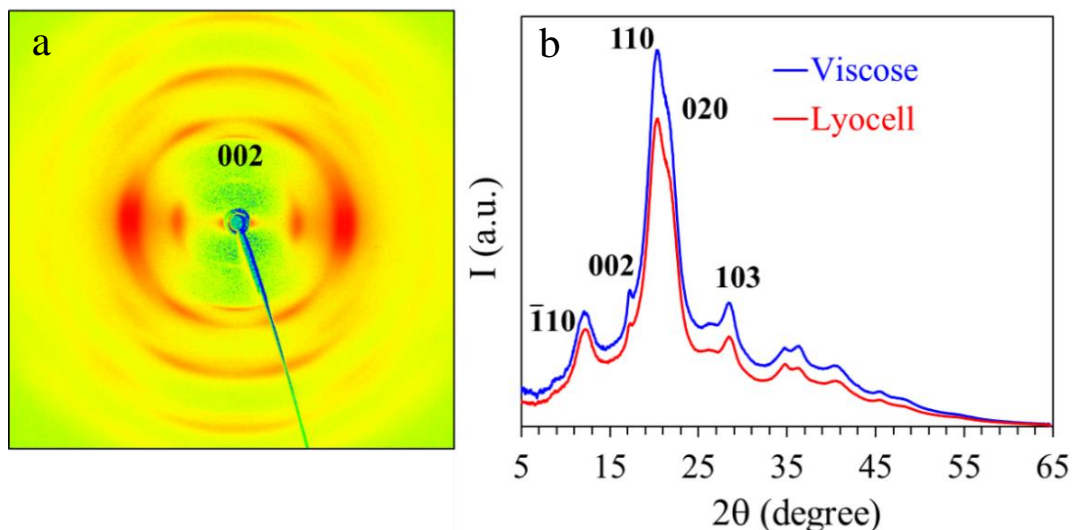
Figure 3.3 (a) 2D wide-angle x ray pattern showing highly anisotropic scattering from regenerated cellulose fibers. (b) 1D data for Lyocell and Viscose fibers indexed based on the literature.[19,29]

3.3.3 Model:

In previous chapter (**section 2.4.2**),[25] we described a phenomenological model to fit the linear mechanical response data for semicrystalline fibers with a glassy amorphous phase. As shown schematically in **Figure 3.4**, the model comprises of parallel connected units having a spring in series with a Kelvin-Voigt element. To describe the slow relaxation of the amorphous phase, we assume a variation in dashpot relaxation times (τ) across the units while the spring moduli (E_c and E_a) are constant. Phenomenological spring dashpot models have been used extensively in the literature to model different polymer fibers.[30–32] However, while previous models were typically able to capture the fiber response to only specific modes of mechanical deformation, the model in **Figure 3.4** has been demonstrated to capture stress-strain, stress relaxation and stress recovery for several natural and synthetic polymer fibers.
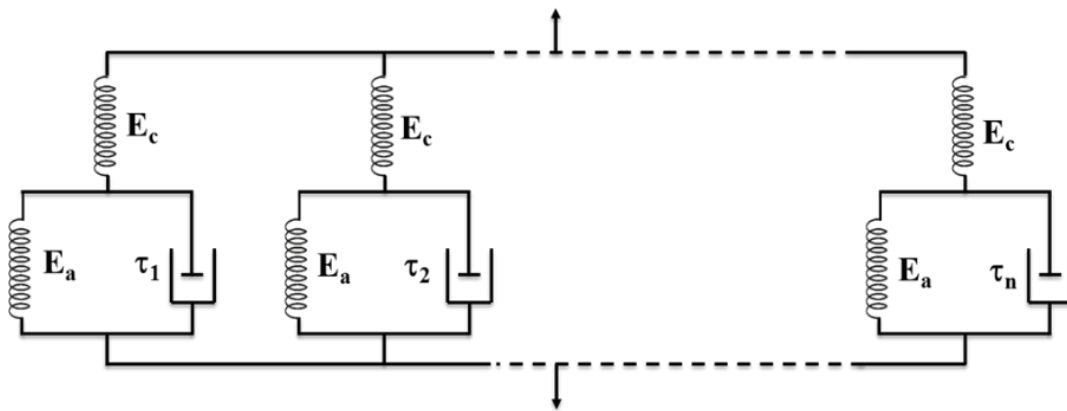
Figure 3.4 Representation of the phenomenological model employed to capture mechanical response of fibers.

Stress-strain and stress relaxation experimental data are fitted using this model using regularization, to obtain the fit parameters, E_c, E_a and $P(\tau)$, that characterize the fibers. We have shown that for semicrystalline fibers with a glassy amorphous phase, E_c corresponds to the crystalline phase while E_a and $P(\tau)$ characterize the response of the amorphous regions of the fiber. E_c from the model fit matches that obtained from independent WAXD experiments, while the activation energy from relaxation time spectra correspond to that reported for sub T_g β−relaxations.

3.4 Results and Discussions:

3.4.1 *Mechanical response and model fit:*

The stress required to elongate cellulose fibers is linear in the extensional strain at low strains. We stretch both Viscose and Lyocell fibers at a strain rate of 4×10^{-3} s^{-1} to a strain of 0.4% and 0.6% respectively, in the linear response region, and then hold for 3600 s and finally decrease the strain until the stress becomes zero (as indicated in the schematic in **Figure 3.5** a). The experimental data and the fit to the phenomenological model (depicted in **Figure 3.4**) is shown in **Figure 3.5** b. The model parameters from the fit, E_c and E_a are shown in **Table 3.1** and $P(\tau)$ are shown in **Figure 3.6**. Previously (Chapter 2),[25] we have shown that the moduli E_c and E_a can be associated with the crystalline and amorphous phases, respectively, and $P(\tau)$ represents the relaxation time spectrum in the glassy amorphous phase.
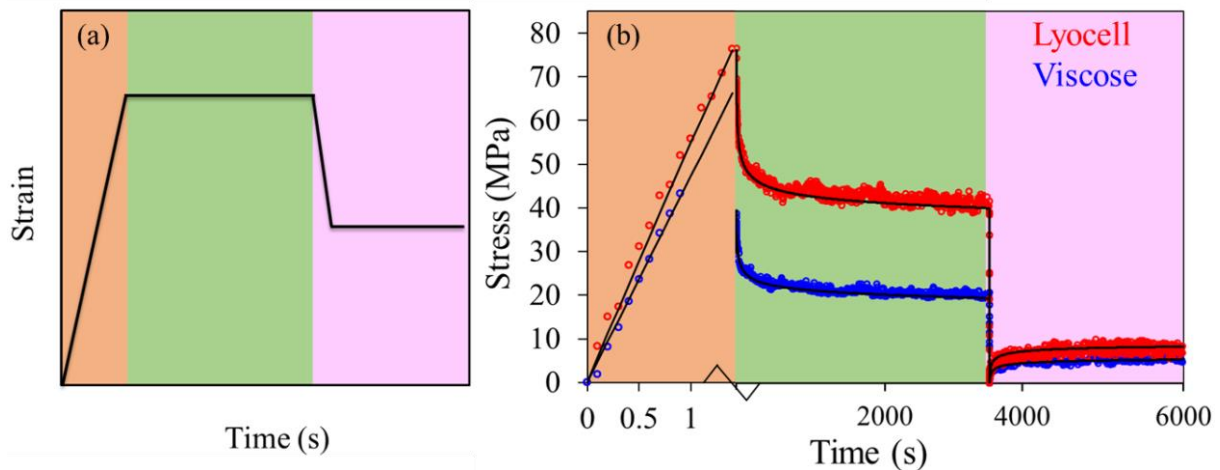
Figure 3.5 (a) Schematic of the extensional strain imposed on the fibers in stress-strain (light orange), stress relaxation (green) and stress recovery (lavender) experiments. (b) Experimental data for stress strain, stress relaxation and stress recovery experiments.

The mechanical response of Lyocell and Viscose fibers exhibit qualitative similarities – however, there are quantitative differences. The slope of the stress-strain data is higher for Lyocell fibers relative to Viscose. Consequently, the crystalline modulus (E_c) for Lyocell fibers (15 GPa) is higher than that for Viscose fibers (12.5 GPa) by about 20%. Here, E_c does not represent the modulus of the unit cell of a cellulose crystal[33–35] – rather, it corresponds to lumped parameter description of the crystalline regions that averages over the details of the semicrystalline microstructure. For both Viscose and Lyocell, E_c is about an order of

magnitude higher than the amorphous phase modulus, E_a. On holding the fibers at constant strain, the stress shows a slow logarithmic relaxation and then plateaus on holding for 3600 s (**Figure 3.5** b, middle). Subsequently, the strain is decreased at 4 x 10^{-3} s^{-1} until the stress goes to zero (at a strain of approximately 0.34% for Lyocell and 0.26% for Viscose). On holding at this strain, the stress is observed to recover (**Figure 3.5** b, right). A broad relaxation time spectrum, $P(\tau)$, is required to capture the slow stress decay and stress recovery. We observe that the data for both Viscose and Lyocell are fitted well by a bimodal $P(\tau)$ (**Figure 3.6**). We note that $P(\tau)$ is broader for Lyocell (relative to Viscose) and extends from over an order of magnitude smaller in time scales to over an order of magnitude higher.
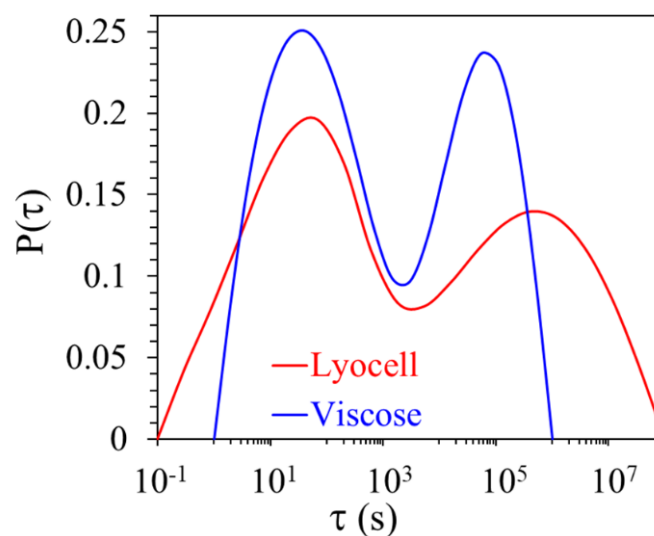
Figure 3.6 Relaxation time spectra for Lyocell and Viscose fibers obtained from the model fitting.

3.4.2 *Wide-angle X ray measurements:*

The moduli of the crystalline and the amorphous phases can be independently determined using WAXD. Cellulose fibers show uniaxial symmetry with the crystal c-axis along the fiber direction. Therefore, fiber stretching results in an increase in the c-axis unit cell dimension (and a corresponding decrease along the a and b axes). We calculate the strain on cellulose crystals from the change in the c lattice parameter of the fibers, as ε_c (= $\frac{\Delta c}{c_o}$). When a semicrystalline fiber is stretched, it has been shown that crystal and amorphous phases experience the same stress.[36–38] Therefore, the crystalline modulus can be calculated as a ratio of the experimentally imposed stress to the WAXD crystalline strain, ε_c. To estimate the

amorphous modulus, we perform WAXD on stretched fibers, after the stress has relaxed to a plateau value. In these experiments, we stretch cellulose fibers to a strain of 1% and then hold the fibers at that strain for over 2 days to ensure that stress relaxation is complete before we perform WAXD. After stress relaxation, the crystal and amorphous regions can be modeled as springs in series.[25,39–41] Therefore, the strain on amorphous phase is calculated as $\varepsilon_a = \varepsilon - \varepsilon_c$ and moduli of crystalline and amorphous phase are calculated as:

$$E_c = \frac{\sigma}{\varepsilon_c} \qquad E_a = \frac{\sigma}{\varepsilon_a}$$

3.1

E_c and E_a obtained from WAXD for both fibers are shown in **Table 3.1**. We observe that these values are in reasonable agreement with those obtained from model fits to the mechanical data. This supports our assertion that the model parameters, E_c and E_a, characterize the crystal and amorphous regions, respectively, of the semicrystalline fiber. We note that our model represents a minimal description of the semicrystalline state, and does not explicitly account for the degree of crystallinity, crystal orientation, spatial variations in microstructure, etc. Therefore, E_c and E_a, represent effective moduli that present a lumped description of the complex semicrystalline microstructure of the fibers. Therefore, we attribute the higher value of E_c for Lyocell to the higher degree of crystallinity and crystal orientation that one associates with this process (relative to Viscose). Similarly, we speculate that the higher value of E_a might correspond to greater coupling between the crystal and amorphous states in the more crystalline Lyocell fiber that results in greater constraints on mobility of the glassy amorphous phase.

Table 3.1 Crystalline and amorphous moduli from model fitting and WAXD.

		Moduli from fitting (GPa)	**Moduli from WAXD (GPa)**
Lyocell	E_c	15.00	16.10
	E_a	2.05	1.91
Viscose	E_c	12.50	14.2
	E_a	1.10	1.78

The glassy amorphous phase in regenerated cellulose fibers is known to be characterized by significant structural heterogeneity. Manabe et. al.[42] have demonstrated that regenerated cellulose fibers obtained from different processes exhibit several distinct dynamical mechanical absorptions. They suggest that the amorphous phase in regenerated cellulose can be characterized by five different dynamical environments that differ in the extent of intra- and intermolecular hydrogen bonding, and by the presence of absorbed water. Further, it has been reported in the literature that polysaccharides (including regenerated cellulose fibers) exhibit different modes (β, β_{wet}, σ, γ) in dielectric relaxation spectra below the glass transition temperature.[42–44] Specifically, the β_{wet} relaxation is attributed to the presence of water in cellulose at room temperature, and is present in addition to the β relaxation. It has been shown that even vacuum dried samples contain a small amount of moisture that is associated with the cellulose, resulting in β_{wet} relaxation.[43] We note that our measurements on "dry" fibers correspond to fibers conditioned at a relative humidity of 55% at room temperature. Therefore, we anticipate that the amorphous phase is characterized by structural heterogeneity in hydrogen bonding and absorbed water. The breadth observed for $P(\tau)$ is consistent with this heterogeneity and it is also not particularly surprising that $P(\tau)$ is not monomodal. However, given the structural complexity in regenerated cellulose, it is not possible to associate $P(\tau)$ with any specific structural motif.

3.4.3 *Temperature dependent mechanical response:*

Temperature dependent measurements were performed on single fibers, using the ARES-G2 rheometer equipped with a forced convection oven. The forced convection oven controls the temperature of dry air that is allowed to flow over the sample, so that the required temperature is attained. Fibers are allowed to equilibrate in the oven atmosphere, characterized by dry air at the set temperature for at least two hours before measurements.

Stress-strain and stress relaxation experiments are performed at different temperatures and the data is fitted to the model (**Figure 3.4**) to obtain fit parameters, E_c, E_a and $P(\tau)$. Temperature dependent $P(\tau)$ for Lyocell and Viscose are shown in **Figure 3.7** a and b, respectively. Temperature dependent moduli, E_c and E_a are shown in **Figure 3.7** c. On heating, we observe a progressive narrowing of $P(\tau)$ for both Lyocell and Viscose. The mode at higher τ moves to shorter times on heating and appears to merge with the lower τ peak,

such that eventually $P(\tau)$ becomes monomodal. The transition to faster monomodal relaxation happens at lower temperature for the Viscose fibers and $P(\tau)$ is monomodal already at 393 K. For Lyocell, $P(\tau)$ becomes monomodal at a temperature between 393 and 473 K. We note that the transition from bimodal $P(\tau)$ at low temperatures to monomodal on heating is reversible, suggesting that heating does not result in chemical degradation of the cellulose fibers. In the literature, it has been demonstrated that the β_{wet} mode disappears above 423 K due to drying of the fibers. Thus, a temperature dependent transition occurs from multimodal low temperature relaxation spectra to monomodal at high temperature.[43–45] Our results are broadly consistent with these reports. Our data also suggests that higher temperatures are required for the higher crystallinity Lyocell fibers to transition to faster monomodal relaxations.
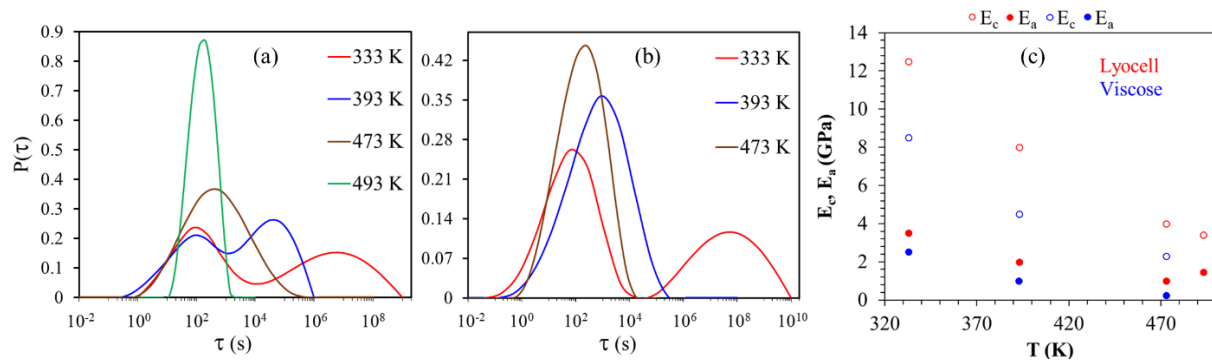
Figure 3.7 Relaxation time spectra for (a) Lyocell and (b) Viscose at increasing temperatures. (c) Variation in the values of E_c and E_a obtained from the model with temperature.

There is a monotonic decrease in both E_c and E_a for Lyocell and Viscose on heating (**Figure 3.7** c). There is a 3-4 fold reduction in the value of crystalline modulus on heating from 333 to 473 K, for both Lyocell and Viscose. At all temperatures, $E_c > E_a$. The values of E_c and E_a for Lyocell are higher than the corresponding values for Viscose. A decrease in the solid modulus of regenerated cellulose fibers on heating has been previously reported.[46] Molecular dynamics simulations[47] of the temperature dependent modulus of crystalline unit cells in native cellulose indicate conformational changes in cellulosic chains present in the unit cell. There is thermal expansion in the unit cell on heating and a decrease in the hydrogen bonding, resulting in a decrease in the crystalline modulus. We anticipate that similar

processes take place in regenerated cellulose on heating. A decrease in the crystalline modulus and conformational changes in the cellulose chains result in the observed decrease in E_c, the effective modulus that characterizes the crystalline phase. The decrease in E_a is consistent with the increased motional freedom in the glassy amorphous phase indicated by the temperature dependent $P(\tau)$.

3.4.4 *Apparent yield of fibers on stretching:*

On stretching, there is a decrease in the slope of the stress-strain curve for Lyocell fibers above a strain of 1.2% and for Viscose fibers above a strain of 1.3% (**Figure 3.8** a). Stress increases linearly above the critical strain until the fiber fails. Lyocell and Viscose show qualitatively similar response – however, as in the linear response region, there are quantitative differences above the critical strain as well. This critical strain has been previously reported and it has been suggested that this is a consequence of plastic yielding of the fiber.[26,28] Therefore, it is referred to as the fiber yield point in the literature. The critical strain is very reproducible across different fibers produced using one particular process, and the values that we obtain are comparable to those reported in the literature.[12,17,28,48] Therefore, the critical strain appears to be a function of the fiber microstructure that develops during the regeneration process.

When Lyocell or Viscose fibers are stretched to a strain (= 4%, rate = 4 x 10^{-3} s^{-1}) higher than the critical value, we observe a decrease in slope of the stress-strain curve at the critical strain, followed by a subsequent monotonic increase (**Figure 3.8** b, c). On unloading the fiber at the same rate, we observe that the stress does not trace the same path. Rather, it decays to zero at a strain of about 2%. Thus, there is residual strain in the fiber on unloading. When the same fiber is stretched in a second loading cycle, the stress does not increase immediately since the residual strain results in slack in the fiber. Once the strain exceeds the slack in the fiber, stress increases with strain, at a slope comparable to the low strain elastic modulus of the original fiber (**Figure 3.8** b, c). At a nominal strain of 4% (relative to the original fiber length), the fiber shows the same value of stress in the second loading cycle as in the first. On unloading the fiber after the second cycle of stretching, the stress decreases along the same path as for the first unloading cycle (**Figure 3.8** b, c). Thus, there appears to be a qualitative change in the stress-strain response of the fibers once it is stretched beyond the critical strain. This behavior is qualitatively similar for Lyocell and Viscose fibers. We now perform stress-strain measurements on a fiber that was stretched to 4% strain, viz. above the critical strain,

and was then unloaded and kept in the unloaded state for a long time (1 day in our experiments). We observe that the stress-strain curve for this sample is unchanged from the original sample (**Figure 3.8** b, c). Therefore, the change in both Lyocell and Viscose fibers due to "yielding" when they are strained to above the critical strain is not a permanent plastic deformation. Rather, the fiber is able to recover to its original state over an extended period of time. This observation suggests that, in contrast to what has been suggested in the literature,[26,28] it is not appropriate to term the critical strain as the yield point for the fiber. Therefore, we refer to this strain as the apparent yield point.
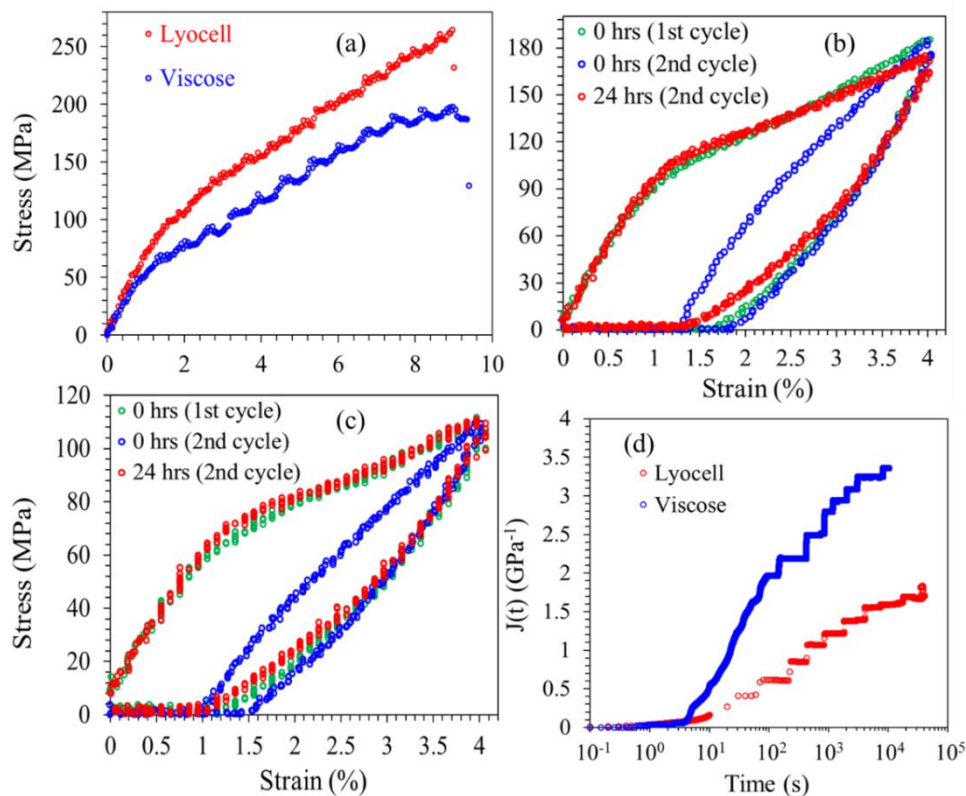
Figure 3.8 (a) Stress vs strain data for dry fibers. Cyclic loading/unloading performed on (b) Lyocell and (c) Viscose fibers immediately after the first cycle and 24 hrs later. (d) Creep compliance for Lyocell and Viscose fibers unloaded to 6 MPa after loading beyond critical strain.

Since the kinetics of structural recovery in fibers stretched above the critical strain are very slow, we use creep measurements to quantify the time-dependent changes. Here, a fiber is stretched to a strain greater than the critical strain and is then unloaded to zero stress.

Subsequently, we impose a small probe stress on the fiber ($\sigma = 6$ MPa in our experiments) and observe the change in fiber strain with time. We maintain the fiber at constant stress and observe that the strain decreases with time as can be seen from the creep compliance ($J = \frac{|\varepsilon(t)|}{\sigma}$) (**Figure 3.8** d). We observe a slow, logarithmic increase in creep compliance with time suggesting that the structural recovery of the fiber after apparent yield is slow and is characterized by a wide distribution of time scales. We notice that the strain recovers faster in case of Viscose fibers than for Lyocell fibers. However, for both Viscose and Lyocell, there is no permanent set and the fibers recover over a long time. The nature of the structural change in the fiber at the apparent yield point and of the slow recovery are not known at this time and require further investigation.

3.4.5   *Cyclic loading/unloading measurements to investigate the apparent yield point:*

When we stretch either Lyocell or Viscose fibers to a strain (= 0.4%) below the critical strain, we observe that the stress during unloading traces the same path as during loading (**Figure 3.9** a). Both elongation and unloading are performed at a strain rate of 4×10^{-3} s^{-1}. Thus, fibers elongated to strains lower than the critical strain recover elastically. On stretching the fibers to strains (= 4%) exceeding the critical strain, we observe apparent yield on loading and a residual strain on unloading (**Figure 3.9** b). When the fiber is immediately subjected to a second loading-unloading cycle, we no longer observe yielding during the loading step. We observe that during loading the fiber during the second cycle, the slack in the fiber, viz. the strain at which the stress increases above zero is lower than the residual stress during unloading in the first cycle. This is consistent with the literature.[26,27] Over subsequent cycles of loading and unloading the same fiber, we observe that the slack in the fiber during loading (relative to the first cycle) becomes equal to the residual strain on unloading. Thus, the stress-strain curve for loading-unloading cycles forms a loop, and there is hysteresis between loading and unloading (**Figure 3.9** b). In all the cycles, the maximum stress observed on stretching to 4% strain remains the same as in the first loading experiment.

We perform cyclic loading/unloading experiments at different value of imposed strain (ε_m) and plot the experimentally observed residual strain (ε_r) versus the imposed strain (**Figure 3.9** c). A fresh fiber is used for each experiment at a different value of ε_m. At low imposed strains, we see elastic fiber response and the residual strain is zero. Extrapolating the residual strain to zero linearly allows us to determine the critical point for apparent yield for the fibers. We confirm that this value of strain is the same as that obtained from the kink in the

stress-strain plot (=1.2% and 1.3% for Lyocell and Viscose, respectively), viz. the apparent yield point for the fiber. In all these experiments, both Viscose and Lyocell fibers show the same qualitative behavior.
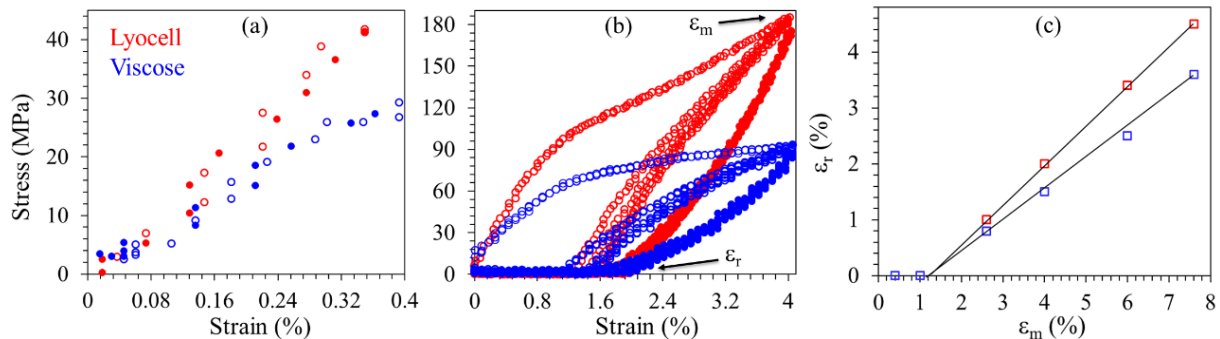
Figure 3.9 Cyclic loading/unloading experiments performed (a) below the critical strain (at 0.4%) and (b) above critical strain (at 4%) (Unfilled circles – loading, filled circles - unloading). (c) Variation of the residual strain with the maximum loading strain. Black line is the extrapolation of data points.

We now repeatedly stretch a single fiber and cycle it to progressively increasing strains above the apparent yield (**Figure 3.10**). We reiterate that the apparent yield strain is very reproducible and is a characteristic of the regeneration process. The values of the apparent yield obtained in our experiments are consistent with the values reported in the literature.[12,17,28,48] In our experiment, we first stretch Lyocell and Viscose fibers to a strain of 4% (above the apparent yield ≈ 1%), corresponding to a maximum stress, σ_1 (= 125 MPa for Viscose and = 230 MPa for Lyocell fibers, **Figure 3.10** a). We then unload the fiber and then stretch it out so that the slack in the fiber is removed. The fiber is then subjected to a second stretching cycle to a strain of 5% (higher than in the first cycle). We observe that the stress increases smoothly (and approximately linearly) until σ_1 and then exhibits a kink beyond which the slope of the stress-strain curve decreases (**Figure 3.10** b). Thus, the apparent yield point is now defined by the memory of the maximum stress experienced by the fiber in the previous loading cycle. We repeat this process by stretching the fiber through two more cycles, to strains of 6.2% for Lyocell and 6.8% for Viscose (**Figure 3.10** c) and 7% for Lyocell and 8% for Viscose (**Figure 3.10** d). As in the second cycle, we observe that the position of the apparent yield strain keeps shifting with each cycle and is defined by the maximum stress experienced in the previous cycle. Further, the slopes of the initial (before

kink) and post apparent yield stress-strain data is approximately preserved for each cycle. Therefore, the "low strain" fiber modulus remains the same for all cycles, independent of the apparent yield point. Thus, our data suggests that the apparent yield strain is characteristic of the fiber structure. The fiber structure set by regeneration and the spinning process determines the apparent yield of the as spun fiber. On stretching the fiber beyond the apparent yield, there is a change in fiber structure that encodes the memory of the maximum stress experienced by the fiber. In subsequent stretching cycles, the apparent yield moves to higher strains determined by the maximum stress in the previous cycle. This memory decays slowly, logarithmically in time, eventually recovering the apparent yield determined by the regeneration and spinning processes.
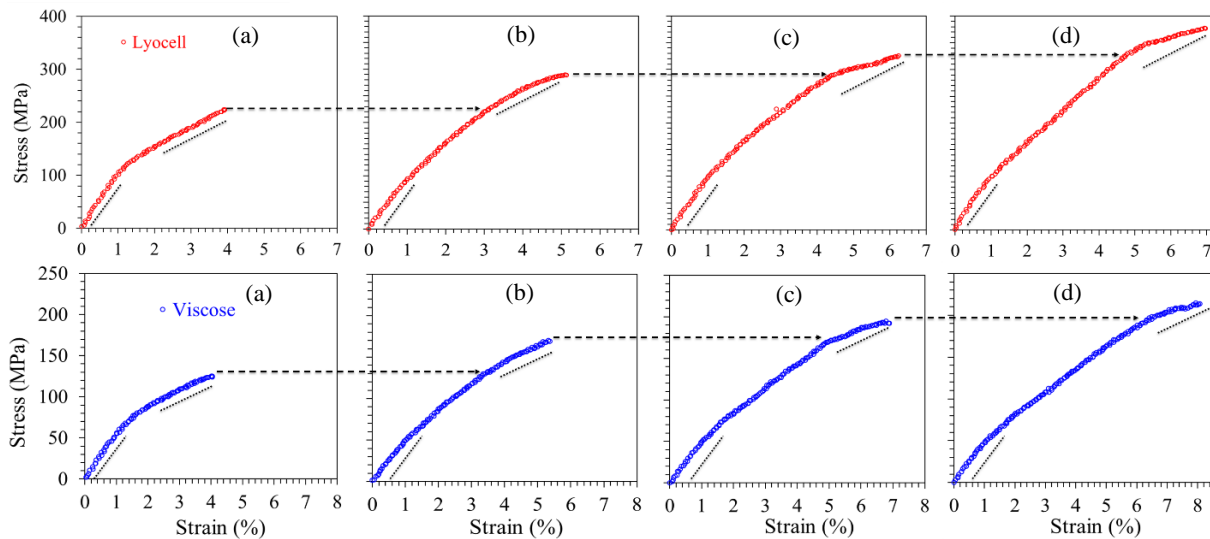
Figure 3.10 Single fibers loaded to different increasing strains in different cycles. Black dashed arrows show shift in the position of kink.

It is remarkable that the mechanical response of Lyocell and Viscose fibers are qualitatively similar, despite the differences in cellulose molecular weight, process differences and structural differences (manifested in the cross-sectional shape of the fibers and the radial variations in their semicrystalline microstructure). In the final section, we investigate the effect of wetting cellulose fibers with water, and show that this reveals qualitative differences between Lyocell and Viscose fibers.

3.4.6 Mechanical response of wet fibers:

On wetting with water, there is a dramatic decrease in the modulus of both Viscose and Lyocell fibers. The modulus of Viscose fibers decreases by about an order of magnitude from the dry state, while there is a 3.6-fold decrease for Lyocell fibers (**Figure 3.11** a). Further, there is a qualitative change in the shape of the stress strain curve for fibers soaked in water. Unlike the dry fibers, we no longer observe a well-defined apparent yield strain. Therefore, it is not clear from the stress-strain data if wet fibers experience apparent yielding.

We now perform repeated cycles of loading/unloading experiments on the wet fibers. For low values of strain (for example, 1%, **Figure 3.11** b), we observe that the decrease in stress on unloading a fiber follows the same path as during loading. Thus, similar to the case of dry fibers, there is an elastic region at low strain. When fibers are subjected to higher strains (for example, 8%, **Figure 3.11** c), we observe that the decrease of stress on unloading no longer follows the same path as the increase on stretching. Similar to the case of the dry fibers, the stress decreases to zero at a non-zero residual strain. When wet fibers subjected to high strains are unloaded and held in the unloaded state, we observe slow logarithmic recovery. However, the rate of recovery is so slow that we never observe full recovery in case of wet fibers.

To determine the critical apparent yield strain in wet fibers, we obtain the residual strain (ε_r) obtained during unloading when the fiber is subjected to the first loading/unloading cycle. When ε_r is plotted as a function of the imposed strain on the fibers, ε_m, we obtain the apparent yield by extrapolating ε_r to zero (**Figure 3.11** d). Thus, even when there is no abrupt change in the slope of the stress-strain curve, we can obtain the apparent yield strain from the extrapolation of ε_r to zero. Using this, we observe that the apparent yield strain for Lyocell fibers is estimated as 1.2%, similar to the value for the dry fiber. In contrast, there is a large increase in the apparent yield strain for the Viscose fibers, with wet fibers showing an apparent yield of 4.8%, as compared to 1.3% for dry fibers.
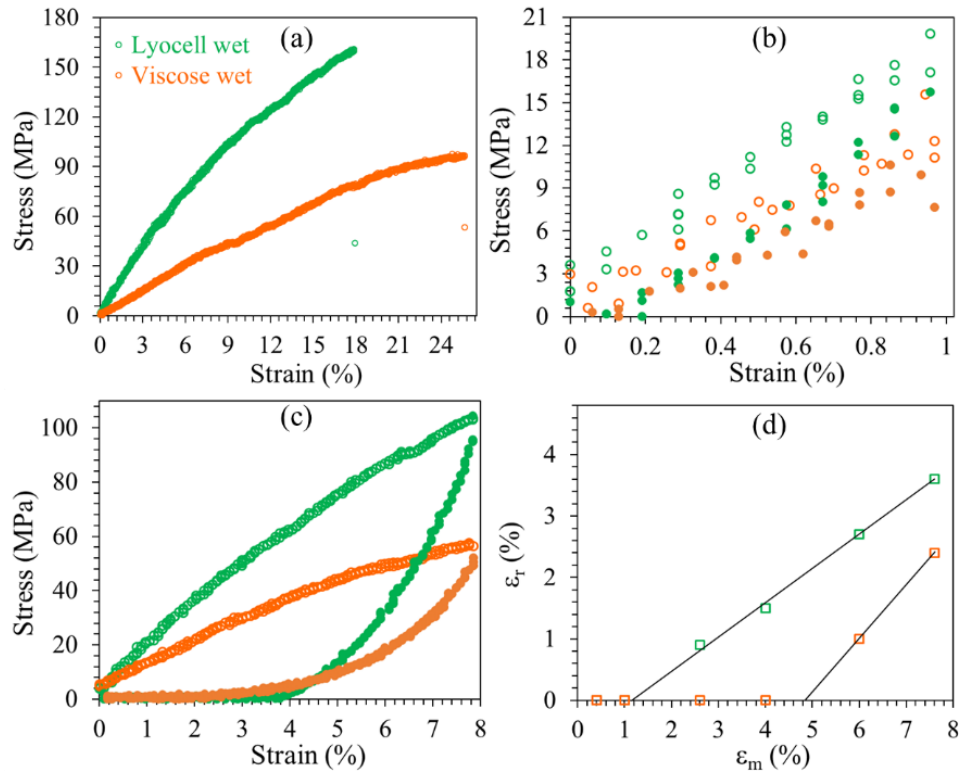
Figure 3.11 (a) Stress vs strain data for water soaked fibers. Wet fibers cyclic loading (b) at low strains and (c) at high strains. (Unfilled circles – loading, filled circles - unloading) (d) Extrapolation of residual strain data for fibers in wet state.

What are the structural underpinnings of the differences in behavior of the apparent yield strain on wetting for Lyocell and Viscose fibers? It is not possible to directly address this question based on the existing data. However, we note that the higher decrease in the wet state modulus relative to dry for the Viscose fibers, and the increase in apparent yield strain on wetting are consistent with the picture of Viscose fibers having a lower crystallinity and less constrained glassy amorphous phase. Additionally, when we compared the humidity uptake of both fibers (by conditioning them at 95% humidity at 30ºC), we observed that Viscose fibers absorb 28-29% moisture by weight (relative to oven dried samples). In contrast, Lyocell fibers absorb 22-24% moisture, clearly lower than Viscose. Absorption of higher amounts of moisture by the Viscose probably results in significant changes in the hydrogen bonded structure in the glassy amorphous phase and consequently, in a greater enhancement in mobility. It is possible that the change in the apparent yield strain on wetting is another manifestation of such structural differences in the organization of semicrystalline microstructure in Viscose and Lyocell fibers.

3.5 Conclusions:

Structural differences between regenerated cellulose fibers prepared using the Lyocell and Viscose processes do not result in qualitative differences in the stress-strain, stress relaxation and stress recovery behavior. This is remarkable since, even at a gross macroscopic level, there are remarkable differences between Lyocell and Viscose fibers: Lyocell fibers are characterized by a smooth, approximately circular cross-section and are radially uniform, while Viscose fibers have a highly irregular cross-section and have a high crystallinity core surrounded by a lower crystallinity shell. Our results suggest that the mechanical response of semicrystalline fibers in the linear response region can be adequately described by a minimal model that invokes only crystal-amorphous coexistence. Fitting the mechanical data on the fibers to a model reveals quantitative differences between the fibers. Lyocell fibers have a higher crystalline and amorphous moduli and a broader relaxation spectrum relative to Viscose. We attribute these differences to a higher degree of crystallinity that is more intimately associated with the glassy amorphous phase in Lyocell. This is consistent with higher water absorption in Viscose fibers and with a dramatic wetting-induced change in apparent yielding. Indeed, the change in the apparent yield strain on wetting Viscose is the only qualitative difference relative to Lyocell (where wetting does not significantly influence the apparent yield strain). We also explore the apparent yield observed on subjecting cellulose fibers to large strains. In the literature, the critical strain above which there is a decrease in the stress-strain curve of cellulose fibers has been identified as the yield point. However, we demonstrate for the first time that this does not represent a true plastic yield process. Fibers stretched above this apparent yield exhibit slow, logarithmic recovery over about a day, to recover their original as-spun state. The structural implications of the apparent yield strain are unclear at this time. When Lyocell or Viscose fibers are stretched above the apparent yield point, the fibers retain the memory of this mechanical history. This memory is not permanent but decays logarithmically as the fiber regains its original structure.

3.6 References:

(1)   Zhang, S.; Chen, C.; Duan, C.; Hu, H.; Li, H. Regenerated Cellulose by the Lyocell Process , a Brief Review of the Process and Properties. *BioResources* **2018**, *13(2)*, 4577–4592.

(2)   Woodings, C. *Regenerated Cellulose Fibres*; Woodhead Publishing Limited, 2001.

(3)   Schuster, K. C.; Aldred, P.; Villa, M.; Baron, M.; Loidl, R.; Biganska, O.; Patlazhan, S.; Navard, P.; Rüf, H.; Jericha, E. Characterising the Emerging Lyocell Fibres Structures by Ultra Small Angle Neutron Scattering (USANS). *Lenzinger Berichte* **2003**, *82*, 107–117.

(4)   Rous, M. A.; Manian, A. P.; Röder, T.; Lichtscheidl, I.; Schuster, K. C. Fluoresent Molecular Probes for the Characterization of Fibre Structure and Distribution of Textile Resin Finishing on Lyocell. *Lenzinger Berichte* **2004**, *83*, 92–98.

(5)   Abu-Rous, M.; Ingolic, E.; Schuster, K. C. Visualisation of the Nano-Structure of Tencel®(Lyocell) and Other Cellulosics as an Approach to Explaining Functional and Wellness Properties in Textiles. *Lenzinger Berichte* **2006**, *85*, 31–37.

(6)   Morehead, F. F.; Sisson, W. A. Skin Effect in Viscose Rayon. *Text. Res. J.* **1945**, *15*, 443–450.

(7)   Kato, K. Reactive Dye Staining for Differentiation of Skin and Core of Viscose Rayon Fibers. *Text. Res. J.* **1959**, *15*, 661–664.

(8)   Lenz, J.; Schurz, J.; Wrentschur, E. Properties and Structure of Solvent-Spun and Viscose-Type Fibres in the Swollen State. *Colloid Polym. Sci.* **1993**, *271* (5), 460–468.

(9)   Jiang, G.; Huang, W.; Li, L.; Wang, X.; Pang, F.; Zhang, Y.; Wang, H. Structure and Properties of Regenerated Cellulose Fibers from Different Technology Processes. *Carbohydr. Polym.* **2012**, *87* (3), 2012–2018.

(10)   Cai, J.; Zhang, L.; Zhou, J.; Qi, H.; Chen, H.; Kondo, T.; Chen, X.; Chu, B. Multifilament Fibers Based on Dissolution of Cellulose in NaOH/Urea Aqueous Solution: Structure and Properties. *Adv. Mater.* **2007**, *47* (22), 8676–8683.

(11)   Gindl, W.; Martinschitz, K. J.; Boesecke, P.; Keckes, J. Orientation of Cellulose Crystallites in Regenerated Cellulose Fibres under Tensile and Bending Loads. *Cellulose* **2006**, *13* (6), 621–627.

(12)   Adusumalli, R.-B.; Muller, U.; Weber, H.; Roeder, T.; Sixta, H.; Gindl, W. Tensile Testing of Single Regenerated Cellulose Fibres. *Macromol. Symp* **2006**, *244*, 83–88.

(13)   Kim, D. B. Dry Jet-Wet Spinning of Cellulose/N-Methylmorpholine N-Oxide Hydrate

Solutions and Physical Properties of Lyocell Fibers. *Text. Res. J.* **2005**, *75* (4), 331–341.

(14)   Fink, H. P.; Weigel, P.; Purz, H. J.; Ganster, J. Structure Formation of Regenerated Cellulose Materials from NMMO-Solutions. *Prog. Polym. Sci.* **2001**, *26* (9), 1473–1524.

(15)   Fink, H. P.; Philipp, B.; Paul, D.; Serimaa, R.; Paakkari, T. The Structure of Amorphous Cellulose as Revealed by Wide-Angle X-Ray Scattering. *Polymer.* **1987**, *28* (8), 1265–1270.

(16)   Bryant, G. M.; Walter, A. T. Stiffness and Resiliency of Wet and Dry Fibers as a Function of Temperature. *Text. Res. J.* **1959**, *29* (3), 211–219.

(17)   Kong, K.; Eichhorn, S. J. The Influence of Hydrogen Bonding on the Deformation Micromechanics of Cellulose Fibers The Influence of Hydrogen Bonding on the Deformation Micromechanics of Cellulose Fibers. *J. Macromol. Sci. Part B Phys.* **2005**, *44* (6), 1123–1136.

(18)   Kong, K.; Davies, R. J.; McDonald, M. A.; Young, R. J.; Wilding, M. A.; Ibbett, R. N.; Eichhorn, S. J. Influence of Domain Orientation on the Mechanical Properties of Regenerated Cellulose Fibers. *Biomacromolecules* **2007**, *8* (2), 624–630.

(19)   Jiang, G.; Yuan, Y.; Wang, B.; Yin, X.; Mukuze, K. S.; Huang, W.; Zhang, Y.; Wang, H. Analysis of Regenerated Cellulose Fibers with Ionic Liquids as a Solvent as Spinning Speed Is Increased. *Cellulose* **2012**, *19* (4), 1075–1083.

(20)   Kong, K.; Wilding, M. A.; Ibbett, R. N.; Eichhorn, S. J. Molecular and Crystal Deformation of Cellulose: Uniform Strain or Uniform Stress? *Faraday Discuss.* **2008**, *139*, 283–298.

(21)   Kreze, T.; Strnad, S.; Stana-Kleinschek, K.; Ribitsch, V. Influence of Aqueous Medium on Mechanical Properties of Conventional and New Environmentally Friendly Regenerated Cellulose Fibers. *Mater. Res. Innov.* **2001**, *4* (2–3), 107–114.

(22)   Ganser, C.; Kreiml, P.; Morak, R.; Weber, F.; Paris, O.; Schennach, R.; Teichert, C. The Effects of Water Uptake on Mechanical Properties of Viscose Fibers. *Cellulose*

2015, *22* (4), 2777–2786.

(23)   Eichhorn, S. J.; Young, R. J.; Davies, G. R. Modeling Crystal and Molecular Deformation in Regenerated Cellulose Fibers. *Biomacromolecules* **2005**, *6* (1), 507–513.

(24)   Zhang, S.; Wang, W.; Li, F.; Yu, J. Non-Linear Viscoelastic Behavior of Novel Regenerated Cellulose Fiber in Dry and Wet Condition. *Cellul. Chem. Technol.* **2013**, *47*, 353–358.

(25)   Sharma, A.; Kumaraswamy, G.; Thakre, S. Modeling the Universal Viscoelastic Response of Polymer Fibers. *Phys. Rev. Mater.* **2018**, *2* (6), 062601.

(26)   Meredith, R. 12—a Comparison of the Tensile Elasticity of Some Textile Fibres. *J. Text. Inst. Trans.* **1945**, *36* (7), T147–T164.

(27)   Meredith, R. 10—the Tensile Behaviour of Raw Cotton and Other Textile Fibres. *J. Text. Inst. Trans.* **1945**, *36* (5), T107–T130.

(28)   Gindl, W.; Keckes, J. Strain Hardening in Regenerated Cellulose Fibres. *Compos. Sci. Technol.* **2006**, *66* (13), 2049–2053.

(29)   Chen, X.; Burger, C.; Fang, D.; Ruan, D.; Zhang, L.; Hsiao, B. S.; Chu, B. X-Ray Studies of Regenerated Cellulose Fibers Wet Spun from Cotton Linter Pulp in NaOH/Thiourea Aqueous Solutions. *Polymer.* **2006**, *47* (8), 2839–2848.

(30)   Wilding, M. A.; Ward, I. M. Creep and Stress-Relaxation in Ultra-High Modulus Linear Polyethylene. *J. Mater. Sci.* **1984**, *19* (2), 629–636.

(31)   Krasnov, I.; Diddens, I.; Hauptmann, N.; Helms, G.; Ogurreck, M.; Seydel, T.; Funari, S. S.; Muller, M. Mechanical Properties of Silk: Interplay of Deformation on Macroscopic and Molecular Length Scales. *Phys. Rev. Lett.* **2008**, *100* (4), 2–5.

(32)   Manich, A. M.; Marino, P. N.; Castellar, M. D. D. E.; Saldivia, M.; Sauri, R. M. Viscoelastic Modeling of Natural and Synthetic Textile Yarns. *J. Appl. Polym. Sci.* **2000**, *76*, 2062–2067.

(33)   Mann, J.; Roldan-Gonzales, L. X-Ray Measurements of the Elastic Modulus of

Cellulose Crystals. *Polymer.* **1962**, *3*, 549–553.

(34) Nishino, T.; Takano, K.; Nakamae, K. Elastic Modulus of the Crystalline Regions of Cellulose Polymorphs. *J. Polym. Sci. Part B Polym. Phys.* **1995**, *33* (11), 1647–1651.

(35) Sakurada, I.; Ito, T.; Nakamae, K. Elastic Moduli of the Crystal Lattices of Polymers. *J. Polym. Sci. Part C Polym. Symp.* **1966**, *15* (1), 75–91.

(36) Sirichaisit, J.; Brookes, V. L.; Young, R. J.; Vollrath, F. Analysis of Structure/Property Relationships in Silkworm (*Bombyx Mori*) and Spider Dragline (*Nephila Edulis*) Silks Using Raman Spectroscopy. *Biomacromolecules* **2003**, *4* (2), 387–394.

(37) Yeh, W. Y.; Young, R. J. Molecular Deformation Processes in Aromatic High Modulus Polymer Fibres. *Polymer.* **1999**, *40* (4), 857–870.

(38) Young, R. J. Monitoring Deformation Processes in High-Performance Fibres Using Raman Spectroscopy. *J. Text. Inst.* **1995**, *86* (2), 360–381.

(39) Dulmage, W. J.; Contois, L. E. A Study of the Elastic Modulus and Extensibility of the Crystalline Regions in Highly Oriented Polymers. *J. Polym. Sci.* **1958**, *28* (117), 275–284.

(40) Sakurada, I.; Nukushina, Y.; Ito, T. Experimental Determination of the Elastic Modulus of Crystalline Regions in Oriented Polymers. *J. Polym. Sci.* **1962**, *57* (165), 651–660.

(41) Sakurada, I.; Ito, T.; Nakamae, K. Elastic Moduli of Polymer Crystals for the Chain Axial Direction. *Die Makromol. Chemie* **1964**, *75*, 1–10.

(42) Manabe, S.; Iwata, M.; Kamide, K. Dynamic Mechanical Absorptions Observed for Regenerated Cellulose Solids in the Temperature Range from 280 to 600 K. *Polym. J.* **1986**, *18* (1), 1–14.

(43) Einfeldt, J.; Meißner, D.; Kwasniewski, A. Contributions to the Molecular Origin of the Dielectric Relaxation Processes in Polysaccharides - The High Temperature Range. *J. Non. Cryst. Solids* **2003**, *320* (1–3), 40–45.

(44) Meißner, D.; Einfeldt, J.; Kwasniewski, A. Contributions to the Molecular Origin of

the Dielectric Relaxation Processes in Polysaccharides - the Low Temperature Range. *J. Non. Cryst. Solids* **2000**, *275* (3), 199–209.

(45) Einfeldt, J.; Kwasniewski, A.; Meißner, D.; Gruber, E.; Henricks, R. Dielectric Spectroscopic Results and Chemical Accessibility of Sulfite Pulps. *Macromol. Mater. Eng.* **2000**, *283*, 7–14.

(46) Zhou, S.; Tashiro, K.; Hongo, T.; Shirataki, H.; Yamane, C.; Ii, T. Influence of Water on Structure and Mechanical Properties of Regenerated Cellulose Studied by an Organized Combination of Infrared Spectra, X-Ray Diffraction, and Dynamic Viscoelastic Data Measured as Functions of Temperature and Humidity. *Macromolecules* **2001**, *34* (5), 1274–1280.

(47) Bergenstråhle, M.; Berglund, L. A.; Mazeau, K. Thermal Response in Crystalline Ibeta Cellulose: A Molecular Dynamics Study. *J. Phys. Chem. B* **2007**, *111* (30), 9138–9145.

(48) Gindl, W.; Martinschitz, K. J.; Boesecke, P.; Keckes, J. Changes in the Molecular Orientation and Tensile Properties of Uniaxially Drawn Cellulose Films. *Biomacromolecules* **2006**, *7* (11), 3146–3150.

Chapter 4.

In-situ Studies of the Viscose and Lyocell fibers to Mechanical Deformation: Comparison of the Microstructural Response of Dry and Wet Fibers

4.1 Graphical Abstract:
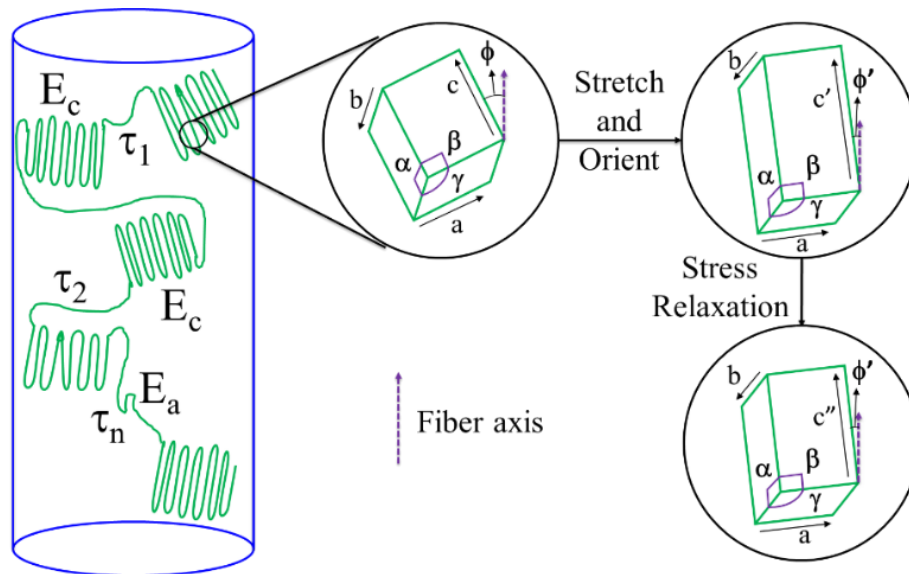
4.2 Introduction:

Cellulose is a natural plant-derived semicrystalline polymer found abundantly on earth.[1] Natural cellulose is converted into continuous fibers by dissolving it in a solvent and extruding it into a non-solvent.[2] During this process, the cellulose is recrystallized and regenerated by extrusion and drawing at high draw ratios.[2,3] Drawing induces orientation in the crystalline as well as in the amorphous phases. The extent of microstructural orientation depends on the processing parameters like, for example, the solvents used, stretching speeds, temperatures etc. The different processes for manufacturing regenerated cellulose fibers arise from differences in these parameters.[2,4–7] The two major manufacturing processes to produce commercial regenerated cellulose fibers are the Lyocell and Viscose processes. Briefly, the Viscose process is an old process that involves reaction of cellulose pulp sequentially with sodium hydroxide and carbon disulphide. The cellulose xanthate thus formed is extruded

through spinneret holes into an aqueous solution of H_2SO_4 with small concentrations of $ZnSO_4$ and Na_2SO_4. On the other hand, Lyocell is a relatively recent process in which an aqueous solution of N-Methylmorpholine N-oxide (NMMO) is utilized to dissolve cellulose pulp and form dope. This dope is then extruded using spinnerets, through an air gap, into water. Apart from the solvents used, there are other differences in the Lyocell and Viscose processes e.g. degree of polymerization of the dope, temperature etc. These differences have been commented on (**Section 1.2**) in the literature by us[8] and by other groups.[2,9,10]

Differences in the spinning process result in the structure of fibers developing differently. For example, as it has been reported[8,11,12] that Viscose fibers exhibit skin-core morphology where the skin is more oriented than the core of the fiber. Such radial variations are not observed in Lyocell fibers. There are other morphological differences between Viscose and Lyocell fibers as well, such as, the cross sectional shape of the fiber, microvoid structure in the fiber, etc.[5,13,14] These structural attributes have been studied using techniques like SEM, TEM, small angle X-ray scattering etc. Structural differences are also evident at smaller length scales. For example, it is widely known that Lyocell fibers have higher crystallinity and crystalline orientation than the Viscose fibers.[5,15–17]

The effects of the process differences that result in differences in structural features, and therefore in the properties of Viscose and Lyocell fibers have been extensively studied in literature.[3,5,18–24] We too have reported quantitative differences in the mechanical response Lyocell and Viscose fibers (chapter 3).[8,25] Specifically, we have demonstrated that Lyocell fibers exhibit higher moduli when compared to Viscose fibers, in accord with the previous literature. For both fibers, stress increases linearly with strain for small deformations. Remarkably, we observe that it is the crystals that respond to stretching the fiber. When the fiber is stretched, the crystal unit cell is stretched along the c-axis. We have reported that there is a shift in the meridional (002) peak to lower 2θ during stretching [green curve **Figure 2.5** (b)]. On holding at a constant strain, this peak moves to an intermediate 2θ (blue curve) indicating a decrease in crystalline strain during stress relaxation, but not complete recovery (**Section 2.4**).[25] We note that on holding both Viscose and Lyocell fibers at a specific constant strain, the stress relaxes logarithmically with time. A mechanical model, represented schematically in **Figure 2.1** (c), was proposed to capture the viscoelastic response from Viscose and Lyocell fibers. For dry fibers, where the glassy phase is amorphous, we have demonstrated that the model parameters can be related to microstructural features: for

example, E_c and E_a represent the effective crystalline phase and amorphous phase modulus, respectively. We obtain a distribution of relaxation times, $P(\tau)$ from a fit of the mechanical data to the model, that we relate to sub-T_g relaxations in regenerated cellulose.[25] For both Viscose and Lyocell fibers, we obtain a bimodal relaxation time distribution,[8] representing different complex relaxation modes. We note that the fit parameters present a "lumped" description of the semicrystalline microstructure, and account for the degree of crystallinity, crystal/amorphous orientations etc. While the same model provides an excellent fit to the data from both Viscose and Lyocell fibers, quantitative differences in the fit parameters capture the differences in the properties of Lyocell and Viscose fibers.

Here, we go beyond the learnings from our simplified model and explore the detailed microstructural response to fiber stretching. Specifically, we are interested in the effect of mechanical deformation on microstructural orientation. There have been previous attempts to study this. For example, Gindl and coworkers have studied the variation in crystalline orientation with strain.[26] They show that crystal orientation increases linearly with strain. Lenz and coworkers[15] have shown the effect of increase in tensile strength on crystalline and amorphous orientation. They reported a systematic increase in the orientation with tensile strength and modulus. Similarly, the effect of tensile modulus and elongation on break has been studied.[16] However, most of the previous work focuses on orientation change during elongation. The evolution of crystal and amorphous orientation during stress relaxation has largely been ignored. We demonstrate that an investigation of the development of orientation in both crystal and amorphous regions during fiber stretching and stress relaxation provides new insights into the microstructural response of Viscose and Lyocell fibers. We use in-situ WAXD and optical microscopic experiments to capture the effect of deformation on the molecular orientation of crystal and amorphous phase during stretching and stress relaxation measurements. We report that quantitative differences in the orientation response between Lyocell and Viscose fibers can be related to process-induced microstructural differences.

We also examine the mechanical response of water soaked regenerated cellulose fibers, that show qualitatively different trends as compared to dry fibers. The effect of water on the properties of regenerated cellulose fibers has been studied.[27–30] This is important since these fibers are used in textile applications where wet fiber properties have implications for product quality. Literature reports show a decrease in modulus on wetting for both Viscose and Lyocell fibers – however, Lyocell fibers are less affected by water when compared to

Viscose fibers. However, none of the studies report the crystal/amorphous orientation response for wet cellulose fibers and its comparison with the dry fibers. We compare the relaxation spectrum obtained for Viscose and Lyocell fibers from our model and demonstrate qualitative differences between the structural response of wet and dry regenerated cellulose fibers.

4.3 Materials and Methods

Regenerated cellulose fibers manufactured from Lyocell and Viscose processes were provided by Aditya Birla Science and Technology Company Pvt. Ltd. The linear mass density of Lyocell fibers is 1.15 ± 0.29 den and that of Viscose fibers is 1.2 ± 0.13 den. Experiments were performed on "dry" fibers, conditioned at 25ºC and 55% RH for over a day, as well as on "wet" fibers i.e. fibers soaked in water for at least 30 minutes and kept wet during the measurements. During measurements on wet fibers, the fibers are kept in contact with a pool of water so that they do not dry out during the experiment.

4.3.1 Mechanical Measurements:

Stress-strain and stress relaxation experiments were performed on wet fibers using the ARES G2 rheometer (TA Instruments). A single fiber was clamped in the torsion fixture of the rheometer using a paper frame set up as described by Adusumalli and co-workers[22] for each measurement. As described previously (**Sections 2.3.1**, **3.3.1**),[25] we obtain the stress by dividing the normal force from the rheometer by the average fiber cross sectional area. **Figure 4.1** schematically shows the experimental protocol for mechanical experiments. Stress-strain experiments (a) are performed by stretching a single fiber at a constant strain rate of 4×10^{-3} s^{-1}, until failure. For stress relaxation measurements (b), fibers are stretched at a strain rate of 4×10^{-3} s^{-1} to a specified final strain. The strain is then held constant to monitor the evolution of stress.
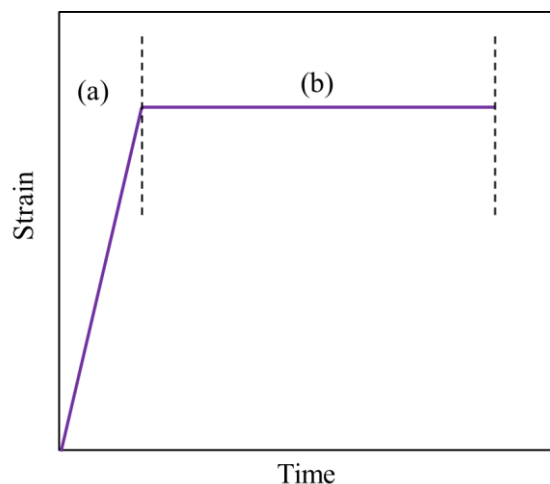
Figure 4.1 Experimental protocol for mechanical deformation during WAXD and birefringence experiments.

4.3.2   *Wide Angle X-Ray Diffraction (WAXD):*

WAXD measurements are made on a bunch of fibers in dry as well as wet state. Fibers are combed to straighten them and are then clamped in the WAXD. Measurements are made using Rigaku R Axis IV++ equipped with a microfocus source (Cu K_α radiation, $\lambda = 0.154$ nm, 1.2 kW rotating anode generator). For in situ diffraction measurements during deformation, a stretching device (Linkam Tensile Stress Testing System - TST350) is mounted on the WAXD instrument. WAXD measurement is performed on fibers in the unstretched state, on fibers stretched to different strains (**Figure 4.1** (a)) and while the stretched fibers are held at a constant strain (**Figure 4.1** (b)).

2D air background is subtracted from the WAXD data obtained for each sample after normalizing for sample absorption and scattering time. A representative 2D image of regenerated cellulose fibers is shown in **Figure 4.2** (a). 2D data is converted to 1D data as shown in **Figure 4.2** (b) using RIGAKU 2DP software. The peaks are indexed based on literature.[3,11]
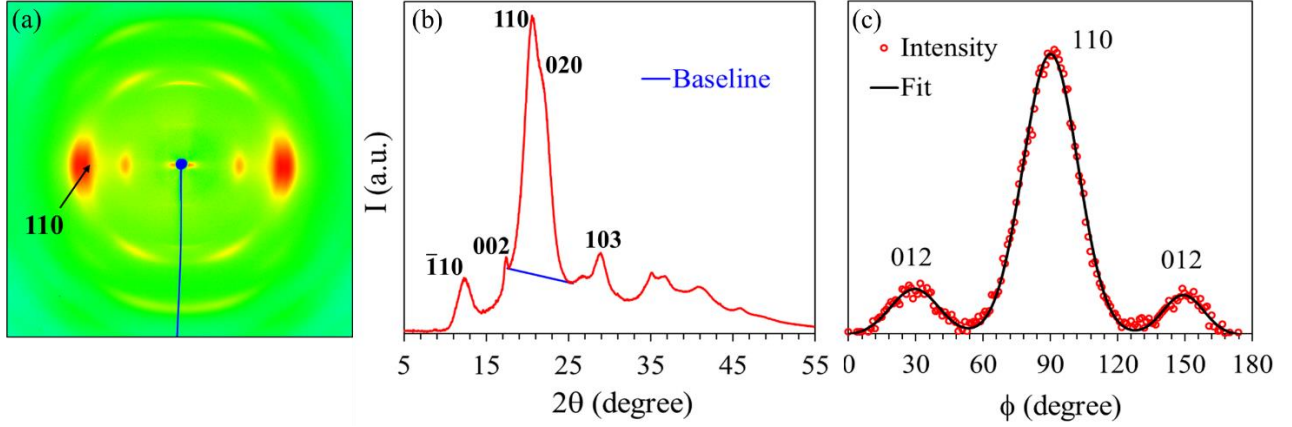
Figure 4.2 (a) 2D WAXD pattern of regenerated cellulose fibers (b) corresponding 1D data and baseline for separating amorphous scattering (c) azimuthal scan at $2\theta = 20.5^{\circ}$ fitted using three Gaussian functions.

4.3.3   *Calculations of Hermans orientation parameter (f_c):*

Crystalline orientation for peak 110 is calculated using Hermans orientation parameter (f_c). We perform azimuthal scans at $2\theta = 20.5^{\circ}$ (**Figure 4.2** (c)), which shows peaks from two crystal planes: 110 and 012. Scattering from the amorphous phase is obtained from the baseline of the 1D data at that 2θ and is subtracted from the azimuthal scan[31] as shown in **Figure 4.2** (b). We note that after subtracting the amorphous scattering, the azimuthal scan does not show any ϕ-independent scattered intensity, viz. we do not observe any scattering from unoriented crystals. We fit the azimuthal scan using three Gaussian functions as shown in **Figure 4.2** (c). Using only the fitted 110 Gaussian peak, $I_{110}(\phi)$, we calculate Hermans orientation parameter [32,33] as follows:

$$f_c = \frac{3\langle\cos^2\phi\rangle - 1}{2}$$

4.1

where,

$$\langle\cos^2\phi\rangle = \frac{\int_0^{\pi/2} I_{110}(\phi)\,\sin\phi\,\cos^2\phi\,d\phi}{\int_0^{\pi/2} I_{110}(\phi)\,\sin\phi\,d\phi}$$

4.2

Here, $-0.5 < f_c < 1$; a negative value of f_c indicates preferred orientation in a direction perpendicular to the fiber axis, a positive value indicates preferred orientation in the fiber direction and 0 indicates completely isotropic orientation.

4.3.4 *Birefringence experiments:*

Birefringence experiments were used to determine amorphous phase orientation (f_a). These experiments were performed on single fibers clamped in the stretching device mounted on a Nikon Eclipse E600 optical microscope using a U-CBE Olympus compensator. All the experiments were performed on dry and water soaked fibers at a magnification of 20X. We measure the compensation angle for unstretched fibers, after stretching and during relaxation. Using the compensator manufacturer-provided tables, the value of retardation is obtained against corresponding compensation angle. Birefringence (Δn) is calculated by dividing the retardation value with the diameter of the fiber measured during the experiment. Δn is related to the orientation of amorphous phase (f_a) as[3,34,35]

$$\Delta n = x \, f_c \, \Delta n_{c\,(max)} + (1-x) \, f_a \, \Delta n_{a\,(max)}$$

4.3

where, x is the crystallinity index calculated from the ratio of intensity under crystalline peaks to total intensity in WAXD. Thus, when x and f_c are obtained from WAXD and Δn from birefringence measurements, we can use equation 4.3 to calculate the amorphous phase orientation, f_a. To calculate x, we subtract incoherent Compton scattering for cellulose as reported in the literature,[36] and obtain x as the ratio of the area under the crystalline peaks to the total area under the scattered curve. The values of x thus calculated are 0.3 for Viscose and 0.4 for Lyocell. These values are in accord with literature reports – however, we note that the literature reports for the crystallinity of regenerated cellulose fibers vary in a wide range from x = 0.155 to 0.74.[3,5,28,37–41] f_c is the crystal orientation measured using WAXD, $\Delta n_{c\,(max)}$ and $\Delta n_{a\,(max)}$ are the maximum values of crystal and amorphous birefringence for cellulose fibers. Based on the literature, we use $\Delta n_{c\,(max)} = \Delta n_{a\,(max)} = 0.059$ for all our calculations.

4.4 Results and Discussions:

We use the Hermans orientation parameter, calculated for the 110 reflection to characterize the crystal orientation, f_c, using equations 4.1 and 4.2. We then measure the fiber birefringence and use equation 4.3 to calculate the amorphous orientation parameter, f_a. The

values of crystal and amorphous orientation parameter for unstretched dry Viscose fibers (f_c = 0.79 ± 0.03, f_a = 0.62 ± 0.03) are lower than those for the Lyocell fibers (f_c = 0.86 ± 0.03, f_a = 0.72 ± 0.03). We repeat the WAXD and birefringence experiments on 10 samples for each Viscose and Lyocell fibers and calculate standard deviation based on variation within the measurements. **Figure 4.3** (a) shows the increase in the crystalline phase orientation parameter when stretched to different strains. Here, birefringence and WAXD were recorded as the strain approached the maximum value. We observe that for both Viscose and Lyocell, the crystal orientation parameter increases linearly with strain. This trend is consistent with the literature.[26] Similarly, the amorphous orientation parameter linearly increases with increasing strain for both fibers as shown in **Figure 4.3** (b). However, there is no noticeable difference between Viscose and Lyocell fibers in the rate of increase in orientation with strain.
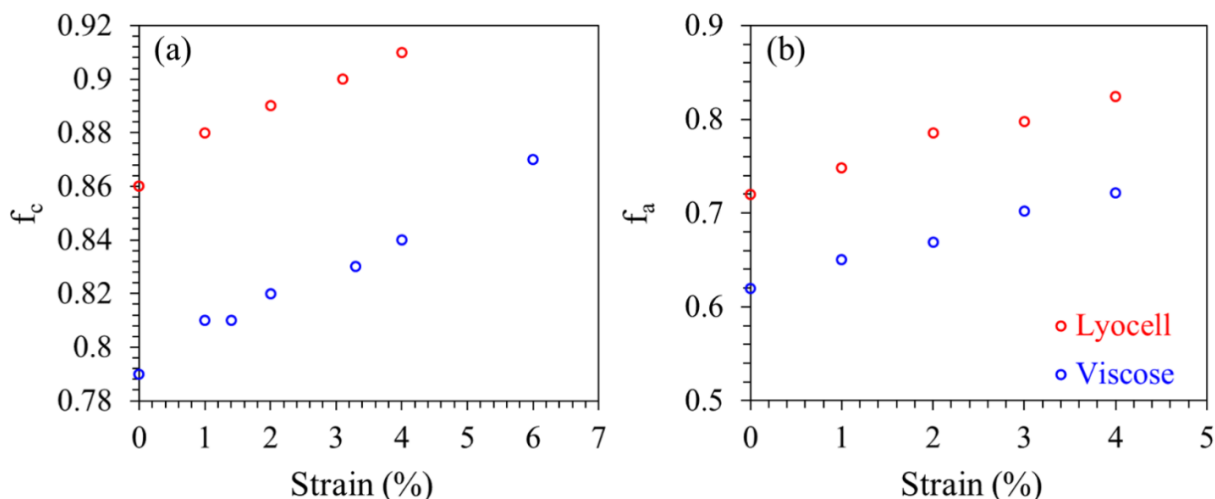
Figure 4.3 Evolution of the crystalline phase (a) and amorphous phase (b) orientations with stretching to different strains at a strain rate of 4 x 10^{-3} s^{-1}.

Interestingly, on holding the fibers at a constant strain, there is no change in the crystalline orientation of both fibers during stress relaxation as shown in **Figure 4.4** (a). However, the amorphous orientation gradually *increases* with stress relaxation as shown in **Figure 4.4** (b). Increase in the amorphous orientation is logarithmic in time, which is in line with the logarithmic stress relaxation observed in these systems.[8,25] We observe that the rate of increase in orientation is faster for Viscose fibers than the Lyocell fibers. We performed these experiments at two different strains of 1% and 4% (above and below the apparent yield

point) as shown in **Figure 4.4** and observe that the variation in crystal and amorphous orientation is qualitatively similar for both strains.
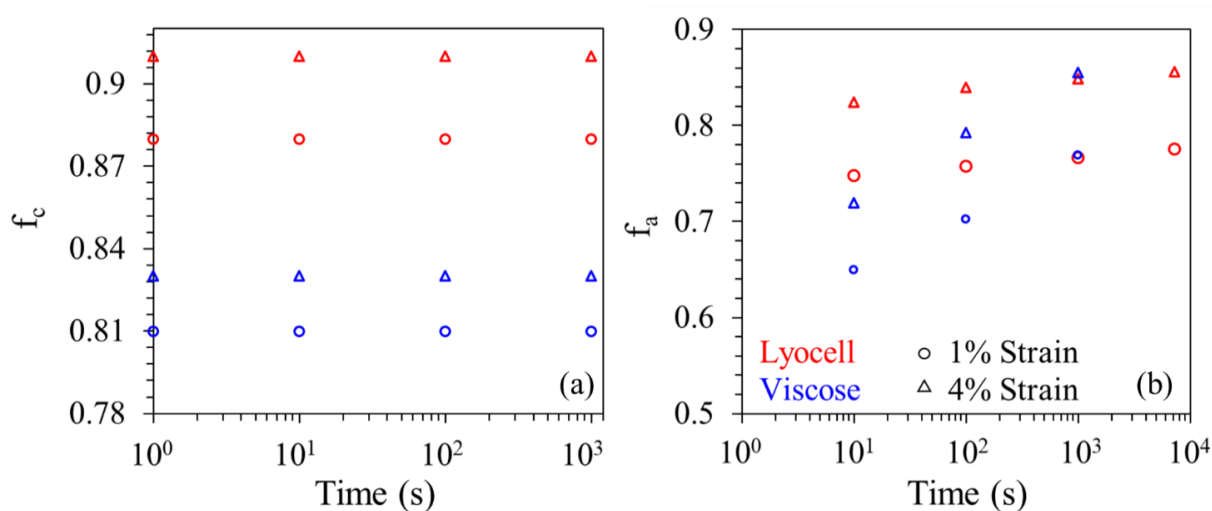
Figure 4.4 Evolution of crystalline phase (a) and amorphous phase (b) orientations during stress relaxation experiments performed at 1% and 4% strains.

The positive values of f_c and f_a indicate preferred orientation of crystalline unit cell and stretching of amorphous chains along the fiber axis. We anticipate that during spinning, cellulose chains are stretched in the fiber direction: therefore, the crystal unit cell c-axis is oriented along the fiber axis. Viscose fibers show lower as-spun orientation than Lyocell fibers. This is consistent with our expectation. In the Viscose process, cellulose xanthate is spun into aqueous acid to regenerate the fiber, while in the Lyocell process, the dope is spun through an air gap into the non-solvent bath. It has been reported in the literature[9] that the presence of the air gap in the manufacturing process is important for formation of highly oriented microstructure. Therefore, as expected, we observe higher crystal/amorphous orientation in case of Lyocell fibers. The linear increase in the crystalline orientation of both fibers with increasing strain is consistent with the literature.[26] We observe that the amorphous phase orientation also shows a linear increase with strain. This is reasonable since the amorphous phase is coupled with the crystalline domains.

We schematically represent the response of crystalline unit cell during stretching and stress relaxation in **Figure 4.5**. In-situ WAXD results show that on stretching, the crystal unit cell is elongated in the c-axis direction and there is an increase in crystal orientation, f_c. On holding the strain constant, the stress relaxes logarithmically. During stress relaxation, there is no change in f_c – however, there is a decrease in the stretching of the crystal unit cell along

the c-axis. Previously (Chapter 2), we had shown that during stress relaxation, strain is transferred from the crystal regions to amorphous phase.[25] Our results indicate that stretching the fiber results in higher orientation of the crystals along the fiber direction and in elongation of the crystal unit cell along the c-axis. During stress relaxation, the crystals stay oriented – however, there is a decrease in the c-axis elongation. Concomitantly, there is a logarithmic increase in f_a. with time. Thus, during stress relaxation, transfer of strain from the crystal unit cell to the amorphous phase results in increased amorphous phase orientation. Previously, we reported that Lyocell fibers exhibit longer relaxation times than Viscose fibers.[8] Consistent with this, we observe a slower increase in the orientation of the amorphous phase for Lyocell fibers compared to Viscose fibers.
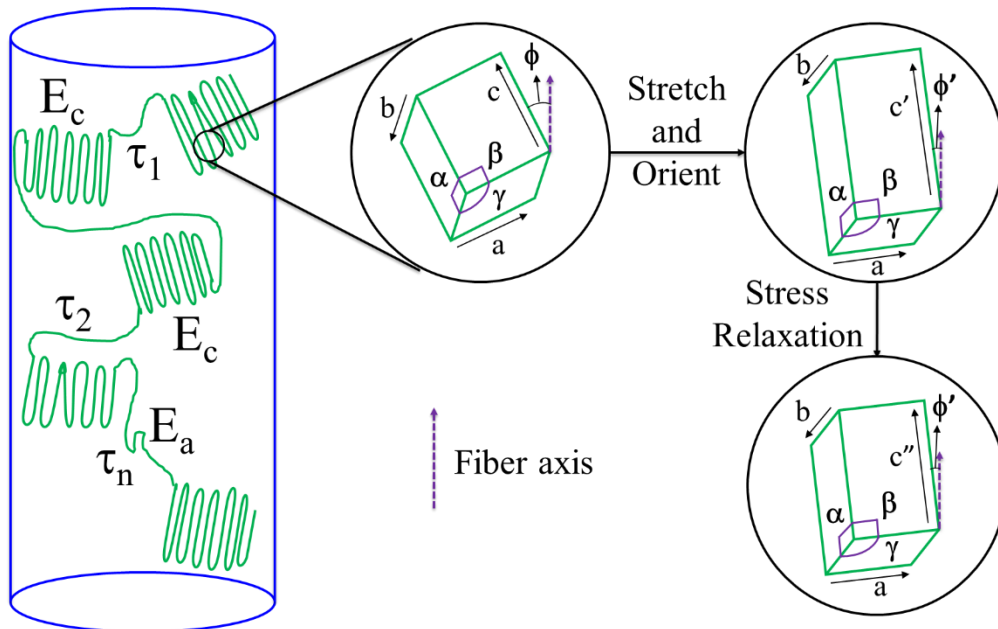
Figure 4.5 Schematic representation of the effect of stretching and stress relaxation experiments on the unit cell strain and orientation.

So far, we have presented results on the effect of mechanical deformation on the microstructure of dry Viscose and Lyocell fibers. It is known that wetting regenerated cellulose fibers with water significantly changes their mechanical response.[27–30] Therefore, we now investigate the effect of mechanical deformation on crystalline and amorphous phase orientation of wet Viscose and Lyocell fibers.

4.4.1   *Fibers soaked in water:*

We calculated the orientation parameters for the crystalline and the amorphous phase of Viscose (f_c = 0.79, f_a = 0.53) and Lyocell (f_c = 0.86, f_a = 0.6) fibers in water soaked

condition as described in the experimental section. We notice that the crystalline orientation of the as-spun fibers does not change from the dry state to the wet condition. However, there is a decrease in the amorphous orientation for both fibers as compared to the dry state. We attribute this to water-induced plasticization of the amorphous phase, as reported in the literature.[28,42]

On stretching, we notice that, within experimental error, there is no measurable increase in the crystal orientation of wet Viscose and Lyocell fibers as shown in **Figure 4.6** (a) – qualitatively different from the case of dry fibers. We stretch the fibers at two different strains of 1% and 4% and observe that this observation is independent of strain. Further, on stretching the fibers, the meridional peak (002) does not show any change in the position (**Figure 4.6** (a), inset) – unlike for dry fibers.[8] WAXD measurements were performed (short exposure time = 3 s) as the fibers were stretched to the maximum strain (=1% or 4%). Therefore, neither does stretching water soaked fibers impart crystal orientation nor does it result in strain on the crystals. However, there is an increase in Δn on stretching, viz. the amorphous phase shows a systematic increase in the orientation with stretching as shown in **Figure 4.6** (b).
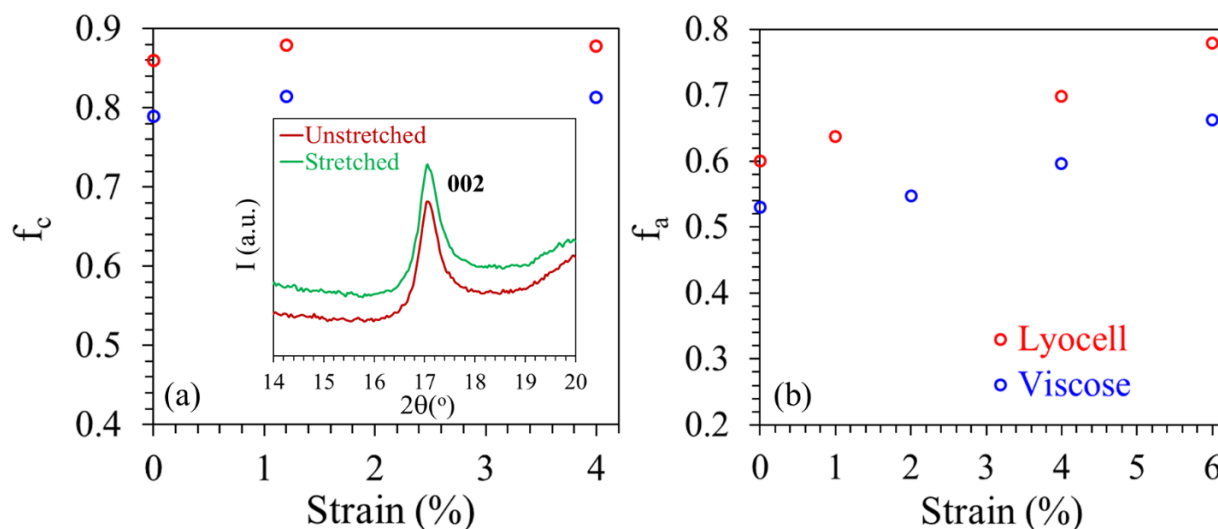
Figure 4.6 Effect of stretching on (a) crystalline phase orientation and meridional peak position (inset) and (b) amorphous phase orientation of wet regenerated cellulose fibers.

The effect of stretching on crystalline strain and orientation for wet fibers is in contrast with that for dry fibers. We have shown earlier[25] that on stretching regenerated cellulose fibers, the crystalline regions predominantly get strained. This happens because the

amorphous phase is glassy at room temperature,[42,43] characterized by long relaxation times that prevent it from responding at practical strains rates. However, it has been reported that on soaking the cellulose fibers in water, the amorphous phase T_g drops below the room temperature.[18,42] It is possible that due to plasticization by water, at least some fraction of the amorphous domains are rendered mobile. Thus, the stretching the fiber results in amorphous phase deformation, rather crystal phase orientation or deformation. Thus, we observe an increase in f_a but not in f_c.

4.4.2 Variation of amorphous orientation during stress relaxation:

Figure 4.7 shows the effect of stress relaxation on the amorphous orientation of Lyocell and the Viscose fibers in wet state. As observed for the dry fibers, the amorphous orientation increases logarithmically in time for the wet fibers as well. For dry fibers, the rate of increase of amorphous orientation during stress relaxation is lower for Lyocell fibers as compared to Viscose fibers. However, in wet condition, Lyocell fibers exhibit a higher rate of increase in amorphous orientation than the Viscose fibers.
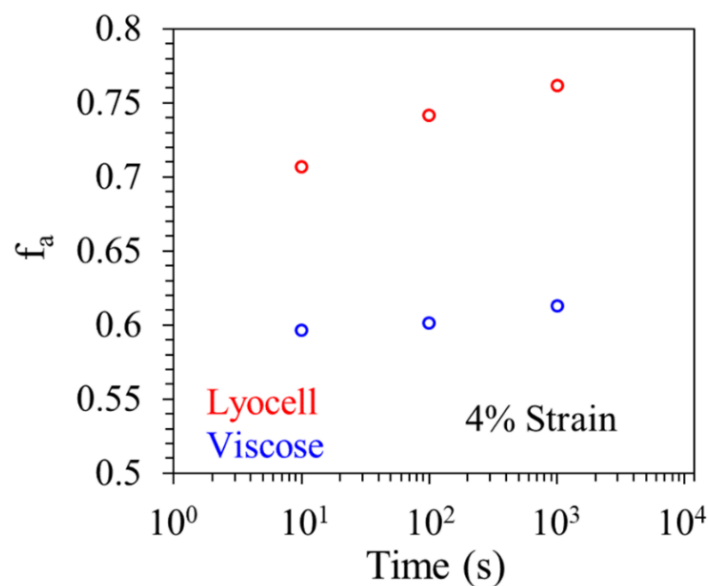
Figure 4.7 Evolution of amorphous phase orientation during stress relaxation experiments performed at 4% strain for Viscose and Lyocell fibers in water soaked state.

In dry condition, amorphous orientation of Viscose fibers increases at a higher rate than the Lyocell fibers during stress relaxation (**Figure 4.4** (b)). This has been explained based on the longer relaxation times for Lyocell fibers than the Viscose fibers. On the other hand, in the water soaked state, amorphous phase orientation increase at a faster pace for

Lyocell fibers than Viscose fibers. This reversal of trend indicates a decrease in the relaxation times for Lyocell fibers below that of the Viscose fibers on wetting. To verify this observation, we compare the relaxation times obtained from the stress relaxation data.

4.4.3 *Fitting the mechanical response from wet fibers:*

We use the model presented in **Figure 2.1** (c) to fit the mechanical response from wet Viscose and Lyocell fibers. **Figure 4.8** (a) shows the fitted stress-strain and the stress relaxation data for the wet Lyocell and Viscose fibers and the values of the E_c and E_a. We notice that for both fibers, $E_c = E_a$. Relaxation time spectra for both fibers show a monomodal distribution as shown in the **Figure 4.8** (b). We observe that the relaxation times for Viscose fibers are greater than for the Lyocell fibers in wet state.
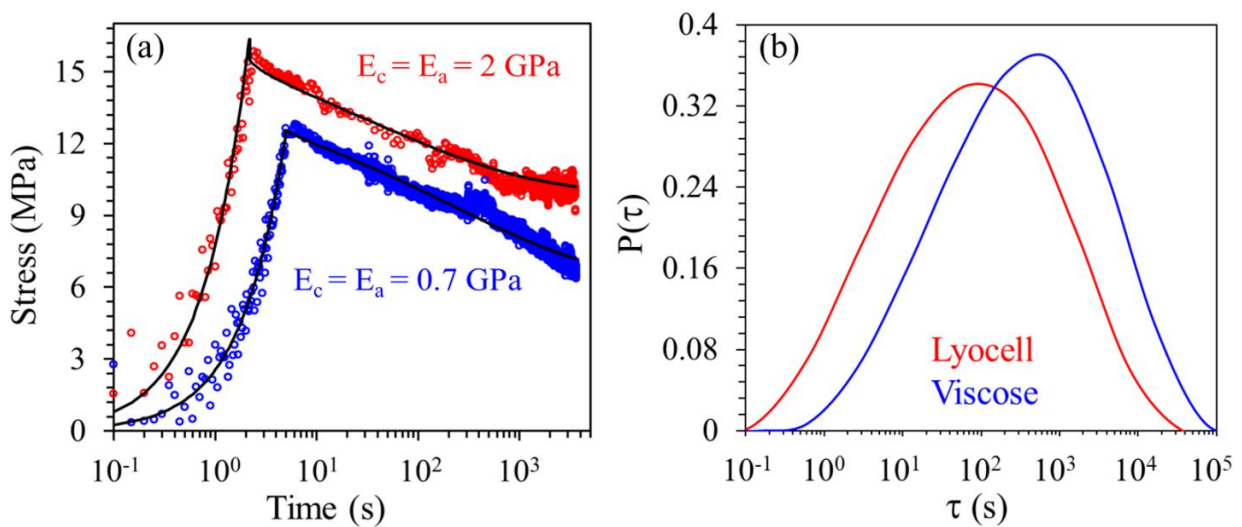
Figure 4.8 (a) Fitted stress-strain and stress relaxation data from Lyocell and Viscose fibers with fitted values of spring moduli, E_c and E_a (b) fitted relaxation time distribution.

The fitting results for both fibers show that $E_c = E_a$ whereas, for dry fiber we observed that $E_c > E_a$. We recall that for the case of dry fibers, in-situ WAXD measurements showed elongation of the c-axis unit cell parameter. Previously, we had demonstrated that this crystal strain could be used to independently estimate the crystal and amorphous moduli, and that these corresponded closely to the E_c and E_a, respectively, obtained from the model.[8] For the case of wet fibers, we do not observe any change in the meridional peak position (002) on stretching. Hence, it is not possible to attribute a microstructural origin to E_c and E_a obtained from fitting the mechanical response of wet fibers. The relaxation time spectrum obtained from the model arises largely from fitting the time-dependence of stress relaxation. We

believe that this is a manifestation of molecular relaxation processes in the fibers. Hence, we attribute the relaxation time spectra to microstructural relaxations in the fibers.

The single mode relaxation time spectra observed for wet fibers is in contrast to the bimodal relaxation time distribution for dry fibers. We had shown that for dry fibers, multimodal distribution is obtained due to the presence of multiple relaxation modes (β, β_{wet}, σ, γ etc.) corresponding to different hydrogen bonded environments. It is reported in the literature that with increase in water content in cellulose fibers, multiple dielectric relaxation modes, specifically β_{wet} and β, merge and a single mode is obtained.[44] Therefore, it is expected that due to plasticization and drop in T_g to below room temperature, the multiplicity of slow relaxation modes are either eliminated or merged with faster modes of relaxation. Thus, the shape of the relaxation time spectra are transformed so that the wet fibers are characterized by monomodal $P(\tau)$. Comparison of relaxation times obtained from two types of fibers shows that the microstructural relaxation in the Viscose fibers occurs more slowly compared to Lyocell fibers. This is in agreement with the comparison of rate of increase in amorphous orientation for wet Lyocell and Viscose fibers. To rationalize the reversal of relaxation rates in Lyocell and Viscose fibers on wetting, we compare the dry fiber relaxation time spectra obtained from the model fitting[8] with that for the wet fibers (**Figure 4.9**).

Wetting results in decrease in the spread of relaxation times and for the highest relaxation times for both Viscose and Lyocell fibers relative to the dry fibers (**Figure 4.9**). This decrease is more prominent for Lyocell fibers. Here, the relaxation mode at longer time scales for the dry fiber appears to largely disappear. The monomodal relaxation for the wet Lyocell fiber is peaked at about the same τ as the "fast" mode for the dry fibers. In contrast, for Viscose fibers, the monomodal relaxation for the wet fibers is observed to peak at τ between the peaks of the bimodal relaxation for dry fibers (**Figure 4.9**). We rationalize this in terms of the differences in the structure of the crystal/amorphous regions in Viscose and Lyocell fibers. In Lyocell fibers, the slowest relaxing amorphous regions appear to be accessible to water and are plasticized on wetting. In contrast, for the Viscose fibers, water is unable to plasticize some of the slow relaxing amorphous modes. It is clear that the relaxation time spectrum for dry fibers extends to longer times for Lyocell versus Viscose. However, for wet fibers, Viscose exhibits slower relaxations than Lyocell. This is consistent with the trends in the rate of birefringence increase for wet and dry fibers (compare **Figure 4.4** (b) and **Figure 4.7**). We believe that these qualitative differences arise from the difference in the

crystal/amorphous microstructure that forms when fibers are prepared using the Lyocell and Viscose processes. It is possible that the greater orientation and higher crystallinity in Lyocell fibers results in tighter crystal/amorphous coupling in the dry fibers, resulting in very slow relaxing amorphous modes (compared to the Viscose). This same structure makes water ingress more facile on wetting the fiber, such that these slowest relaxing amorphous modes are readily plasticized.

We note that these microstructural differences between Lyocell and Viscose also manifest in the wetting-induced change in the apparent yield point that we have previously investigated (**Section 3.4.6**).[8] We had shown that there is no change in the apparent yield strain on wetting Lyocell fibers. However, for Viscose fibers, there is significant increase in the apparent yield strain from 1.3% to 4.8% on wetting. This observation relates to microstructural differences in the spatial organization of the crystal/amorphous regions in Lyocell and Viscose fibers and is consistent with the differences reported here.
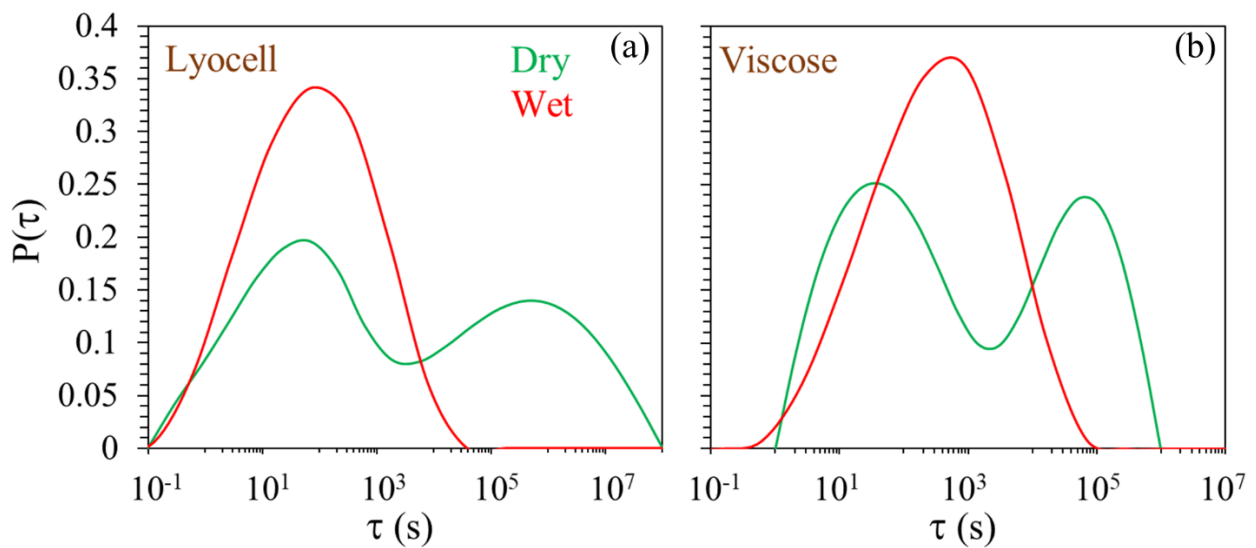
Figure 4.9 Comparison of relaxation time spectra in dry and wet condition for (a) Lyocell and (b) Viscose fibers.

4.5 Conclusions:

We study the differences in the structural response of regenerated cellulose fibers obtained from Viscose and Lyocell process in terms of crystalline and amorphous phase orientations. We use wide angle X-ray diffraction and birefringence experiments during mechanical deformation and show that on stretching the dry fibers, orientation of crystalline and amorphous increases linearly. However, on holding at a constant strain the crystals do not

change their orientation whereas, amorphous phase orientation increases logarithmically. We interpret this in terms of a structural response: crystals relax only by changing strain and not by change in orientation. Amorphous orientation increases more rapidly in Viscose fibers than the Lyocell fibers in the dry state, that we attribute to the higher relaxation time for Lyocell fibers. This trend is reversed when fibers are soaked in water. In wet condition, Viscose fibers show a slower increase in amorphous orientation than the Lyocell fibers. This is supported by the comparison of relaxation time spectra obtained by fitting a previously reported mechanical model to wet fibers data. In-situ WAXD experiments on wet fibers during stretching indicate that the crystalline phase does not respond during stretching. Whereas, amorphous orientation of wet fibers increases linearly during stretching. Therefore, we show that the structural response of wet fibers is qualitatively and quantitatively different from the dry fibers. Wet fiber response is governed largely by the ability of water to plasticize the amorphous regions. This is strongly dependent on the crystal/amorphous microstructure that forms as a consequence of the spinning process.

4.6   References:

(1)   Lavanya, Devabaktuni Kulkarni, P. K.; Dixit, M.; Raavi, P. K.; Krishna, L. N. V. Sources of Cellulose and Their Applications - A Review. *Int. J. DRUG Formul. Res.* **2011**, *2* (6), 19–38.

(2)   Woodings, C. *Regenerated Cellulose Fibres*; Woodhead Publishing Limited, 2001.

(3)   Jiang, G.; Yuan, Y.; Wang, B.; Yin, X.; Mukuze, K. S.; Huang, W.; Zhang, Y.; Wang, H. Analysis of Regenerated Cellulose Fibers with Ionic Liquids as a Solvent as Spinning Speed Is Increased. *Cellulose* **2012**, *19* (4), 1075–1083.

(4)   Zhang, L.; Ruan, D.; Zhou, J. Structure and Properties of Regenerated Cellulose Films Prepared from Cotton Linters in NaOH/Urea Aqueous Solution. *Ind. Eng. Chem. Res.* **2001**, *40* (25), 5923–5928.

(5)   Jiang, G.; Huang, W.; Li, L.; Wang, X.; Pang, F.; Zhang, Y.; Wang, H. Structure and Properties of Regenerated Cellulose Fibers from Different Technology Processes. *Carbohydr. Polym.* **2012**, *87* (3), 2012–2018.

(6)   Chen, J. H.; Guan, Y.; Wang, K.; Xu, F.; Sun, R. C. Regenerated Cellulose Fibers Prepared from Wheat Straw with Different Solvents. *Macromol. Mater. Eng.* **2015**,

300 (8), 793–801.

(7)   Chen, X.; Burger, C.; Fang, D.; Ruan, D.; Zhang, L.; Hsiao, B. S.; Chu, B. X-Ray Studies of Regenerated Cellulose Fibers Wet Spun from Cotton Linter Pulp in NaOH/Thiourea Aqueous Solutions. *Polymer.* **2006**, *47* (8), 2839–2848.

(8)   Sharma, A.; Nagarkar, S.; Thakre, S.; Kumaraswamy, G. Structure – Property Relations in Regenerated Cellulose Fibers : Comparison of Fibers Manufactured Using Viscose and Lyocell Processes. *Cellulose* **2019**, *26* (6), 3655–3669.

(9)   Zhang, S.; Chen, C.; Duan, C.; Hu, H.; Li, H. Regenerated Cellulose by the Lyocell Process , a Brief Review of the Process and Properties. *BioResources* **2018**, *13(2)*, 4577–4592.

(10)   Fink, H. P.; Weigel, P.; Purz, H. J.; Ganster, J. Structure Formation of Regenerated Cellulose Materials from NMMO-Solutions. *Prog. Polym. Sci.* **2001**, *26* (9), 1473–1524.

(11)   Müller, M.; Riekel, C.; Vuong, R.; Chanzy, H. Skin/Core Micro-Structure in Viscose Rayon Fibres Analysed by X-Ray Microbeam and Electron Diffraction Mapping. *Polymer.* **2000**, *41* (7), 2627–2632.

(12)   Morehead, F. F.; Sisson, W. A. Skin Effect in Viscose Rayon. *Text. Res. J.* **1945**, *15*, 443–450.

(13)   Abu-Rous, M.; Ingolic, E.; Schuster, K. C. Visualisation of the Nano-Structure of Tencel®(Lyocell) and Other Cellulosics as an Approach to Explaining Functional and Wellness Properties in Textiles. *Lenzinger Berichte* **2006**, *85*, 31–37.

(14)   Abu-Rous, M.; Ingolic, E.; Schuster, K. C. Visualisation of the Fibrillar and Pore Morphology of Cellulosic Fibres Applying Transmission Electron Microscopy. *Cellulose* **2006**, *13* (4), 411–419.

(15)   Lenz, J.; Schurz, J.; Wrentschur, E. Properties and Structure of Solvent-Spun and Viscose-Type Fibres in the Swollen State. *Colloid Polym. Sci.* **1993**, *271* (5), 460–468.

(16)   Lenz, J.; Schurz, J.; Wrentschur, E. On the Elongation Mechanism of Regenerated Cellulose Fibres. *Holzforschung* **1994**, *48* (s1), 72–76.

(17) Röder, T.; Moosbauer, J.; Wöss, K.; Schlader, S.; Kraft, G. Man-Made Cellulose Fibres – a Comparison Based on Morphology and Mechanical Properties. *Lenzinger Berichte* **2013**, *91*, 7–12.

(18) Bryant, G. M.; Walter, A. T. Stiffness and Resiliency of Wet and Dry Fibers as a Function of Temperature. *Text. Res. J.* **1959**, *29* (3), 211–219.

(19) Kong, K.; Eichhorn, S. J. The Influence of Hydrogen Bonding on the Deformation Micromechanics of Cellulose Fibers The Influence of Hydrogen Bonding on the Deformation Micromechanics of Cellulose Fibers. *J. Macromol. Sci. Part B Phys.* **2005**, *44* (6), 1123–1136.

(20) Kong, K.; Davies, R. J.; McDonald, M. A.; Young, R. J.; Wilding, M. A.; Ibbett, R. N.; Eichhorn, S. J. Influence of Domain Orientation on the Mechanical Properties of Regenerated Cellulose Fibers. *Biomacromolecules* **2007**, *8* (2), 624–630.

(21) Kim, D. B. Dry Jet-Wet Spinning of Cellulose/N-Methylmorpholine N-Oxide Hydrate Solutions and Physical Properties of Lyocell Fibers. *Text. Res. J.* **2005**, *75* (4), 331–341.

(22) Adusumalli, R.-B.; Muller, U.; Weber, H.; Roeder, T.; Sixta, H.; Gindl, W. Tensile Testing of Single Regenerated Cellulose Fibres. *Macromol. Symp* **2006**, *244*, 83–88.

(23) Gindl, W.; Keckes, J. Strain Hardening in Regenerated Cellulose Fibres. *Compos. Sci. Technol.* **2006**, *66* (13), 2049–2053.

(24) Cai, J.; Zhang, L.; Zhou, J.; Qi, H.; Chen, H.; Kondo, T.; Chen, X.; Chu, B. Multifilament Fibers Based on Dissolution of Cellulose in NaOH/Urea Aqueous Solution: Structure and Properties. *Adv. Mater.* **2007**, *47* (22), 8676–8683.

(25) Sharma, A.; Kumaraswamy, G.; Thakre, S. Modeling the Universal Viscoelastic Response of Polymer Fibers. *Phys. Rev. Mater.* **2018**, *2* (6), 062601.

(26) Gindl, W.; Martinschitz, K. J.; Boesecke, P.; Keckes, J. Orientation of Cellulose Crystallites in Regenerated Cellulose Fibres under Tensile and Bending Loads. *Cellulose* **2006**, *13* (6), 621–627.

(27) Ganser, C.; Kreiml, P.; Morak, R.; Weber, F.; Paris, O.; Schennach, R.; Teichert, C.

The Effects of Water Uptake on Mechanical Properties of Viscose Fibers. *Cellulose* **2015**, *22* (4), 2777–2786.

(28) Zhou, S.; Tashiro, K.; Hongo, T.; Shirataki, H.; Yamane, C.; Ii, T. Influence of Water on Structure and Mechanical Properties of Regenerated Cellulose Studied by an Organized Combination of Infrared Spectra, X-Ray Diffraction, and Dynamic Viscoelastic Data Measured as Functions of Temperature and Humidity. *Macromolecules* **2001**, *34* (5), 1274–1280.

(29) Kreze, T.; Strnad, S.; Stana-Kleinschek, K.; Ribitsch, V. Influence of Aqueous Medium on Mechanical Properties of Conventional and New Environmentally Friendly Regenerated Cellulose Fibers. *Mater. Res. Innov.* **2001**, *4* (2–3), 107–114.

(30) Nazari, B.; Utomo, N. W.; Colby, R. H. The Effect of Water on Rheology of Native Cellulose/Ionic Liquids Solutions. *Biomacromolecules* **2017**, *18* (9), 2849–2857.

(31) Kumaraswamy, G.; Verma, R. K.; Kornfield, J. A.; Yeh, F.; Hsiao, B. S. Shear-Enhanced Crystallization in Isotactic Polypropylene . In-Situ Synchrotron SAXS and WAXD. *Macromolecules* **2004**, *37* (24), 9005–9017.

(32) Hermans, J. J.; Hermans, P. H.; Vermaas, D.; Weidinger, A. Quantitative Evaluation of Orientation in Cellulose Fibres From the X-Ray Pibre Diagram. *Recl. des Trav. Chim. des Pays-Bas* **1946**, *65* (6), 427–447.

(33) Alexander, L. E. *X-Ray Diffraction Methods in Polymer Science*; John Wiley & Sons, Inc., **1969**.

(34) Stein, R. S. The X-Ray Diffraction, Birefringence, and Infrared Dichroism of Stretched Polyethylene. III. Biaxial Orientation. *J. Polym. Sci.* **1958**, *31* (123), 335–343.

(35) Taylor, G. R.; Darin, S. R. Birefringence and Crystallization in Elastomers. *J. Appl. Phys.* **1955**, *26* (9), 1075–1079.

(36) Driemeier, C.; Calligaris, G. A. Theoretical and Experimental Developments for Accurate Determination of Crystallinity of Cellulose I Materials. *J. Appl. Crystallogr.* **2011**, *44*, 184–192.

(37) Dieter, K.; B., P.; Thomas, H.; Ute, H.; Wagenknecht, W. *Comprehensive Cellulose*

Chemistry Volume 1 Fundamentals and Analytical Methods; WILEY-VCH Verlag GmbH, **1998**.

(38)   Stana-Kleinschek, K.; Ribitsch, V.; Kreže, T.; Sfiligoj-Smole, M.; Peršin, Z. Correlation of Regenerated Cellulose Fibres Morphology and Surface Free Energy Components. *Lenzinger Berichte* **2003**, *82*, 83–95.

(39)   Kreze, T.; Stana-Kleinschek, K.; Ribitsch, V. The Sorption Behaviour of Cellulose Fibres. *Lenzinger Berichte* **2001**, *80*, 28–33.

(40)   Kreze, T.; Jeler, S.; Strnad, S. Correlation between Structure Characteristics and Adsorption Properties of Regenerated Cellulose Fibers. *Mater. Res. Innov.* **2003**, *5* (6), 277–283.

(41)   Peng, S.; Shao, H.; Hu, X. Lyocell Fibers as the Precursor of Carbon Fibers. *J. Appl. Polym. Sci.* **2003**, *90* (7), 1941–1947.

(42)   Akim, E. L.; Naimark, N. I.; Vasil'yev, B. V.; Fomenko, B. A.; Ignat'eva, E. V.; Zhegalova, N. N. Effect of Plasticizing Liquid Media on the Glass Transition Temperatures of Cellulosic Materials. *Polym. Sci. U.S.S.R.* **1971**, *13* (10), 2522–2529.

(43)   Szczes´niak, L.; Rachocki, A.; Tritt-Goc, J. Glass Transition Temperature and Thermal Decomposition of Cellulose Powder. *Cellulose* **2008**, *15* (3), 445–451.

(44)   Einfeldt, J.; Meißner, D.; Kwasniewski, A. Contributions to the Molecular Origin of the Dielectric Relaxation Processes in Polysaccharides - The High Temperature Range. *J. Non. Cryst. Solids* **2003**, *320* (1–3), 40–45.

Chapter 5.

Characterizing microvoids in regenerated cellulose fibers obtained from Viscose and Lyocell process

5.1 Graphical Abstract:

5.2 Introduction:

About a fourth of the global production of synthetic polymers is used by converting into fiber form. Naturally available polymers such as cellulose are converted into fibers by regenerating the polymer out of solution during spinning. Such regenerated cellulose fibers are widely used in textile applications. The industrially predominant process for the preparation of regenerated cellulose fibers is the Viscose process.[1,2] However, there are growing environmental concerns about the use of carbon disulphide solvent in this process. Therefore, alternate processes that are more environmentally benign, such as the Lyocell process, have been developed wherein cellulose fibers are regenerated by spinning from an

Characterizing Microvoids in Regenerated Cellulose Fibers obtained from Viscose and Lyocell Process

N-methyl morpholine N-oxide/water solution into a water bath.[2,3] The microstructure of regenerated cellulose fibers is greatly influenced by the processing technique used for fiber formation. For example, regenerated cellulose fibers produced using the Lyocell process exhibit higher crystallinity and higher crystalline orientation compared to Viscose fibers.[2,3] This results in Lyocell fibers, having a significantly higher modulus but with a lower elongation to break. The microstructural differences between Viscose and Lyocell fibers have been investigated in the literature,[4–7] [8,9] However, these reports have focused largely on determining the crystallinity and crystalline/amorphous organization in the fibers. In this work, we focus on an aspect that has not been investigated in detail in the literature and characterize the differences between microvoids in these regenerated cellulose fibers. We also demonstrate the limitations of literature methods used to analyze scattering from microvoids, that call into question the conclusions from previous studies.[10–14]

Microvoids are pores or defect sites of microscopic size induced in a material during processing. It has been suggested that microvoids play an important role in determining the fiber properties, including mechanical failure, water uptake etc.[12,15–18] Microvoids are observed in most polymer fibers, especially those that have a glassy amorphous phase e.g. Kevlar, cellulose, PAN fibers, etc.[19–22] In cellulosic fibers as well, both native and regenerated, the presence of microvoids has been reported in the literature.[10–13] It has also been reported that there are differences in the microvoids in regenerated cellulose fibers, depending on whether they are manufactured using the Viscose or Lyocell process.[12–14] The characteristics of microvoids are governed by the molecular structure of the polymer and the fiber formation process. During fiber drawing, microvoids get elongated and oriented in the fiber direction for regenerated fibers.

In the literature, microvoid structure has been studied using small angle scattering techniques.[20–23] Ruland claimed that the fan-like equatorial scattering pattern observed from the SAXS of dry fibers originates from the microvoids elongated in the fiber direction.[22] He showed the evolution of this scattering pattern when cellulose fibers were heat treated to make carbon fibers. He used the spread of the intensities in the azimuthal angle to obtain the average length and average misorientation of the microvoids. Later, this method was extensively used by several researchers.[20,24–28] Shioyaet. al.[29] and Crawshawet. al.[26] used small angle scattering to measure the cord length, radius of gyration, mean cross-section and volume fraction of the microvoids. Schurz et.al. used the small angle scattering curve to

determine the invariant and hence the volume fraction and average chord length of the microvoids.[12]

We note that in all these literature reports, the structural analysis is based on scattering data at small angles, in the region of $q = 0.1$ to 2 nm^{-1}. There is only one report in the literature on ultra-small angle neutron scattering of regenerated cellulose fibers.[30] This report clearly suggests that the small angle data (near $q = 0.1$ nm^{-1}) cannot be extrapolated to lower q and calls the previously reported analyses into question. However, unfortunately the ultra-small angle scattering data has not been analyzed in detail to obtain microvoid size.

Here, we report combined small angle X-ray (SAXS) and medium resolution-small angle neutron scattering (MSANS) to analyze the structure of microvoids in regenerated cellulose fibers. We show that combination of MSANS and SAXS can be used to analyze the microvoids in regenerated cellulose fibers. We demonstrate that regenerated cellulose fibers manufactured using different processes i.e. Viscose and Lyocell show differences in the average microvoid size and average orientation of microvoids, presumably induced by differences in processing techniques. We also quantify the microvoid volume fractions using SAXS and MSANS data and show that the void volume fraction in Viscose and Lyocell fibers are comparable.

5.3   Materials and methods:

Small angle X-ray scattering experiments were performed on commercial regenerated cellulose fibers manufactured using Lyocell and Viscose processes. These fibers were commercial fibers generously provided by Aditya Birla Science and Technology Company Pvt. Ltd. Experiments were performed on dry fibers, conditioned at 25°C and 55% RH for a day. Under these conditions, cellulose is known to absorb up to 10% water. It is reported that, at 55% RH, water present in cellulose is either (i) absorbed in amorphous cellulose by forming inter and intra chain hydrogen bonds or (ii) adsorbed as monomolecular layers.[31,32] Sorption and NMR data show that water aggregation to form spatially heterogeneous pockets occurs only above RH of 60-65%.[33] Therefore, in our experiments, it is reasonable to assume that the water is uniformly absorbed in the amorphous phase, and that no water pockets are expected at length scales ~O(100 nm). Therefore, scattering contrast in both SAXS and MSANS arise from the same structural features, viz. microvoids.

5.3.1 *Small angle X-ray scattering:*

SAXS was performed using the Rigaku Nano-Viewer equipped with a microfocus source (Cu K_α radiation, $\lambda = 0.154$ nm, 1.2KW rotating anode generator) and a two dimensional detector (HyPix-3000 with a radiation hardened semiconductor sensor). We comb a bunch of fibers so as to straighten them and clamp them aligned in the vertical direction. We perform SAXS experiments on such fiber samples to obtain a 2D SAXS pattern, as shown in **Figure 5.1**. We prepare 3D isotropic samples by hand, by knotting and repeatedly winding fibers in different directions to form a bundle, shown schematically in **Figure 5.1**. We check for isotropy of such fiber bundles by obtaining scattering patterns at several different orientations and by confirming that the scattering patterns are isotropic at all orientations. Samples that are observed in this manner to be isotropic are used to obtain isotropic 2D scattering data, an example of which is shown in **Figure 5.1** (b).
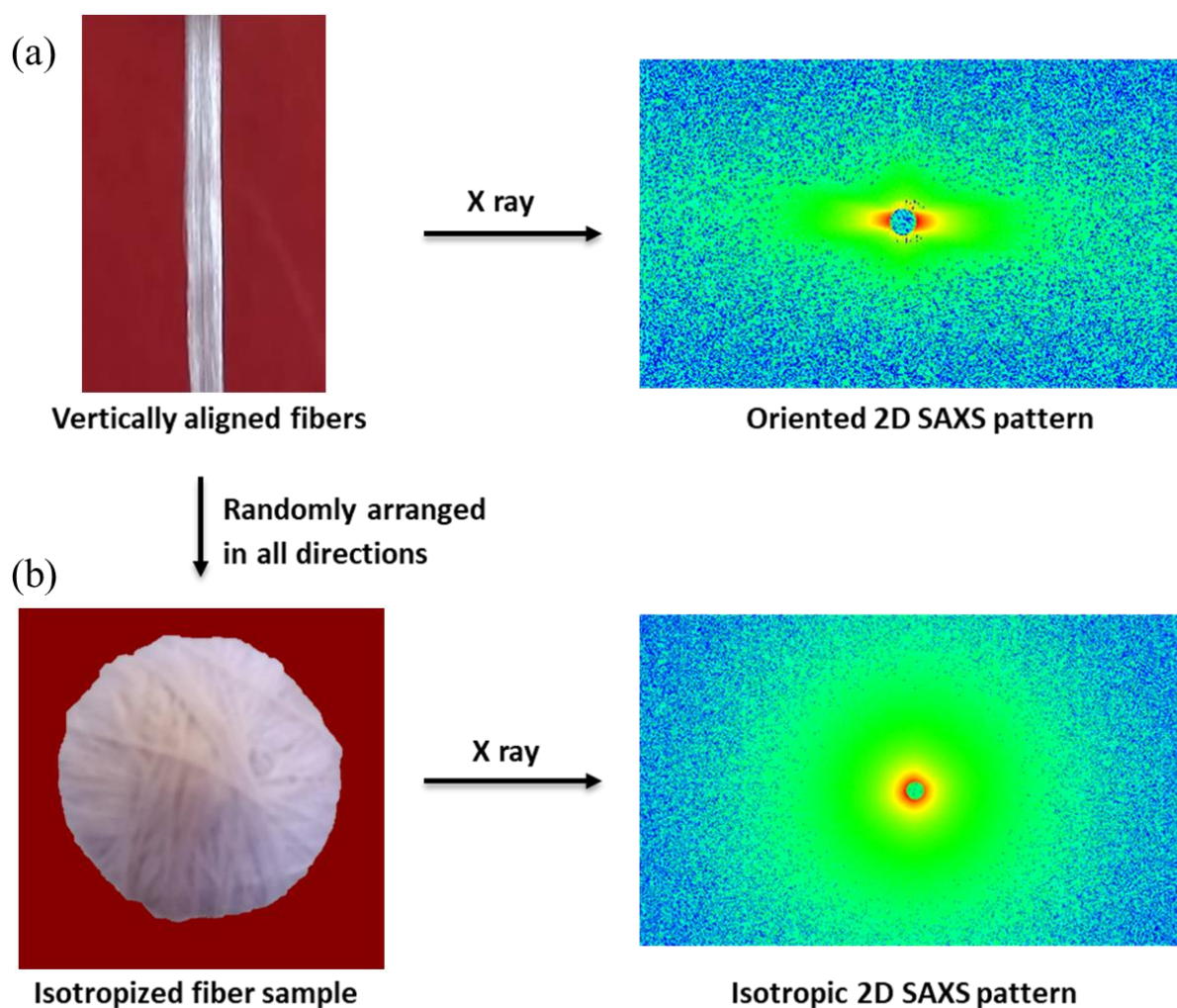
Figure 5.1 Schematic of the scattering experiment on vertically aligned and isotropized fibers.

5.3.2   *SAXS Data treatment:*

We perform azimuthal scans using the Rigaku 2DP software at various values of q to obtain the angular dependence of the 2D data, (I vs. ϕ going from 0 to 180°). 2D data from both the anisotropic and isotropized samples were converted into 1D intensity vs q (I vs. q) data by circularly averaging the 2D data using Rigaku 2DP software. Scattered intensity is normalized by the transmission (T) and by the time of exposure. We directly measure the sample transmission. We allow the direct X-ray beam to incident on the detector (after replacing the beam stop with an attenuator to prevent damage to the detector) and obtain T as the ratio of the direct beam intensity at the detector in the presence of the fiber sample to that in the absence of sample. By definition, $T = e^{-\mu t}$, where, μ is the absorption coefficient and t is

the thickness of the sample. We calculate μ for cellulose as described by Alexander.[34] To convert data into absolute units, the effective thickness of sample in X-ray beam is required, which is calculated as $t = (1/\mu) \times \ln(1/T)$. Data is converted into absolute units using the procedure described by Phinjaroenphan et.al.[35] using water as the standard.

We calculate the electron density, $\rho(e^-)$ of the cellulose fibers as follows:

$$\rho(e^-) = \frac{\rho(m)}{M} n_e \, N_A$$

5.1

where, $\rho(m)$ is the mass density (g/nm³), M is the molecular weight (g/mole), n_e is the number of electrons per mole and N_A is Avogadro's number. We note that the electron density is related to the scattering length density for SAXS through the Thomson scattering length, r_e = 2.82 fm. We report the scattered intensity in units of nm⁻³, since we work with electron density rather than scattering length density. The scattered intensity can be readily converted into units of nm⁻¹ by multiplying with r_e^2.

5.3.3 *Medium-resolution small angle neutron scattering:*

To access lower wave vector transfer, scattering experiments were performed using a double crystal based medium resolution small-angle neutron scattering facility (MSANS) at the Guide Tube Laboratory of Dhruva reactor, Mumbai, India.[36,37] Scattered intensities were collected as a function of wave vector transfer q [= $4\pi\sin(\theta)/\lambda$, where 2θ is the scattering angle and λ (= 0.312 nm) is the incident neutron wavelength]. The isotropically arranged fiber specimens were placed on a sample holder with a circular slit of 1.5 cm diameter. Measured SANS profiles were corrected for background and instrument resolution.[38]

5.3.4 *Ruland equatorial steak analysis:*

Anisotropic scattering from the elongated structures is analyzed using the method proposed by Ruland to obtain the average length (L) and the average misorientation (B$_g$).[20,22] We obtain the azimuthal variation of scattered intensity from the equatorial streaks at different q values. The breadth of the azimuthal scan (B), measured as the full width at half maximum is related to the scattering vector (q), L and B$_g$ as:

$$\frac{B^2 q2}{4\pi^2} = \frac{1}{L^2} + \frac{B_g^2 q^2}{4\pi^2}$$

5.2

5.3.5   Porod's analysis:

According to Porod's law, scattering from surfaces with a sharp interface is observed at high q values where the intensity varies as:

$$I = K_p \, q^{-4}$$

5.3

where K_p is Porod's constant given as:

$$K_p = 2\pi \Delta\rho^2 \, S_p/V_s$$

5.4

where, $\Delta\rho$ is the electron density difference between the phases, S_p is the total surface area of the scatterers in a scattering volume V_s. We note that S_p/V_s represents the average surface area of the scatterers in the scattering volume, and not the average specific surface area for a scatterer.

5.3.6   Invariant calculation:

We calculate the invariant by combining SAXS and MSANS data and by extrapolating to low and high q regions. We use SAXS intensity in absolute units and scale the MSANS data to overlap with the SAXS data in the q range where SAXS and MSANS data are both available. We extrapolate to lower q as $I = Aq^{-1}$ (from q_1 0.0030 nm^{-1} to q = 0 nm^{-1}, A is a constant). At high q (for q > q_2 = 0.42 nm^{-1}), we extrapolate the scattered intensity using Porod's law. Thus, the invariant (Q) is calculated using the absolute intensity I as:

$$Q = \int_0^\infty Iq^2 dq = \int_0^{q_1 = \,=0.003\ nm^{-1}} Iq^2 dq + \int_{q_1=0.003\ nm^{-1}}^{q_2=0.42\ nm^{-1}} Iq^2 dq + \int_{q_2=0.42\ nm^{-1}}^\infty Iq^2 dq$$

$$= \; \tfrac{1}{2} Aq_1^2 + \int_{q_1}^{q_2} Iq^2 dq + K_P/q_2 \;\; = 2\pi^2 \Delta\rho^2 \chi(1-\chi)$$

5.5

Where, $\Delta\rho$ is the electron density contrast and χ is the volume fraction of the scatterers.

5.3.7 *Lognormal distribution function:*

We assume that the microvoid radii R follow a lognormal distribution, given as:

$$f(R) = \frac{N}{\sqrt{2\pi}\, sR^p} \exp\left(-\frac{(\ln(R) - \ln(\mu))^2}{2s^2}\right)$$

5.6

where, N is a normalization parameter, p is the shape parameter, μ is the mean, s characterizes the width of the distribution.

5.4 Results and Discussion:

5.4.1 *Small angle X-ray scattering on fibers:*

Figure 5.2 a and b show the 2D small angle X-ray scattering patterns for oriented Lyocell and Viscose fibers, respectively. We observe that the patterns are highly anisotropic with pronounced streaking in the equatorial direction, indicating oriented scatterers elongated in the fiber direction.[22] The scattering pattern for regenerated cellulose fibers is qualitatively consistent with the literature.[13,22] We analyze the anisotropy of the scattering pattern using Ruland's equatorial streak method[20,22] as described in the Experimental section. Thus, we obtain the average length, L, and angular spread of the scatterers, B_g around the fiber direction. A representative azimuthal scan for the 2D SAXS pattern obtained at $q = 0.17$ nm^{-1} for Lyocell fibers is shown in **Figure 5.2** c. We observe that the distribution of intensities is fitted well by a Gaussian. We observe that a plot of $\frac{B^2 q^2}{4\pi^2}$ with $\frac{q^2}{4\pi^2}$ is linear, consistent with equation 5.2 (**Figure 5.2** d). According to equation 5.2 we obtain the slope as B_g^2. The SAXS data is extrapolated to $q = 0$ to obtain the intercept as L^{-2}. Thus, we obtain average microvoid length for Lyocell and Viscose fibers as 403 nm and 271 nm respectively. The misorientation of microvoids is characterized by an angular spread around the fiber axis of 29.7° for Lyocell fibers and 34.3° for Viscose fibers. Our results are broadly consistent with the literature.[20,24–28] Jiang et. al. investigated the average length of microvoids in regenerated cellulose fibers prepared through different processing techniques and reported values varying in the range of 250 – 1300 nm.[13,14] The average microvoid lengths obtained by us are consistent with these values.
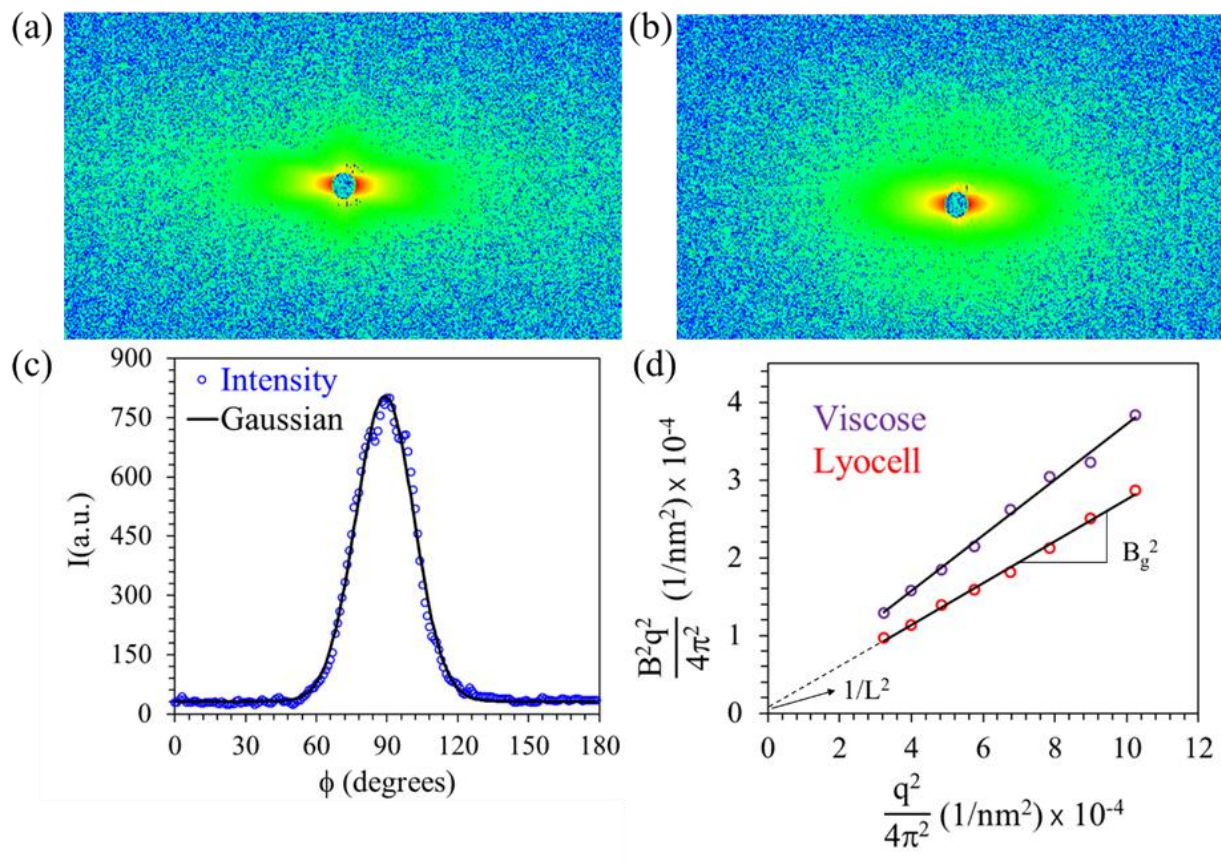
Figure 5.2 2D SAXS pattern of Lyocell (a) and Viscose (b) taken on fibers aligned in vertical direction. (c) Intensity distribution in the azimuthal scan of 2D SAXS pattern for Lyocell at q = 0.17 nm^{-1}. Black line represents the fitted Gaussian function. (d) Plot of $B^2q^2/4\pi^2$ vs $q^2/4\pi^2$, extrapolated to q = 0 to obtain L and B_g.

Next, we obtain SAXS from isotropized samples of Lyocell and Viscose fibers and circularly average this data to obtain a 1D plot of intensity as a function of q (**Figure 5.3**). We observe that, after correcting for the background, the scattered data varies as q^{-4} over the entire q-range for the SAXS data.
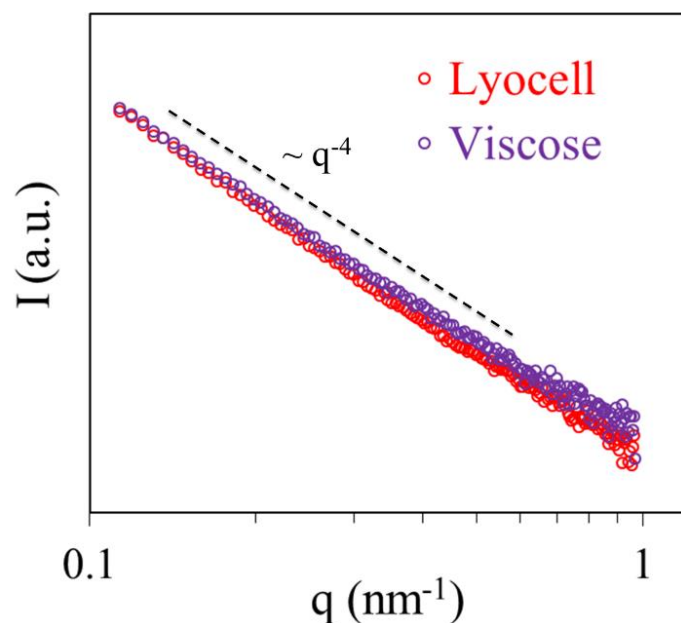
Figure 5.3 1D SAXS data obtained by circularly averaging data from isotropized Lyocell and Viscose samples.

5.4.2 *Medium resolution small angle neutron scattering on fibers:*

MSANS experiments were performed on isotropized samples of Viscose and Lyocell fibers. 1D data for both the fibers is shown in **Figure 5.4**. We note that the shape of the MSANS data is similar to that of the SAXS data in the q range where there is overlap. Therefore, we vertically shift the MSANS data so that it overlaps with the SAXS data (plotted as absolute intensity in units of nm^{-3}, as discussed in the Methods section). The MSANS intensity for Lyocell fibers show a distinct transition to a q^{-1} dependence at low q, below 10^{-2} nm^{-1} suggesting that the scatterers are elongated objects with rod-like symmetry. For Viscose fibers too, we observe that the MSANS data scales as q^{-4} for $q > 5 \times 10^{-2}$ nm^{-1} and transitions to a weaker q dependence at lower q, near 0.003 nm^{-1}. MSANS measurements on the Viscose fibers do not give us data at sufficiently low q to unambiguously confirm a q^{-1} dependence of the scattered intensity. However, the SAXS data is characterized by equatorial streaks, similar to that for Lyocell fibers. Therefore, following the data on the Lyocell fibers, we believe that this data too will scale as q^{-1} at even lower q.
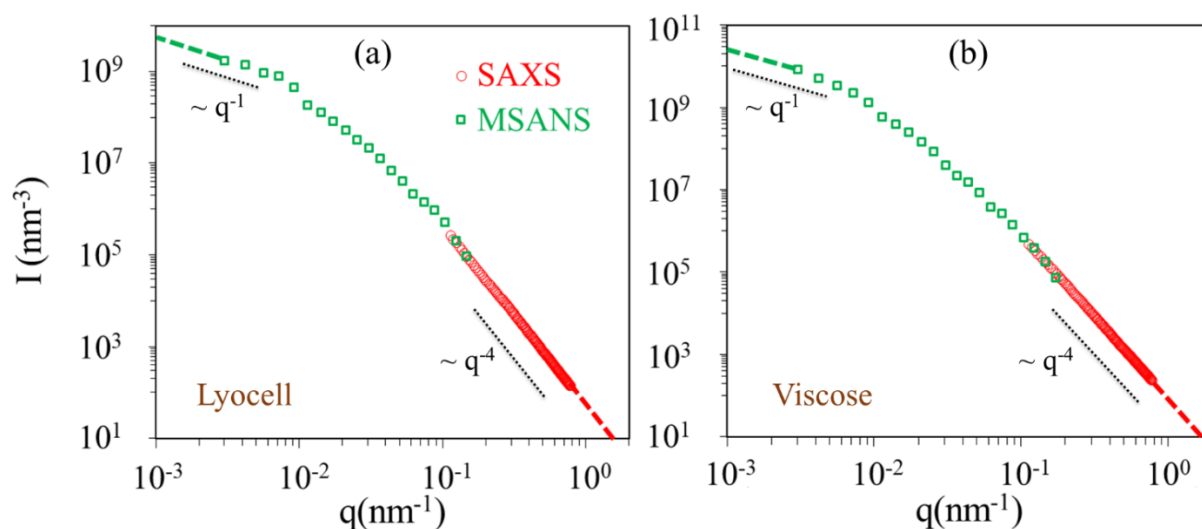
Figure 5.4 Combined MSANS (green) and 1D SAXS (red) data for (a) Lyocell and (b) Viscose fibers. Dashed lines represent extrapolated data points. As mentioned in the Methods section, the MSANS data is scaled so as to match the SAXS data in the range where data from both techniques are available.

The intensity of X-ray scattering depends on the size and shape of the scatterer and on the electron density contrast between the scatterer and the medium. For regenerated cellulose fibers, scattering can result from contrast between the crystal and amorphous phases of the cellulose and from scattering from microvoids. We calculate the electron densities using equation 5.1, using literature values for mass density of amorphous and crystalline cellulose.[39] We obtain electron densities of amorphous and crystalline phase as 479.5 e^-/nm^3 and 508.3 e^-/nm^3 respectively. Thus the contrast between the crystal and amorphous phases in the regenerated cellulose fiber is in the region of 30 e^-/nm^3. In comparison, the contrast between the electron density of the cellulose and air (assumed to be 0 e^-/nm^3) is in the region of 500 e^-/nm^3. The literature indicates that small angle X-ray and neutron scattering from regenerated cellulose fibers is dominated by microvoids rather than crystal/amorphous contrast.[13,22] This is consistent our expectation based on the differences in electron density between cellulose and air and between crystal and amorphous phases. Therefore, we assume that the observed scattering in our experiments is predominantly due to microvoids.

The highly anisotropic scattering from aligned fibers, with prominent streaks in the equatorial direction and the q^{-1} dependence of the low q MSANS intensity strongly indicates that the microvoids are elongated and aligned in the fiber direction. Our scattering data is consistent with literature reports of needle shaped microvoids, elongated along the fiber axis.[22] The

geometry of fiber spinning also suggests that the microvoids are elongated and aligned in the fiber direction. Therefore, we analyze the scattering data considering the microvoids to be long cylindrical structures that are predominantly aligned along the fiber axis. A schematic of oriented cylindrical microvoids and the corresponding 2D SAXS pattern from this sample is shown in **Figure 5.5**.
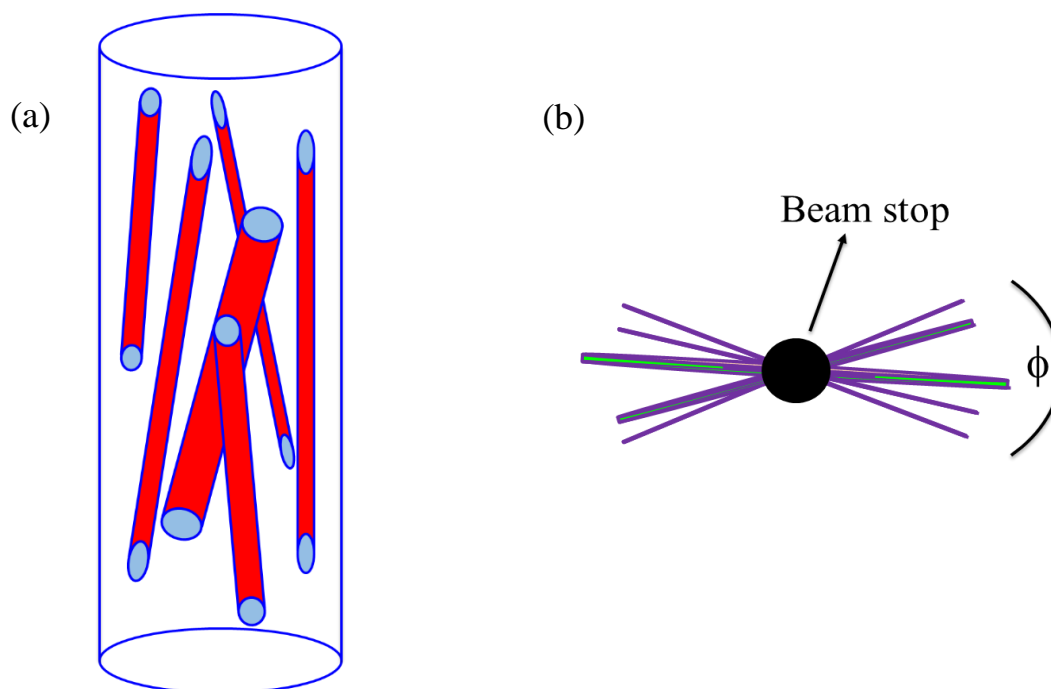
Figure 5.5 (a) Schematic of the oriented cylindrical model and (b) corresponding the 2D SAXS pattern

A q^{-4} dependence of SAXS intensity has been described by Porod as arising from a sharp density change at the interphase between two phases.[40] Therefore, we use equation 5.3 to obtain Porod's constant (K_p) from absolute intensity data of isotropized fibers (**Figure 5.4**). We obtained $K_p = 85$ nm^{-7} for Viscose and $K_p = 50$ nm^{-7} for Lyocell fibers. We measure the crystallinity of Viscose (30%) and Lyocell (40%) fibers using wide angle X-ray diffraction[41] and use these values to estimate the average electron density of the cellulose phase (as a weighted average of the crystalline and amorphous regions). Using this in equation 5.4, we obtain $S_p/V_s = 3.31 \times 10^{-5}$ nm^{-1} for Lyocell and 5.63×10^{-5} nm^{-1} for Viscose fibers. We reiterate that S_p/V_s is the total surface area of all microvoids per unit volume of the sample. We observe that Viscose fibers possess larger microvoid surface area per unit scattering volume of the sample when compared with the Lyocell fibers. This is in

agreement with literature reports that show higher moisture adsorption for Viscose fibers compared with Lyocell.[42,43]

Jiang et. al.[13,14] have obtained the radius of microvoids for regenerated cellulose fibers by following the approach of Statton[44,45] who analyzed the scattering data along the equatorial streak using the method of Guinier. A Guinier form[40] was fitted to the intensity to obtain microvoid radii in the range of $1 – 7$ nm. We note that over the entire range of q for a typical SAXS experiment, the scattered intensity scales as q^{-4}. This precludes a Guinier analysis of the data, suggesting that the estimates of microvoid radii reported in the literature are erroneous. To illustrate this, we refer to a schematic representation of the q-dependence of scattering from microvoids (**Figure 5.6**). For microvoids characterized by an average length, L and radius, R, where $L \gg R$, scattering at extremely low q ($\ll L^{-1}$) is given by $I_o\exp(-q^2R_g^2/3)$, where I_o is the scattering at $q = 0$ and R_g is the radius of gyration of the microvoid. In this regime, a plot of $\ln(I)$ vs $\ln(q)$ is horizontal. For a microvoid length of 271 to 403 nm, this regime would be observed at $q \ll 0.0037$ to 0.0025 nm^{-1}. Clearly, we do not access this q range even in the MSANS experiment. For intermediate q, where $L^{-1} < q < R^{-1}$, and when the samples are isotropized such that the microvoids are isotropically oriented, then the scattering is scaled by a Lorentz correction, given by q^{-1}. Thus, a plot of $\ln(I)$ vs $\ln(q)$ is characterized by a slope of -1. In this regime, it is possible to obtain the average microvoid radius from a plot of $\ln(qI)$ vs q^2. For much higher q, we obtain Porod scattering, primarily from the air-cellulose interface in the microvoids, as discussed earlier. We note that our MSANS data include only a few data points at sufficiently low q, where the scattered intensity scales as q^{-1}. Therefore, rather than fitting the low q MSANS data to a Guinier model, we adopt a different approach, as detailed below.
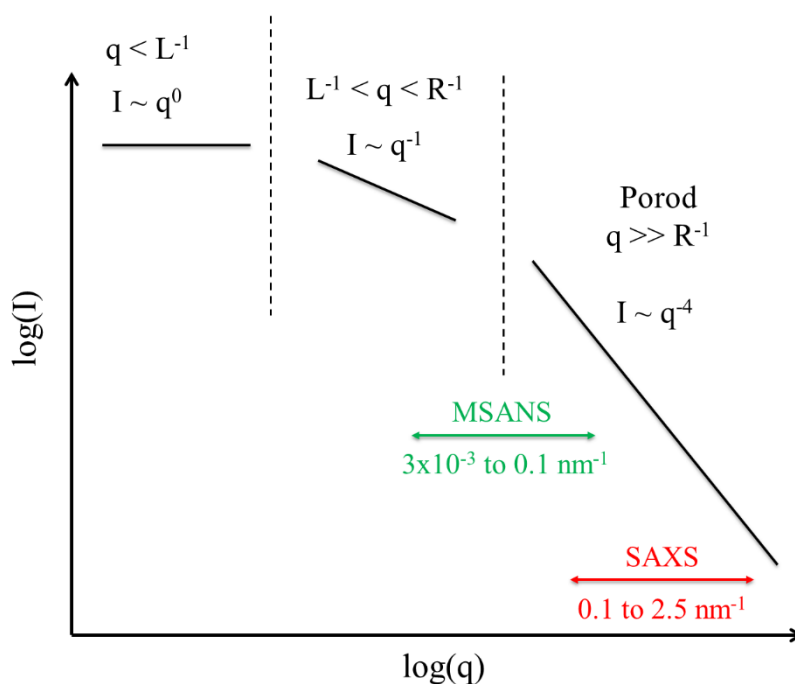
Figure 5.6 Schematic for q dependence of scattering intensity from cylindrical microvoids.

We obtain the invariant by integrating the scattering data from q = 0 to ∞. This requires that the experimental scattering intensity be extrapolated to lower and to higher q. Since we can estimate the Porod constant, K_P from our data, it is easy to extrapolate the scattering data to high q. To extrapolate to low q, we assume that the scattered intensity scales as q^{-1}. Since the invariant is calculated by integrating q^2I, the error introduced by assuming an extrapolation of the low q intensity as q^{-1} is small. Therefore, an analytical form can be obtained for the low q and high q integrations, as shown in equation   5.5. Since the value of the low q integral goes as q_1^2, the error introduced by assuming that the scattered intensity scales as q^{-1} all the way to q = 0 is small. We note that, here too, it is critical to have experimental MSANS data that guides the low q extrapolation. Using scattering data in the Porod limit and extrapolating this to low q (as has been done in the literature[25,26]) will result in large errors in the estimation of the invariant as well.

Figure 5.4 shows the combined SAXS and MSANS absolute intensity data, extrapolated as described in the Methods section. The invariants calculated using equation   5.5 are Q = 2007.3 nm^{-3} for Lyocell and Q = 2508.5 nm^{-3} for Viscose fibers. The void volume fractions (χ) obtained from equation   5.5 are 4 x 10^{-4} for Lyocell fibers and 5 x 10^{-4} for Viscose fibers. For calculating microvoid volume fraction (χ), we made few assumptions e.g.

extrapolation of the lower q USANS data as q^{-1}, considering electron density of air microvoids 0 e^-/nm^3 etc. We estimate the error induced due to these assumptions one by one.

5.4.3 Error from low q extrapolation:

We extrapolate intensity as I $\propto$ q^{-1} in the lower q region of USANS (q < 0.003 nm^{-1}) to evaluate invariant. However, below certain value of q, intensity should decay as q^0.[1] We estimate the possible error generated due to this assumption by extrapolating the data as I $\propto$ q^0 for q < 0.003 nm^{-1} and calculating invariant from this extrapolation. The difference in χ obtained by this extrapolation and the method reported above is below 10^{-5}. This is very small when compared to the microvoid volume fractions of 4 x 10^{-4} and 5 x 10^{-4} for Lyocell and Viscose respectively.

5.4.4 Errors from electron density contrast calculations:

We obtain the average electron density of cellulose by taking the weighted average of crystalline and amorphous phase electron densities as described earlier. Electron density of air microvoids is assumed to be zero. Electron density contrasts ($\Delta\rho$) calculated with these values is used for obtaining χ. However, actual value of the air electron density is non-zero. Also, the fraction of crystalline phase used to calculate the weighted average is obtained from the WAXD crystallinity index, which is not an accurate measurement of crystallinity. Therefore, we obtain χ using the actual electron density of air (0.36 e^-/nm^3) and using the crystalline electron density as highest and amorphous electron density as lowest electron density possible for cellulose. The error in χ calculated based on these electron densities is within $\pm$ 2 x 10^{-5}.

Values of cumulative errors due to extrapolation and electron density contrast calculations are likely to be smaller than 10%. Therefore, neglecting these errors would not affect our results significantly.

We divide S_p/V_s by χ to obtain the average specific surface area of the microvoids. From this, the average radius (R) of cylindrical microvoids is calculated as:

$$S_p/ \chi V_s = (S/V)_p = 2/R, \qquad R = 2 \chi V_s/S_p$$

$$5.7$$

We obtain R = 18 nm for the Viscose fibers and R = 26 nm for the Lyocell fibers. Note that the radius obtained from the Porod analysis is not a number weighted average. For an average length L, it is defined as:

$$R = 2 \frac{\sum_i V_i}{\sum_i S_i} = 2 \frac{\sum_i \pi R_i^2 L x_i}{\sum_i 2\pi R_i L x_i} = \frac{\sum_i R_i^2 x_i}{\sum_i R_i x_i}$$

5.8

where x_i is the fraction of pores with radius = R_i.

Finally, with this information, we fit the combined MSANS and SAXS data from the isotropized samples, assuming that the scattering arises from highly elongated microvoids. We assume that the microvoids comprise sufficiently long cylinders so that the shape of the scattering curve is not strongly influenced by the exact value of the microvoid length. We assume that the radii are polydisperse and choose a lognormal form for the distribution of radius sizes as described by equation 5.6. For fitting the scattering data, we use SASfit software (version 0.94.5).[46] We use the inbuilt form factor - Porod's approximation of long cylinder and lognormal function to estimate the distribution of radii. We constrain the fit by fixing the microvoid radius to the average value obtained from Porod's analysis, as described above. Thus, we use $\mu = 18$ nm for Viscose fibers and $\mu = 26$ nm for Lyocell fibers as the mean radius for the fit. Therefore, there are effectively only two fitting parameters in the model – the width, s of the microvoid radius distribution and the shape parameter, p. **Figure 5.7** (a) shows the best fits obtained from the model fitting and the corresponding radii distributions obtained as fit parameters (**Figure 5.7** b). We obtain a significantly higher value of s for Viscose fibers (s = 1.1, p = 2.15) than for the Lyocell fibers (s = 0.85, p = 2.3). This gives rise to a wider radius distribution for Viscose fibers as evident from **Figure 5.7** (b). Wider radii distribution causes the intensity at lower q to deviate from a clear q^{-1} dependence for Viscose fibers. The radii obtained using equation 5.8 from these distributions are: Viscose = 25.5 nm and Lyocell = 29.4 nm, which are similar to the values obtained from the simple Porod analysis described earlier in the paper.

Characterizing Microvoids in Regenerated Cellulose Fibers obtained from Viscose and Lyocell Process
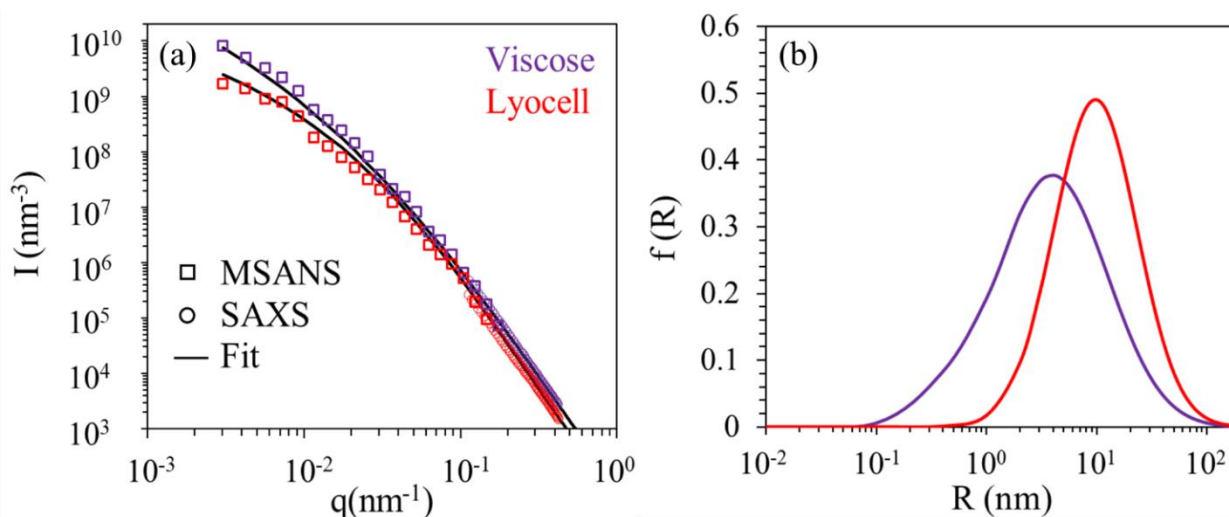
Figure 5.7 (a) Fitted cylindrical model to the combined MSANS and SAXS data from Lyocell and Viscose fibers. (b) Corresponding radius distribution obtained as fit parameters.

Finally, we compare the results for the Viscose and the Lyocell fibers. For the Lyocell fibers, we observe that the microvoids are larger and are more highly oriented. This is consistent with our expectations, based on the fiber formation process. It has been reported[1] that the absence of an air gap during fiber formation in the Viscose process reduces the orientation and alignment of the fiber structure. On the other hand, cellulose polymers get oriented and stretched in the air gap as the dope is spun into the water bath through an air gap in the Lyocell process, leading to better oriented crystalline structure. Therefore, it is not unexpected that during drawing, the microvoids also get more elongated and oriented for Lyocell fibers when compared with Viscose fibers.

We note that the microvoid volume fraction is very small in both Lyocell (4×10^{-4}) and Viscose fibers (5×10^{-4}). This suggests that the differences in the fiber formation processes do not significantly affect the void volume fraction of the regenerated cellulose fibers. However, the size of the microvoids appears to be strongly influenced by the process parameters during fiber formation e.g. air gap, draw ratio etc. Differences in the microvoid structure are expected to have significant implications for the failure properties of the fibers.[16,17] It is reported in literature that Lyocell fibers break at lower strains than the Viscose fibers.[13] Our results show that the average microvoid size in Lyocell fibers is larger than in Viscose fibers. It is possible that this might contribute to the failure of Lyocell fibers at lower strain relative to Viscose fibers. However, a detailed study is required to relate microvoid size to the strain at break for these fibers. This study represents an important first step in that

direction since we report, for the first time, a detailed description of the microvoid characteristics in regenerated cellulose fibers and their relation with the method for fiber manufacture.

5.5   Summary:

We demonstrate the differences in the microvoid structure of regenerated cellulose fibers manufactured from Viscose and Lyocell process using small angle X-ray and medium resolution small angle neutron scattering. Earlier methods present in literature incorrectly fit a Guinier form to the SAXS data from regenerated cellulose fibers,[13,14,44,45] yielding unphysically low value of microvoid radii. We show that SAXS measurements alone are insufficient to correctly characterize microvoids in regenerated cellulose fibers. Combining MSANS and SAXS experiments, we show that microvoids can be modeled as elongated cylinders. Microvoid size (average length and radius), average misorientation and void fraction are calculated using Ruland's equatorial streak method and from our estimate of the invariant and Porod's constant. We show that microvoids in Lyocell fibers are, on average, larger and better oriented than for Viscose fibers. Microvoids in Viscose fibers also show a larger distribution of microvoid radii relative to Lyocell fibers. These structural differences could have implications for the mechanical failure of the fibers.

5.6   References:

(1)   Zhang, S.; Chen, C.; Duan, C.; Hu, H.; Li, H. Regenerated Cellulose by the Lyocell Process, a Brief Review of the Process and Properties. *BioResources* **2018**, *13(2)*, 4577–4592.

(2)   Woodings, C. *Regenerated Cellulose Fibres*; Woodhead Publishing Limited, **2001**.

(3)   Fink, H. P.; Weigel, P.; Purz, H. J.; Ganster, J. Structure Formation of Regenerated Cellulose Materials from NMMO-Solutions. *Prog. Polym. Sci.* **2001**, *26* (9), 1473–1524.

(4)   Lenz, J.; Schurz, J.; Wrentschur, E. Properties and Structure of Solvent-Spun and Viscose-Type Fibres in the Swollen State. *Colloid Polym. Sci.* **1993**, *271* (5), 460–468.

(5)   Kim, D. B. Dry Jet-Wet Spinning of Cellulose/N-Methylmorpholine N-Oxide Hydrate Solutions and Physical Properties of Lyocell Fibers. *Text. Res. J.* **2005**, *75* (4), 331–341.

(6)   Adusumalli, R.-B.; Muller, U.; Weber, H.; Roeder, T.; Sixta, H.; Gindl, W. Tensile Testing of Single Regenerated Cellulose Fibres. *Macromol. Symp* **2006**, *244*, 83–88.

(7)   Cai, Z.; Zhang, Y.; Li, J.; Xue, F.; Shang, Y.; He, X.; Feng, J.; Wu, Z.; Jiang, S. Real Time Synchrotron SAXS and WAXS Investigations on Temperature Related Deformation and Transitions of β-IPP with Uniaxial Stretching. *Polymer.* **2012**, *53* (7), 1593–1601.

(8)   Sharma, A.; Kumaraswamy, G.; Thakre, S. Modeling the Universal Viscoelastic Response of Polymer Fibers. *Phys. Rev. Mater.* **2018**, *2* (6), 062601.

(9)   Sharma, A.; Nagarkar, S.; Thakre, S.; Kumaraswamy, G. Structure – Property Relations in Regenerated Cellulose Fibers : Comparison of Fibers Manufactured Using Viscose and Lyocell Processes. *Cellulose* **2019**, *26* (6), 3655–3669.

(10)   Chen, X.; Burger, C.; Wan, F.; Zhang, J.; Rong, L.; Hsiao, B. S.; Chu, B.; Cai, J.; Zhang, L. Structure Study of Cellulose Fibers Wet-Spun from Environmentally Friendly NaOH / Urea Aqueous Solutions. *Biomacromolecules* **2007**, *8*, 1918–1926.

(11)   Crawshaw, J.; Vickers, M.; Briggs, N. The Hydration of TENCEL® Cellulose Fibres Studied Using Contrast Variation in Small Angle Neutron Scattering. *Polymer* **2000**, *41* (5), 1873–1881.

(12)   Schurz, J.; Lenz, J.; Wrentschur, E. Inner Surface and Void System of Regenerated Cellulose Fibers. *Die Angew. Makromol. Chemie* **1995**, *229*, 175–184.

(13)   Jiang, G.; Huang, W.; Li, L.; Wang, X.; Pang, F.; Zhang, Y.; Wang, H. Structure and Properties of Regenerated Cellulose Fibers from Different Technology Processes. *Carbohydr. Polym.* **2012**, *87* (3), 2012–2018.

(14)   Jiang, G.; Yuan, Y.; Wang, B.; Yin, X.; Mukuze, K. S.; Huang, W.; Zhang, Y.; Wang, H. Analysis of Regenerated Cellulose Fibers with Ionic Liquids as a Solvent as Spinning Speed Is Increased. *Cellulose* **2012**, *19* (4), 1075–1083.

(15) Costa, M. L.; Rezende, M. C.; Almeida, S. F. M. De. Effect of Void Content on the Moisture Absorption in Polymeric Composites. *Polym. Plast. Technol. Eng.* **2006**, *45* (6), 691–698.

(16) Chambers, A. R.; Earl, J. . S.; Squires, C. A.; Suhot, M. A. The Effect of Voids on the Flexural Fatigue Performance of Unidirectional Carbon Fibre Composites Developed for Wind Turbine Applications. *Int. J. Fatigue* **2006**, *28*, 1389–1398.

(17) Varna, J.; Joffe, R.; Berglund, L. A.; Lundstriim, T. S. Effect of Voids on Failure Mechanisms in RTM Laminates. *Compos. Sci. Technol.* **1995**, *53*, 241–249.

(18) Zhang, A.; Li, D.; Lu, H.; Zhang, D. Qualitative Separation of the Effect of Voids on the Bending Fatigue Performance of Hygrothermal Conditioned Carbon/Epoxy Composites. *Mater. Des.* **2011**, *32* (10), 4803–4809.

(19) Grubb, D. T.; Prasad, K.; Adams, W. Small-Angle X-Ray Diffraction of Kevlar Using Synchrotron Radiation. *Polymer* **1991**, *32* (7), 1167–1172.

(20) Thünemann, A. F.; Ruland, W. Microvoids in Polyacrylonitrile Fibers: A Small-Angle X-Ray Scattering Study. *Macromolecules* **2000**, *33* (5), 1848–1852.

(21) Rennhofer, H.; Loidl, D.; Puchegger, S.; Peterlik, H. Structural Development of PAN-Based Carbon Fibers Studied by in Situ X-Ray Scattering at High Temperatures under Load. *Carbon* **2010**, *48* (4), 964–971.

(22) Ruland, W. Small-Angle Scattering Studies on Carbonized Cellulose Fibers. *J. Polym. Sci. Part C Polym. Symp.* **1969**, *28* (1), 143–151.

(23) Zhu, C.; Liu, X.; Yu, X.; Zhao, N.; Liu, J.; Xu, J. A Small-Angle X-Ray Scattering Study and Molecular Dynamics Simulation of Microvoid Evolution during the Tensile Deformation of Carbon Fibers. *Carbon* **2012**, *50* (1), 235–243.

(24) Moss, C. E.; Butler, M. F.; Muller, M.; Cameron, R. E. Microfocus Small-Angle X-Ray Scattering Investigation of the Skin-Core Microstructure of Lyocell Cellulose Fibers. *J. Appl. Polym. Sci.* **2002**, *83*, 2799–2816.

(25) Vickers, M. E.; Briggs, N. P.; Ibbett, R. N.; Payne, J. J.; Smith, S. B. Small Angle X-Ray Scattering Studies on Lyocell Cellulosic Fibres: The Effects of Drying, Re-

Wetting and Changing Coagulation Temperature. *Polymer* **2001**, *42* (19), 8241–8248.

(26) Crawshaw, J.; Cameron, R. A Small Angle X-Ray Scattering Study of Pore Structure in Tencel Cellulose Fibres and the Effects of Physical Treatments. *Polymer* **2000**, *41*, 4691–4698.

(27) Zhu, C. Z.; Yu, X. L.; Liu, X. F.; Mao, Y. Z.; Liu, R. G.; Zhao, N.; Zhang, X. L.; Xu, J. 2D SAXS/WAXD Analysis of Pan Carbon Fiber Microstructure in Organic/Inorganic Transformation. *Chinese J. Polym. Sci.* **2013**, *31* (5), 823–832.

(28) Thunnemann, A. F.; Ruland, W. Lamellar Mesophases in Polyacrylonitrile: A Synchrotron Small-Angle X-Ray Scattering Study. *Macromolecules* **2000**, *33*, 2626–2631.

(29) Shioya, M.; Takaku, A. Characterization of Microvoids in Carbon Fibers by Absolute Small-Angle X-Ray Measurements on a Fiber Bundle. *J. Appl. Phys.* **1985**, *58* (11), 4074–4082.

(30) Schuster, K. C.; Aldred, P.; Villa, M.; Baron, M.; Loidl, R.; Biganska, O.; Patlazhan, S.; Navard, P.; Rüf, H.; Jericha, E. Characterising the Emerging Lyocell Fibres Structures by Ultra Small Angle Neutron Scattering (USANS). *Lenzinger Berichte* **2003**, *82*, 107–117.

(31) Kreze, T.; Strnad, S.; Stana-Kleinschek, K.; Ribitsch, V. Influence of Aqueous Medium on Mechanical Properties of Conventional and New Environmentally Friendly Regenerated Cellulose Fibers. *Mater. Res. Innov.* **2001**, *4* (2–3), 107–114.

(32) Klemm, D.; Philpp, B.; Heinze, T.; Heinze, U.; Wagenknecht, W. *Comprehensive Cellulose Chemistry Volume l Fundamentals and Analytical Methods*; WILEY-VCH Verlag GmbH, **1998**.

(33) Gezici-Koç, Ö.; Erich, S. J. F.; Huinink, H. P.; van der Ven, L. G. J.; Adan, O. C. G. Bound and Free Water Distribution in Wood during Water Uptake and Drying as Measured by 1D Magnetic Resonance Imaging. *Cellulose* **2017**, *24* (2), 535–553.

(34) Alexander, L. E. *X-Ray Diffraction Methods in Polymer Science*; John Wiley & Sons, Inc., **1969**.

(35)   Phinjaroenphan, R.; Soontaranon, S.; Chirawatkul, P.; Chaiprapa, J.; Busayaporn, W.; Pongampai, S.; Lapboonreung, S.; Rugmai, S. SAXS/WAXS Capability and Absolute Intensity Measurement Study at the SAXS Beamline of the Siam Photon Laboratory. *J. Phys. Conf. Ser.* **2013**, *425* (13), 132019.

(36)   Mazumder, S.; Sen, D.; Saravanan, T.; Vijayaraghavan, P. R. A Medium Resolution Double Crystal Based Small-Angle Neutron Scattering Instrument at Trombay. *Curr. Sci.* **2001**, *81* (3), 257–262.

(37)   Mazumder, S.; Sen, D.; Saravanan, T.; Vijayaraghavan, P. R. Performance and Calibration of the Newly Installed Medium Resolution Double Crystal Based Small-Angle Neutron Scattering Instrument at Trombay. *J. Neutron Res.* **2001**, *9*, 39–57.

(38)   Lake, J. A. An Iterative Method of Slit-Correcting Small Angle X-Ray Data. *Acta Cryst.* **1967**, *23* (2), 191.

(39)   Chen, H. *Biotechnology of Lignocellulose: Theory and Practice*; Springer, **2014**.

(40)   Guinier, A.; Fournet, G. *Small-Angle Scattering of X-Rays*; John Wiley & Sons, Inc., **1955**.

(41)   Kasai, N.; Kakudo, M. *X-Ray Diffraction by Macromolecules*; Springer, **2005**.

(42)   Kreze, T.; Jeler, S.; Strnad, S. Correlation between Structure Characteristics and Adsorption Properties of Regenerated Cellulose Fibers. *Mater. Res. Innov.* **2003**, *5* (6), 277–283.

(43)   Kreze, T.; Stana-Kleinschek, K.; Ribitsch, V. The Sorption Behaviour of Cellulose Fibres. *Lenzinger Berichte* **2001**, January 2014, 28–33.

(44)   Statton, W. O. Microvoids in Fibers As Studied By Small-Angle Scattering of X-Rays. *J. Polym. Sci.* **1962**, *58* (166), 205-.

(45)   Statton, W. O. Crystallite Regularity and Void Content in Cellulose Fibers as Shown by Small-Angle X-Ray Scattering. *J. Polym. Sci.* **1956**, *22* (102), 385–397.

(46)   Kohlbrecher, J.; Thu, A. F. Computer Programs SASfit : A Tool for Small-Angle Scattering Data Analysis Using a Library of Analytical Expressions. **2015**, 1587–1598.

Chapter 6.
Summary and Future Work

6.1 Summary:

This thesis focuses on developing robust structure-property links for Viscose and Lyocell regenerated cellulose fibers, in the context of the gaps in the present knowledge identified from a detailed survey of the literature. We use mechanical measurements to study the viscoelastic response of regenerated cellulose fibers. To study the structural features present at multiple length scales, we use wide angle X-ray diffraction, small angle X-ray scattering, medium resolution small angle neutron scattering, microscopy etc. We combine mechanical testing with in-situ structural measurements to map the microstructural origins of viscoelastic response. We present an elegant set of tools and analyse the data from measurements that characterize structure at length scales from $\sim O(\text{Å})$ to $\sim O(100\text{nm})$. These tools are applied to Lyocell and Viscose fibers to investigate up the effect of structural differences between them. We present models to quantitate the links between properties of fibers and the relevant structural features. Here we summarize the major understandings and accomplishments form this thesis:

- We demonstrate that semicrystalline polymer fibers exhibit a universal mechanical response. The linear region mechanical response from semicrystalline fibers with glassy amorphous phase can be captured by invoking only crystalline/amorphous coexistence and present a model to establish a robust structure property relation for these fibers.

- We show that the kink in the stress-strain curve of regenerated cellulose fibers, that is reported as yielding in the literature does not represent a plastic deformation and is recovered logarithmically over a period of a day.

- We quantify the differences in Viscose and Lyocell fibers in dry as well as water soaked state using in-situ WAXD and birefringence measurements.

- We report a methodology to accurately quantify microvoids in Lyocell and Viscose fibers using SAXS and MSANS measurements.

This thesis significantly advances our understanding of structure-property relations for regenerated cellulose fibers.

6.2 Future Work:

Our findings open up new possibilities for exploring the microstructural origin of the properties of regenerated cellulose fibers. In this work, we have characterized the structure of the end product of the spinning process (fibers) at the microscopic level. However, we have not investigated the process of formation of this structure and the factors governing it. The molecular structure of the raw materials and the processing parameters play a crucial role in determining this structure. **Figure 6.1** is a schematic representation of the interplay of molecular structure and processing that gives rise to the formation of microscopic structure in the final products, that govern their properties.
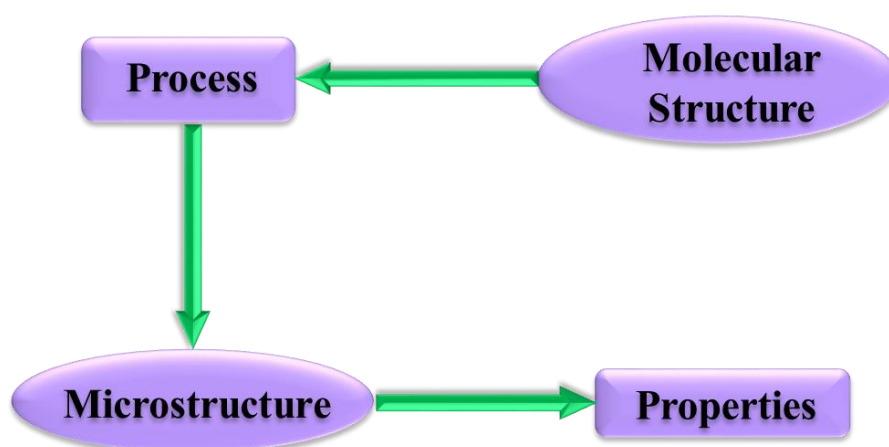

Figure 6.1 Schematic of the link between molecular structure of raw material, process, microstructure of product and the final product properties.

We have reported that there are significant molecular level differences in the cellulose pulp used in Viscose and Lyocell processes e.g. composition, degree of polymerization etc. Also, Lyocell and Viscose processes are characterized by different processing parameters e.g. solvents, operating temperature etc. The learnings from this thesis focus on microstructure-property linkages. We suggest possible future areas of research that could build on our findings and develop the linkages shown in **Figure 6.1**.

6.2.1 *Relaxation time spectra:*

The distribution of relaxation times obtained by fitting our model to the mechanical data has been related to the sub T_g relaxations. The wide spectra represent the heterogeneity in amorphous phase. However, the exact origin of this heterogeneity is not understood at this point. In Chapter 3, we reported that the width of spectra decreases with heating and the two

relaxation modes merge to generated single relaxation mode in both fibers. We also showed that on soaking in water, Viscose and Lyocell fibers exhibit a monomodal relaxation time spectrum and that there is decrease in the relaxation times both fibers. However, Lyocell fibers exhibit pronounced decrease in relaxation times as compared to Viscose fibers, indicating greater plasticization of amorphous phase in Lyocell. The questions that remain unanswered are:

- What is the origin of heterogeneities in the amorphous phase?
- Could the differences in the distribution of relaxation times be related to the distribution of molecular weights in cellulose pulp used for Viscose and Lyocell processes?
- Can the higher relaxation times observed in dry Lyocell relaxation spectrum be correlated to higher molecular weights used in the cellulose pulp?
- Would variation in the molecular weight of the cellulose pulp used for regenerating Lyocell fibers produce fibers with lower crystal orientation, and would this qualitatively change the nature of the amorphous phase?
- What specific difference in the glassy amorphous phase results in greater plasticization of Lyocell fibers by water, relative to Viscose fibers?

Some of the questions posed above e.g. origin of wide relaxation time distribution, effect of temperature and moisture changes could be answered by studying the changes in the amorphous phase with temperature and moisture. However, accurate tools for direct characterization of the amorphous phase are lacking. One way forward could be to use dielectric measurements and solid state nuclear magnetic resonance (NMR) to characterize the amorphous phase relaxations in these fibers. However, we note that it is difficult to develop setups that can perform such measurements in-situ during heating or wetting.

A detailed study of the structure formation during the processing would be useful to answer questions on the effect of molecular weight on the final fiber form. Fibers manufactured from cellulose pulps with different molecular weight distributions could be analysed using our model and the effect of molecular weights on the properties could be studied. Using Lyocell technique to process cellulose pulp with a much lower degree of polymerisation than the conventional range might require significant changes in the manufacturing process to handle low molecular weights. Small scale experimental facilities for fiber preparation, along with

in-situ characterization tools could help to optimize processing parameters accordingly and study structure formation during processing.

The structural feature that leads to differences in the amorphous phase of Lyocell and Viscose is the structural arrangement of crystalline lamellae and amorphous chains. Currently, there are no tools for studies of the crystal/amorphous lamellar structure and interfaces in regenerated cellulose fibers. A direct imaging methodology has been developed by Olley et. al.[1,2] to study the crystal/amorphous structure in polyolefins. This employs an acid etchant to selectively remove the amorphous phase. The relief of the crystal structure is then replicated on a film that can be shadowed with metal and observed under the transmission electron microscope. Such etching/replica/imaging methodology has not been developed for regenerated cellulose fibers. Therefore, one avenue for future investigation is the development of this methodology to image the lamellar arrangement in Viscose and Lyocell fibers. It is possible that there are significant differences in the crystal/amorphous arrangement in Viscose and Lyocell, which might shed some light on the origin of different amorphous phase properties in the two fibers.

6.2.2 *Apparent yield:*

We showed that the transition in stress strain curve to a lower slope in regenerated cellulose fibers does not correspond to a permanent deformation. Rather, it represents a relaxation process, which induces temporary deformation in the fibers and is recovered over long time. However, the molecular underpinnings of apparent yield remain elusive. Clearly, apparent yielding and recovery do not occur through the same mechanism as there is a vast difference in time scales over which these two processes take place. The following questions need to be addressed to understand the apparent yield:

- What microstructural change induces at the apparent yield underlies the response of the fiber?
- What components of the microstructure are responsible for recovery and what are the differences in these features that give rise to different recovery rates in Lyocell and Viscose fibers?
- Why does the apparent yield strain increases drastically in Viscose fibers on wetting but remain unchanged for Lyocell?
- What decides the apparent yield strain – the raw material or processing?

- Can recovery be related to the structural relaxation in these fibers in the same way as the linear region relaxation and recovery?

We noticed that the apparent yield strains for commercial Lyocell and Viscose fibers in dry state are not drastically different from each other. This opens the interesting possibility of manufacturing regenerated cellulose fibers with differences in apparent yield strain. If the apparent yield point is found to be independent of the quantitative differences in the structure of Lyocell and Viscose fibers, it is possible that the structure of native cellulose used as a raw material for manufacturing regenerated cellulose fibers sets the apparent yield strain. On the other hand, we observe differences in the recovery rate for Viscose and Lyocell fibers. The rate of recovery is faster for the Viscose fibers as compared to the Lyocell fibers. Therefore, a systematic study of the semicrystalline structure during recovery could be helpful.

It would be useful to analyse the changes in the amorphous phase of Lyocell and Viscose fibers on wetting using dielectric relaxation, NMR etc. Variation in the apparent yield strain with systematically changing the moisture content should be studied. We reported that wetting induces faster linear region stress relaxation in Lyocell fibers as compared to the Viscose fibers. It is possible that similar structural changes are responsible for wetting induced changes in the Lyocell and Viscose fibers. Therefore, exploring differences in the interaction of water with Viscose and Lyocell fibers might help. Lyocell fibers are regenerated in a water bath. It is possible that due to structure formation in the presence of water, the amorphous phase in Lyocell fibers is easily plasticized with water and there is no effect of water on the apparent yield strain. Would apparent yielding of Lyocell fibers regenerated using solvents other than water be different.

6.2.3 *Failure properties:*

Lyocell and Viscose fibers fail at different strains. There are also differences in the fibrillation properties of two fibers. We have reported a methodology to characterize microvoids in these fibers in dry state. These microvoids might initiate crack formation in the fibers. However, the failure mechanism in these fibers is not well understood. Before one can address the failure problems in these fibers, it is necessary to understand the mechanism of failure in fibers.

Effect of stretching on the microvoid structure should be studied using in-situ SAXS experiments. The structure of fibers stretched to strains near their failure strains could be quantified using the methodologies developed in this thesis. Also, fiber processing

parameters like the size of the air gap could be varied to change crystalline orientation in Lyocell fibers. The differences in the structure of fibers manufactured using different air gaps could be quantified using the methodologies described in this thesis and could be related to the failure properties.

To understand and control fibrillation behaviour, it is necessary to first completely quantify fibrillation. The extent of fibrillation in Lyocell fibers has been quantified earlier.[3] However, the critical stress, moisture content etc. required for fibrillation are not quantified. It is known that the fibrillation occurs on mechanically shearing wet Lyocell fibers. Torsion experiments could be performed on the fibers using a rheometer to quantify the failure stress and strain. Similarly, the effect of moisture content on the fibrillation could be studied. Several reports have presented methodologies for reduction in fibrillation.[4,5] Fibers manufactured from these processes could be compared to the conventional Lyocell fibers in terms of failure stress and strain.

As mentioned earlier, the effect of plasticization is more pronounced in Lyocell fibers as compare to Viscose fibers on soaking in water. It is possible that due to this plasticization, Lyocell structure fibrillates on shearing in wet state. This could be investigated by comparing relaxation time spectra for fibers with different fibrillation tendencies. It is also important to study the fibrillation of Lyocell fibers in solvents other than water. Different solvents affect the glass transition temperature of cellulose to different extents.[6] A comparison of the fibrillation parameters obtained for Lyocell fibers fibrillated in different solvent could help to understand the origin of fibrillation and its link to plasticization. If these are linked, then the roles of the fiber manufacturing process and of the characteristics of the cellulose pulp could be explored. Higher molecular weights in cellulose pulp could be responsible for differences in the plasticity for Lyocell and Viscose fibers. Therefore, a study of fibrillation of fibers produced using pulp with different molecular weight distribution could help understand this problem.

Therefore, the structure-property relations developed in this thesis can be used to identify the relevant process parameters and the molecular structure of raw material. Till date, no predictive models exist for process-structure-property relations in regenerated cellulose fibers. This chapter lists possible lines of enquiry that might lead to the development of predictive models. Such a detailed understanding would result in rational selection of raw material and process conditions to obtain fibers with optimized properties.

6.3 References:

(1)   Olley, R. H.; Bassett, D. C. An Improved Permanganic Etchant for Polyolefines. *Polymer.* **1982**, *23* (12), 1707–1710.

(2)   Olley, R. H.; Hodge, A. M.; Bassett, D. C.; Thomson, J. J. Permanganic Etchant for Polyolefines. *J. Polym. Sci.* **1979**, *17* (4), 627–643.

(3)   Mortimer, S. A.; Péguy, A. A. Methods for Reducing the Tendency of Lyocell Fibers to Fibrillate. *J. Appl. Polym. Sci.* **1996**, *60* (3), 305–316.

(4)   Nemec, H.; Ag, L. Fibrillation of Cellulosic Materials - Can Previous Literature Offer a Solution? *Lenzinger Berichte* **1994**, *9*, 69–72.

(5)   Bates, I.; Maudru, E.; Phillips, D. a S.; Renfrew, a H. M.; Su, Y.; Xu, J. Cross-Linking Agents for the Protection of Lyocell against Fibrillation: Synthesis, Application and Technical Assessment of 2,4-Diacrylamidobenzenesulphonic Acid. *Color. Technol.* **2004**, *120* (6), 293–300.

(6)   Akim, E. L.; Naimark, N. I.; Vasil'yev, B. V.; Fomenko, B. A.; Ignat'eva, E. V.; Zhegalova, N. N. Effect of Plasticizing Liquid Media on the Glass Transition Temperatures of Cellulosic Materials. *Polym. Sci. U.S.S.R.* **1971**, *13* (10), 2522–2529.

List of Publications

1. Sharma, A.; Kumaraswamy, G.; Thakre, S. Modeling the Universal Viscoelastic Response of Polymer Fibers. *Phys. Rev. Mater.* **2018**, *2* (6), 062601

2. Sharma, A.; Nagarkar, S.; Thakre, S.; Kumaraswamy, G. Structure – Property Relations in Regenerated Cellulose Fibers : Comparison of Fibers Manufactured Using Viscose and Lyocell Processes. *Cellulose* **2019**, *26* (6), 3655–3669

3. Sharma A.; Sen D.; Thakre S.; Kumaraswamy G. Characterizing Microvoids in Regenerated Cellulose Fibers Obtained from Viscose and Lyocell Processes. *Macromolecules* **2019**, 52 (11), 3987-3994

4. "Microstructural Differences between Viscose and Lyocell Revealed by In-Situ Studies of Wet and Dry fibers" Aakash Sharma, Shirish Thakre, Guruswamy Kumaraswamy (*Submitted*)